THE UNIVERSITY OF CALGARY

AN ALTERNATIVE TO DIRECT SEQUENCE SPREAD SPECTRUM MULTIPLE ACCESS SYSTEM USING OPTIMIZED WAVESHAPING

by

Kim Giap Chia

A THESIS

SUBMITTED TO THE FACULTY OF GRADUATE STUDIES

IN PARTIAL FULFILLMENT OF THE REQUIREMENTS FOR THE

DEGREE OF MASTER OF SCIENCE

DEPARTMENT OF ELECTRICAL AND

COMPUTER ENGINEERING

CALGARY, ALBERTA

NOVEMBER, 1992

ISBN 0-315-83114-6

Name Kim CHIA

Dissertation Abstracts International is arranged by broad, general subject categories. Please select the one subject which most nearly describes the content of your dissertation. Enter the corresponding four-digit code in the spaces provided.

ELECTRICAL ENGINEERING | 0 5 4 4 | U·M·I

SUBJECT TERM | SUBJECT CODE

Subject Categories

THE HUMANITIES AND SOCIAL SCIENCES

COMMUNICATIONS AND THE ARTS

Architecture 0729
Art History 0377
Cinema 0900
Dance 0378
Fine Arts 0357
Information Science 0723
Journalism 0391
Library Science 0399
Mass Communications 0708
Music 0413
Speech Communication 0459
Theater 0465

EDUCATION

General 0515
Administration 0514
Adult and Continuing 0516
Agricultural 0517
Art 0273
Bilingual and Multicultural 0282
Business 0688
Community College 0275
Curriculum and Instruction 0727
Early Childhood 0518
Elementary 0524
Finance 0277
Guidance and Counseling 0519
Health 0680
Higher 0745
History of 0520
Home Economics 0278
Industrial 0521
Language and Literature 0279
Mathematics 0280
Music 0522
Philosophy of 0998
Physical 0523
Psychology 0525
Reading 0535
Religious 0527
Sciences 0714
Secondary 0533
Social Sciences 0534
Sociology of 0340
Special 0529
Teacher Training 0530
Technology 0710
Tests and Measurements 0288
Vocational 0747

LANGUAGE, LITERATURE AND LINGUISTICS

Language
 General 0679
 Ancient 0289
 Linguistics 0290
 Modern 0291
Literature
 General 0401
 Classical 0294
 Comparative 0295
 Medieval 0297
 Modern 0298
 African 0316
 American 0591
 Asian 0305
 Canadian (English) 0352
 Canadian (French) 0355
 English 0593
 Germanic 0311
 Latin American 0312
 Middle Eastern 0315
 Romance 0313
 Slavic and East European 0314

PHILOSOPHY, RELIGION AND THEOLOGY

Philosophy 0422
Religion
 General 0318
 Biblical Studies 0321
 Clergy 0319
 History of 0320
 Philosophy of 0322
Theology 0469

SOCIAL SCIENCES

American Studies 0323
Anthropology
 Archaeology 0324
 Cultural 0326
 Physical 0327
Business Administration
 General 0310
 Accounting 0272
 Banking 0770
 Management 0454
 Marketing 0338
Canadian Studies 0385
Economics
 General 0501
 Agricultural 0503
 Commerce-Business 0505
 Finance 0508
 History 0509
 Labor 0510
 Theory 0511
Folklore 0358
Geography 0366
Gerontology 0351
History
 General 0578
 Ancient 0579
 Medieval 0581
 Modern 0582
 Black 0328
 African 0331
 Asia, Australia and Oceania 0332
 Canadian 0334
 European 0335
 Latin American 0336
 Middle Eastern 0333
 United States 0337
History of Science 0585
Law 0398
Political Science
 General 0615
 International Law and Relations 0616
 Public Administration 0617
Recreation 0814
Social Work 0452
Sociology
 General 0626
 Criminology and Penology 0627
 Demography 0938
 Ethnic and Racial Studies 0631
 Individual and Family Studies 0628
 Industrial and Labor Relations 0629
 Public and Social Welfare 0630
 Social Structure and Development 0700
 Theory and Methods 0344
Transportation 0709
Urban and Regional Planning 0999
Women's Studies 0453

THE SCIENCES AND ENGINEERING

BIOLOGICAL SCIENCES

Agriculture
 General 0473
 Agronomy 0285
 Animal Culture and Nutrition 0475
 Animal Pathology 0476
 Food Science and Technology 0359
 Forestry and Wildlife 0478
 Plant Culture 0479
 Plant Pathology 0480
 Plant Physiology 0817
 Range Management 0777
 Wood Technology 0746
Biology
 General 0306
 Anatomy 0287
 Biostatistics 0308
 Botany 0309
 Cell 0379
 Ecology 0329
 Entomology 0353
 Genetics 0369
 Limnology 0793
 Microbiology 0410
 Molecular 0307
 Neuroscience 0317
 Oceanography 0416
 Physiology 0433
 Radiation 0821
 Veterinary Science 0778
 Zoology 0472
Biophysics
 General 0786
 Medical 0760

EARTH SCIENCES

Biogeochemistry 0425
Geochemistry 0996
Geodesy 0370
Geology 0372
Geophysics 0373
Hydrology 0388
Mineralogy 0411
Paleobotany 0345
Paleoecology 0426
Paleontology 0418
Paleozoology 0985
Palynology 0427
Physical Geography 0368
Physical Oceanography 0415

HEALTH AND ENVIRONMENTAL SCIENCES

Environmental Sciences 0768
Health Sciences
 General 0566
 Audiology 0300
 Chemotherapy 0992
 Dentistry 0567
 Education 0350
 Hospital Management 0769
 Human Development 0758
 Immunology 0982
 Medicine and Surgery 0564
 Mental Health 0347
 Nursing 0569
 Nutrition 0570
 Obstetrics and Gynecology 0380
 Occupational Health and Therapy 0354
 Ophthalmology 0381
 Pathology 0571
 Pharmacology 0419
 Pharmacy 0572
 Physical Therapy 0382
 Public Health 0573
 Radiology 0574
 Recreation 0575
 Speech Pathology 0460
 Toxicology 0383
Home Economics 0386

PHYSICAL SCIENCES

Pure Sciences

Chemistry
 General 0485
 Agricultural 0749
 Analytical 0486
 Biochemistry 0487
 Inorganic 0488
 Nuclear 0738
 Organic 0490
 Pharmaceutical 0491
 Physical 0494
 Polymer 0495
 Radiation 0754
Mathematics 0405
Physics
 General 0605
 Acoustics 0986
 Astronomy and Astrophysics 0606
 Atmospheric Science 0608
 Atomic 0748
 Electronics and Electricity 0607
 Elementary Particles and High Energy 0798
 Fluid and Plasma 0759
 Molecular 0609
 Nuclear 0610
 Optics 0752
 Radiation 0756
 Solid State 0611
Statistics 0463

Applied Sciences

Applied Mechanics 0346
Computer Science 0984

Engineering
 General 0537
 Aerospace 0538
 Agricultural 0539
 Automotive 0540
 Biomedical 0541
 Chemical 0542
 Civil 0543
 Electronics and Electrical 0544
 Heat and Thermodynamics 0348
 Hydraulic 0545
 Industrial 0546
 Marine 0547
 Materials Science 0794
 Mechanical 0548
 Metallurgy 0743
 Mining 0551
 Nuclear 0552
 Packaging 0549
 Petroleum 0765
 Sanitary and Municipal 0554
 System Science 0790
Geotechnology 0428
Operations Research 0796
Plastics Technology 0795
Textile Technology 0994

PSYCHOLOGY

General 0621
Behavioral 0384
Clinical 0622
Developmental 0620
Experimental 0623
Industrial 0624
Personality 0625
Physiological 0989
Psychobiology 0349
Psychometrics 0632
Social 0451

Nom ______________________________

Dissertation Abstracts International est organisé en catégories de sujets. Veuillez s.v.p. choisir le sujet qui décrit le mieux votre thèse et inscrivez le code numérique approprié dans l'espace réservé ci-dessous.

______________________________ SUJET | ☐☐☐☐ CODE DE SUJET | U·M·I

Catégories par sujets

HUMANITÉS ET SCIENCES SOCIALES

COMMUNICATIONS ET LES ARTS
Architecture 0729
Beaux-arts 0357
Bibliothéconomie 0399
Cinéma 0900
Communication verbale 0459
Communications 0708
Danse 0378
Histoire de l'art 0377
Journalisme 0391
Musique 0413
Sciences de l'information 0723
Théâtre 0465

ÉDUCATION
Généralités 515
Administration 0514
Art 0273
Collèges communautaires 0275
Commerce 0688
Économie domestique 0278
Éducation permanente 0516
Éducation préscolaire 0518
Éducation sanitaire 0680
Enseignement agricole 0517
Enseignement bilingue et multiculturel 0282
Enseignement industriel 0521
Enseignement primaire. 0524
Enseignement professionnel 0747
Enseignement religieux 0527
Enseignement secondaire 0533
Enseignement spécial 0529
Enseignement supérieur 0745
Évaluation 0288
Finances 0277
Formation des enseignants 0530
Histoire de l'éducation 0520
Langues et littérature 0279
Lecture 0535
Mathématiques 0280
Musique 0522
Orientation et consultation 0519
Philosophie de l'éducation 0998
Physique 0523
Programmes d'études et enseignement 0727
Psychologie 0525
Sciences 0714
Sciences sociales 0534
Sociologie de l'éducation 0340
Technologie 0710

LANGUE, LITTÉRATURE ET LINGUISTIQUE
Langues
- Généralités 0679
- Anciennes 0289
- Linguistique 0290
- Modernes 0291

Littérature
- Généralités 0401
- Anciennes 0294
- Comparée 0295
- Mediévale 0297
- Moderne 0298
- Africaine 0316
- Américaine 0591
- Anglaise 0593
- Asiatique 0305
- Canadienne (Anglaise) 0352
- Canadienne (Française) 0355
- Germanique 0311
- Latino-américaine 0312
- Moyen-orientale 0315
- Romane 0313
- Slave et est-européenne 0314

PHILOSOPHIE, RELIGION ET THÉOLOGIE
Philosophie 0422
Religion
- Généralités 0318
- Clergé 0319
- Études bibliques 0321
- Histoire des religions 0320
- Philosophie de la religion 0322

Théologie 0469

SCIENCES SOCIALES
Anthropologie
- Archéologie 0324
- Culturelle 0326
- Physique 0327

Droit 0398
Économie
- Généralités 0501
- Commerce-Affaires 0505
- Économie agricole 0503
- Économie du travail 0510
- Finances 0508
- Histoire 0509
- Théorie 0511

Études américaines 0323
Études canadiennes 0385
Études féministes 0453
Folklore 0358
Géographie 0366
Gérontologie 0351
Gestion des affaires
- Généralités 0310
- Administration 0454
- Banques 0770
- Comptabilité 0272
- Marketing 0338

Histoire
- Histoire générale 0578
- Ancienne 0579
- Médiévale 0581
- Moderne 0582
- Histoire des noirs 0328
- Africaine 0331
- Canadienne 0334
- États-Unis 0337
- Européenne 0335
- Moyen-orientale 0333
- Latino-américaine 0336
- Asie, Australie et Océanie 0332

Histoire des sciences 0585
Loisirs 0814
Planification urbaine et régionale 0999
Science politique
- Généralités 0615
- Administration publique 0617
- Droit et relations internationales 0616

Sociologie
- Généralités 0626
- Aide et bien-àtre social 0630
- Criminologie et établissements pénitentiaires 0627
- Démographie 0938
- Études de l' individu et de la famille 0628
- Études des relations interethniques et des relations raciales 0631
- Structure et développement social 0700
- Théorie et méthodes. 0344
- Travail et relations industrielles 0629

Transports 0709
Travail social 0452

SCIENCES ET INGÉNIERIE

SCIENCES BIOLOGIQUES
Agriculture
- Généralités 0473
- Agronomie. 0285
- Alimentation et technologie alimentaire 0359
- Culture 0479
- Élevage et alimentation 0475
- Exploitation des péturages 0777
- Pathologie animale 0476
- Pathologie végétale 0480
- Physiologie végétale 0817
- Sylviculture et faune 0478
- Technologie du bois 0746

Biologie
- Généralités 0306
- Anatomie 0287
- Biologie (Statistiques) 0308
- Biologie moléculaire 0307
- Botanique 0309
- Cellule 0379
- Écologie 0329
- Entomologie 0353
- Génétique 0369
- Limnologie 0793
- Microbiologie 0410
- Neurologie 0317
- Océanographie 0416
- Physiologie 0433
- Radiation 0821
- Science vétérinaire 0778
- Zoologie 0472

Biophysique
- Généralités 0786
- Medicale 0760

SCIENCES DE LA TERRE
Biogéochimie 0425
Géochimie 0996
Géodésie 0370
Géographie physique 0368
Géologie 0372
Géophysique 0373
Hydrologie 0388
Minéralogie 0411
Océanographie physique 0415
Paléobotanique 0345
Paléoécologie 0426
Paléontologie 0418
Paléozoologie 0985
Palynologie 0427

SCIENCES DE LA SANTÉ ET DE L'ENVIRONNEMENT
Économie domestique 0386
Sciences de l'environnement 0768
Sciences de la santé
- Généralités 0566
- Administration des hipitaux 0769
- Alimentation et nutrition 0570
- Audiologie 0300
- Chimiothérapie 0992
- Dentisterie 0567
- Développement humain 0758
- Enseignement 0350
- Immunologie 0982
- Loisirs 0575
- Médecine du travail et thérapie 0354
- Médecine et chirurgie 0564
- Obstétrique et gynécologie 0380
- Ophtalmologie 0381
- Orthophonie 0460
- Pathologie 0571
- Pharmacie 0572
- Pharmacologie 0419
- Physiothérapie 0382
- Radiologie 0574
- Santé mentale 0347
- Santé publique 0573
- Soins infirmiers 0569
- Toxicologie 0383

SCIENCES PHYSIQUES
Sciences Pures
Chimie
- Genéralités 0485
- Biochimie 487
- Chimie agricole 0749
- Chimie analytique 0486
- Chimie minérale 0488
- Chimie nucléaire 0738
- Chimie organique 0490
- Chimie pharmaceutique 0491
- Physique 0494
- PolymÇres 0495
- Radiation 0754

Mathématiques 0405
Physique
- Généralités 0605
- Acoustique 0986
- Astronomie et astrophysique 0606
- Electronique et électricité 0607
- Fluides et plasma 0759
- Météorologie 0608
- Optique 0752
- Particules (Physique nucléaire) 0798
- Physique atomique 0748
- Physique de l'état solide 0611
- Physique moléculaire 0609
- Physique nucléaire 0610
- Radiation 0756

Statistiques 0463

Sciences Appliqués Et Technologie
Informatique 0984
Ingénierie
- Généralités 0537
- Agricole 0539
- Automobile 0540
- Biomédicale 0541
- Chaleur et ther modynamique 0348
- Conditionnement (Emballage) 0549
- Génie aérospatial 0538
- Génie chimique 0542
- Génie civil 0543
- Génie électronique et électrique 0544
- Génie industriel 0546
- Génie mécanique 0548
- Génie nucléaire 0552
- Ingénierie des systâmes 0790
- Mécanique navale 0547
- Métallurgie 0743
- Science des matériaux 0794
- Technique du pétrole 0765
- Technique minière 0551
- Techniques sanitaires et municipales 0554
- Technologie hydraulique 0545

Mécanique appliquée 0346
Géotechnologie 0428
Matières plastiques (Technologie) 0795
Recherche opérationnelle 0796
Textiles et tissus (Technologie) 0794

PSYCHOLOGIE
Généralités 0621
Personnalité 0625
Psychobiologie 0349
Psychologie clinique 0622
Psychologie du comportement 0384
Psychologie du développement 0620
Psychologie expérimentale 0623
Psychologie industrielle 0624
Psychologie physiologique 0989
Psychologie sociale 0451
Psychométrie 0632

THE UNIVERSITY OF CALGARY

FACULTY OF GRADUATE STUDIES

The undersigned certify that they have read, and recommend to the Faculty of Graduate Studies for acceptance, a thesis entitled, **"A N ALTERNATIVE TO DIRECT SEQUENCE SPREAD SPECTRUM MULTIPLE ACCESS SYSTEM USING OPTIMIZED WAVESHAPING"**, submitted by Kim Giap Chia in partial fulfillment of the requirements for the degree of Master of Science.

Supervisor - Dr. A. Sesay
Dept. of Elec. and Comp. Engg.

Dr. M. Fattouche
Dept. of Elec. and Comp. Engg.

Dr. G. Lachapelle
Dept. of Geomatics Engg.

Date : NOV 10 1992

ABSTRACT

An alternative to the conventional DS-SSMA system is presented for applications where bandwidth is limited. The conventional system uses Gold codes whereas the proposed system spreads with a unique waveform, based upon a linear combination of half-period sinusoids. Transmit waveforms are spectrally efficient, continuous over the entire signaling interval and easily generated. Receiver is of the single-user correlation type and the waveform is selected from the solution of a constrained optimization problem. Four simulation models are built, tested and simulated using SPW, a highly integrated and powerful software tool. Plots of typical waveforms and bit error performances are presented for noncoherent Differential Quadrature Phase Shift Keying (DQPSK) in AWGN and a multipath fading channel. Performances indicate that the system is a viable alternative in bandwidth limited applications. Examples of potential applications are presented for which the proposed system is most suitable.

ACKNOWLEDGMENTS

I wish to thank Dr. A. Sesay for his guidance, support and patience throughout the progress of this research as well as the financial support of The University of Calgary and Telecommunications Research Laboratories (TR Labs).

I would also like to express my appreciation to Grant McGibney for his assistance in eradicating the problems associated with SPW and the computing facilities during the initial phase of this project, Gerald Morrison and Dave Tholl for their help regarding Mac software and the rest of the staff of TR Labs, including students, for making this two years a memorable experience.

Lastly, I like to thank my wife, Susan, for her patience and understanding in our long distance relationship during the past two years.

DEDICATION

I like to dedicate this thesis in living memory of my father who made it possible for me to pursue my education in Canada.

TABLE OF CONTENTS

LIST OF TABLES

LIST OF FIGURES

LIST OF SYMBOLS & ABBREVIATIONS

$\alpha_{k,l}$	Rayleigh distributed gain of the l th path of the k th user
$a(D)$	initial loading of the stages of the shift registers
$\{a_{j+i}\}$	pseudo-random code sequence
$a_k(t)$	spreading code waveform of the k th user
a_l^k	l th chip of the k th user
a_n	n th value of the code sequence
AO/LSE	Auto-Optimal with Least Sidelobe Energy
$b(D)$	output of a R-stage linear feedback shift register generator
$b_k(t)$	complex information signal of the k th user
b_j^k	j th complex data symbol of the k user
$\{b_j\}$	information sequence
b_p^1	p th received complex symbol of user #1
$\hat{b}_p^1$	estimate of the inphase transmitted bit for receiver #1
CDMA	Code Division Multiple Access
Δ	maximum delay spread of the multipath channel
$(\Delta f)_c$	coherence bandwidth
$\delta(t)$	Kronecker delta
D_c^1	desired signal component of the inphase branch of one arm of the optimum DQPSK demodulator for receiver #1

D_s^1 desired signal component of the quadrature branch of one arm of the optimum DQPSK demodulator for receiver #1

DS Direct Sequence

DS-SS Direct Sequence Spread Spectrum

DS-SSMA Direct Sequence Spread Spectrum Multiple Access

DQPSK Differential Quadrature Phase Shift Keying

E_s energy of the transmitted signal

$\phi_{k,l}$ uniformly distributed random phase of the l the path of the k th transmitter

f_c common carrier frequency

FCC Federal Communication Commission

FDMA Frequency Division Multiple Access

FH Frequency Hopped

FH-SS Frequency Hop Spread Spectrum

FM Frequency Modulation

FSK Frequency Shift Keying

γ_0 average signal-to-noise ratio of the desired signal

$g(D)$ generator polynomial

$g_{k,l}$ an element in the k th column and l th row of a Hadamard matrix

$g_k(t)$ transmit waveform of the k th transmitter defined in [0,T)

GINO General Interactive Optimizer

GRG General Reduced Gradient

η sample of Gaussian noise

$h_k(t)$ equivalent lowpass impulse response of the channel for the k th transmitter

I_c^1	interference component of the inphase branch of one arm of the optimum DQPSK demodulator of receiver #1
JTIDS	Joint Tactical Information Distribution System
K	number of users
L	number of Rayleigh distributed paths
LAN	Local Area Network
LPI	Low Probability of Intercept
M	size of Hadamard matrix
MA	Multiple Access
$n(t)$	white Gaussian noise
N	number of transmit waveforms
N_c	code period
η_c	sampled zero mean white Gaussian noise of the inphase branch of the optimum DQPSK demodulator
nsecs	nano seconds
$p_1(t)$	optimized receiver waveform
$p_{i,l}$	an element in the i th column and l th row of a (M x M) matrix
P_e	average probability of error
P_e^1	average probability of error for receiver #1
PCM	Pulse Code Modulation
PCN	Personal Communications Network
PLL	Phase Lock Loop
PN	Pseudo-noise
PSK	Phase Shift Keying

$P_T(t)$	rectangular waveform defined in [0,T)
$P_{T_c}(t)$	rectangular pulse defined in [0,T_c)
θ_k	random carrier phase of the k th transmitter
$\theta_b(k)$	discrete periodic autocorrelation of code *b(D)*
$\theta_{bb'}(k)$	discrete crosscorrelation functions of two codes *b(D)* and *b'(D)*
R	symbol rate in bits/seconds
$r(t)$	received signal
$r_{k,i}(\tau)$	partial crosscorrelation function between the i th receiver code and the k th interfering code defined in [0,τ]
$\hat{r}_{k,i}(\tau)$	partial crosscorrelation function between the i th receiver code and the k the interfering code defined in [τ,T]
$\{s_{j,i}\}$	sequence resulting from the modulo-2 operation of $\{b_j\}$ and $\{a_{j+i}\}$
$s_k(t)$	transmitted signal of the k th user
SNR	signal-to-noise ratio
SS	Spread Spectrum
τ_k	propagation time delay of the k th signal
τ_{rms}	rms delay spread
$t_{k,l}$	delay of the l th Rayleigh path of the k th transmitter through the multipath channel
T	symbol duration
T_c	chip duration
TDMA	Time Division Multiple Access
TH	Time Hopping

t(n)	crosscorrelation function of a pair of Gold codes
WARC-92	World Administrative Radio Conference 1992
ξ	equivalent complex lowpass output of the sampled signal
Z_c^1	sampled lowpass output of the integrator of the inphase branch of one arm of the optimum DQPSK demodulator of receiver #1
Z_s^1	sampled lowpass output of the integrator of the quadrature branch of one arm of the optimum DQPSK demodulator of receiver #1
Z_p^1	detection statistic of receiver #1 for the inphase branch

CHAPTER 1

INTRODUCTION

"Whuh? Oh, " said the missile expert. "I guess I was off base about the jamming. Suddenly it seems to me that's so obvious, it must have been tried and it doesn't work."

"Right, it doesn't. That's because the frequency and amplitude of the control pulses make like purest noise - they're genuinely random. So trying to jam them is like trying to jam FM with an AM signal. You hit it so seldom, you might as well not try."

"What do you mean, random? You can't control anything with random noise."

The captain thumbled over his shoulder at the Luanae Galaxy. "They can. There's a synchronous generator in the missiles that reproduces the same random noise, peak by pulse. Once you do that, modulation's no problem. I don't know how they do it. They just do. The Luanae can't explain it; the planetoid developed it."

England put his head down almost to the table. "The same random," he whispered from the very edge of sanity.

THEODORE STURGEON, "The Pod in the Barrier,"
Galaxy, Sept. 1957;
reprinted in "A Touch of Strange"
Doubleday, 1958

The above passage clearly illustrates some of the peculiar characteristics of a Spread Spectrum (SS) system. It defies common logic that a signal could be modulated with random noise (whose characteristics are known) and have perfect recovery of the original signal at the receiver using an exact copy of the noise. Due to this unusual phenomenon, this process was known as noise modulation during the 50's.

1.1 Historical Developments

Spread Spectrum had its beginnings as early as the mid 20's[1] where the groundwork in information and communication theories were laid by some prominent researchers in that period: Weiner[2], Whittaker[3-6], Hartley[7], Nyquist[8], Kotelnikov[9], Shannon[10] and Gabor[11]. The explosion of activities in SS started during World War II as the Allies and the Germans searched for a secure communication system with anti-jamming capabilities.

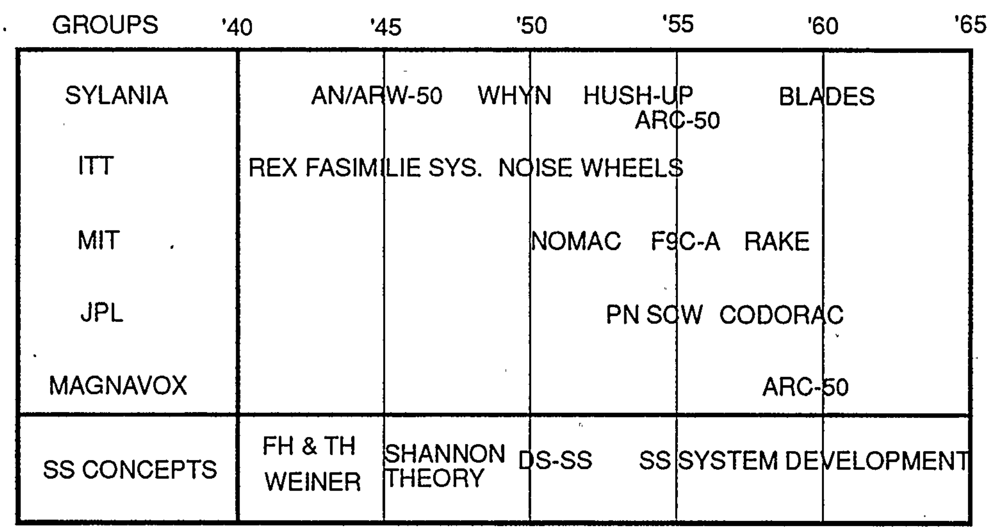

FIG.1.1.1 Approximate time lines for the development of SS systems and concepts [1].

The evolution of SS systems by various research groups can be seen in Fig.1.1.1. Despite the cloak of secrecy over these projects, there were still rampant exchange of ideas resulting in the prototype of BLADES, the first fully operational Frequency Hop Spread Spectrum (FH-SS) system and the ARC-50, the first fully operational Direct Sequence Spread Spectrum (DS-SS) system.

The last decade has been named the "Computer Decade" and now, with the evolution in communications, this decade will be called the "Telecommunications Decade". With an increasing need to communicate, particular attention is focused on the efficient use of the available frequency spectrum. Along with the declassification of documents associated with SS, many companies have proliferated to manufacture SS equipment for commercial uses. In addition, three frequency bands, 902 - 928 MHz, 2400 - 2483.5 MHz and 5725 - 5850 MHz were made available to commercial SS users in 1983 by the U.S. Federal Communication Commission (FCC). These events have stimulated interest in SS, little known to most people until the early 1980s.

1.2 What is Spread Spectrum (SS)?

For a system to be classified as a SS, it must possess certain characteristics whose definition can be stated as follows[12]:

> "Spread spectrum is a means of transmission in which the signal occupies a bandwidth in excess of the minimum necessary to send the information; the band spread is accomplished by means of a code which is independent of the data, and a synchronized reception with the code at the receiver is used for despreading and subsequent data recovery."

According to this definition, it can be seen that not all modulation techniques that use a transmission bandwidth much greater than that required for data transmission can be classified as SS. Some examples of such schemes are FM, PCM and low rate coding.

1.2.1 Model of SS System

The constituents of a SS communication system can be seen from Fig.1.2.1. At the transmitter, the information bits are encoded and then modulated before passing through the channel. Once the transmitted signal is received, it is demodulated and decoded. The blocks described so far are the basic elements of a conventional digital communication system, regardless of the different modulation techniques(eg. PSK, FSK, etc.) and coding schemes(eg. block codes, cyclic codes, etc.) employed.

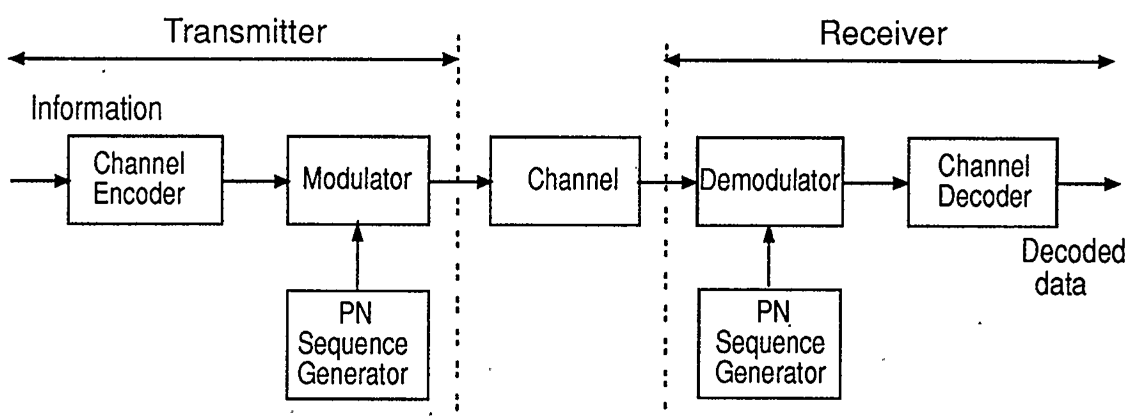

FIG.1.2.1 Model of SS communication system

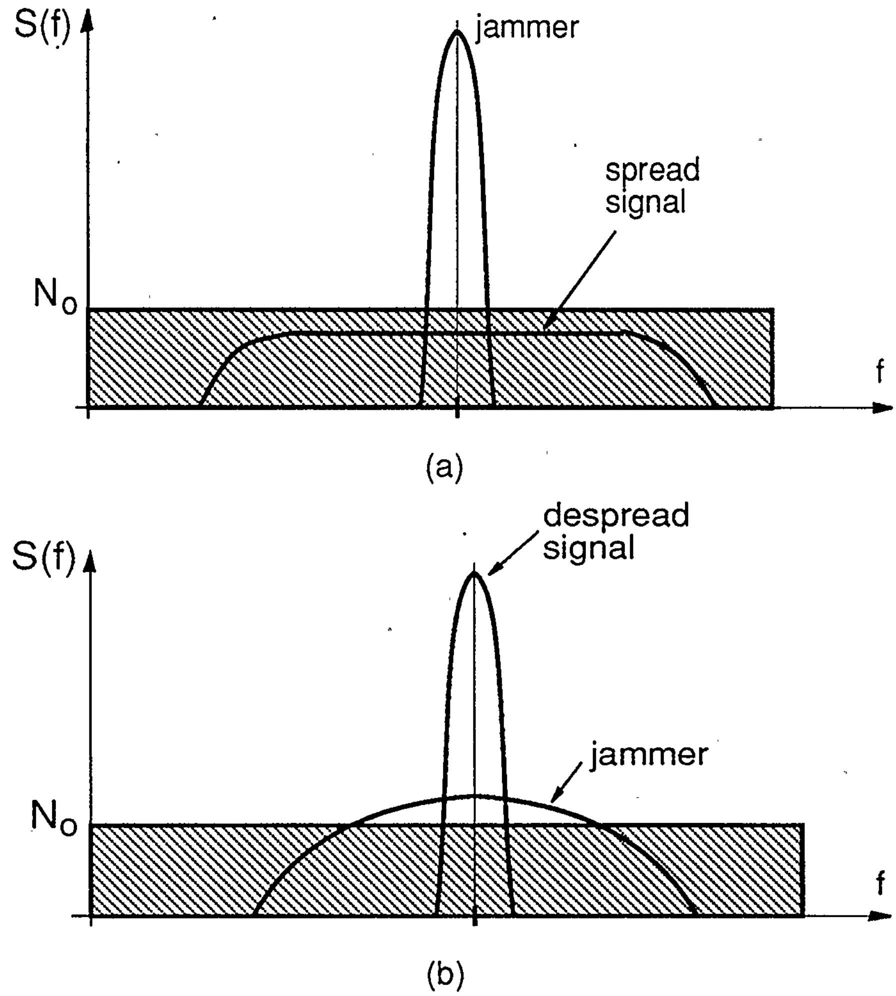

FIG.1.2.2 Power spectrum of original narrowband signal after (a) spreading and (b) despreading.

In the case of a SS system, besides all these elements, there are two identical pseudo-noise (PN) sequences or code generators. The generator output at the transmitter consisting of pseudo-random values of { ± 1 } multiples with the encoded data. This multiplication process is equivalent to correlation in the frequency domain, that is , spreading of the bandwidth of the narrowband signal, thereby minimizing the power per unit bandwidth (W/Hz) as depicted in

Fig.1.2.2. The extent of bandwidth spread is directly related to the length of the PN code generated. The received signal is then demodulated before despreading using a similar PN code generator to remove the random patterns from the signal. In effect, this collapses the wideband signal into a high-energy narrowband signal.

Synchronization of the PN sequences at the transmitter and the receiver is absolutely necessary for the proper decoding of the received signal. Achieving this level of synchronization problem is two-fold. Firstly, the receiver PN code or sequence phase has to be determined from the received signal - a process known as code acquisition. Secondly, the code phase must be continuously maintained, ie. continuous tracking of the code. This tracking process, using a delay-locked loop, is very similar to the phase-locked loop (PLL) which is for the generation of a carrier reference.

1.2.2 Types of SS Systems

The two basic forms of SS are the Frequency-Hopped (FH) and Direct Sequence (DS) systems. In a FH system, the allocated spectrum is divided into a large number of disjoint frequency slots and during transmission, the signal can occupy any one of these slots. The occupancy of the frequency slots, known as the hopping pattern, is determined pseudo-randomly using a PN generator. In contrast, the transmitted signal of a DS system is modulated directly with the pseudo-random signal of a PN generator. Additionally, DS signals occupy the entire bandwidth all the time as compared to the narrow bandwidth taken up by the FH signal during each hop.

Besides FH and DS system, there are other forms of SS systems. One form is Time Hopping (TH) which is analogous to FH. Here, the time interval (much larger than the reciprocal of the information rate) is divided into a large number of time slots and the transmitted signal hops pseudo-randomly in these slots. Other methods involve a combination of SS systems. A possible combination is a hybrid of DS/FH. With all these systems, only the DS-SS system will be discussed extensively.

1.3 Why spread?

In a SS system, the data occupies a large portion of the available spectrum. This seems contradictory because for decades, communication engineers have been trying to compress as much information as possible into an ever decreasing bandwidth. Obviously, there are reasons for spreading and depending upon the application, certain benefits can accrue. Some of the reasons are:

(1) jamming resistance
(2) interference resistance
(3) low probability of intercept (LPI)
(4) multiple access capability
(5) ranging capability
(6) combating multipath effects
(7) coexistence with non-spread signals.

Although SS seems to possess all the key ingredients of a good communication systems, it should be noted that it will not do everything. For instance, SS communication is not totally secure (ie., a persistent listener with the necessary equipment is capable of intercepting the message). However, to ensure security of communication, standard encryption algorithms can be applied which are now available commercially on integrated circuit chips.

1.4 Applications of SS

Traditionally, SS was used extensively by the military for secure and anti-jamming communications. Even today, the military is still a major player of SS as seen by the proliferation of satellite communications and the presence of the Joint Tactical Information Distribution System (JTIDS). This scene is slowly changing in face of the disintegration of the USSR and consequently, a reduction in defense spending. Presently, the military contractors and manufacturers of SS are exploring new venues to export their expertise to commercial applications.

With the attendance of about 1000 delegates representing most of the world's countries in Torremolinos, Spain for the World Administrative Radio Conference 1992 (WARC-92, Feb.3 to Mar.3) dealing with frequency allocation, SS is becoming an increasingly attractive alternative for the elimination of the cost and political considerations involved with the shuffling of the spectrum[13]. This is possible because SS allows new users to share the spectrum with existing users. To illustrate this point, FCC has authorized, in May 1991, a two year demonstration program for a SS Personal Communications Network (PCN) at two locations: Houston, Texas and Orlando, Florida. In both places, the 1.85 - 1.95 GHz band will be shared between SS PCNs and the local gas and electric utilities[14].

Although SS technology is a mature field, its applications in mobile telephony is a recent event. There is a potential that it can replace Time Division Multiple Access (TDMA) which is the current proposed technique for mobile cellular radio communications in North America. With its multiple access capability, it is expected to increase the number of users per cell over that of TDMA. In addition, SS allows asynchronous transmission and thus, could subsist with less stringent timing requirements. The idea of using SS to resolve multipath fading in a mobile environment is fairly new where it can be used to improve system performance.

There is a predicted growth in SS applications in in-building wireless communications network. The major cost of a conventional Local Area Network (LAN) is the hard wiring required to connect all the terminals. Furthermore, those wirings leave behind a confusing and unmanageable maze. If more terminals had to be added or the system reconfigured, the costs would escalate. This escalation in cost increases with the age and complexity of the building. However, with SS, the last 100m of the wiring costs could be eliminated and in addition, cellular technique can be applied to allow frequency reuse between different floors of a building. This would certainly improve the cost effectiveness and flexibility of the system.

Other possible scenarios where SS can be used are wireless alarms, police radar and covert communications. For wireless alarms, each floor of a building can have several sensors placed at different locations without wiring. These sensors would report to a central transceiver, which in turn is connected to a local police or fire station. Since each sensor possesses a unique code, it can indicate the location of trouble.

Among all these possible applications of SS, this thesis will only consider the use of the alternate system in a multi-user indoor wireless communications environment for the transmission of either data or voice where the available bandwidth is limited. Possible applications include the transmissions of public safety (example, fire alarms), utility and distress information from a central transceiver to sensors situated at different locations. In such applications, conventional SS techniques will be ineffective because of the large bandwidth requirement and the limited number of codes, consequently the number of sensors, that can be generated. If security is of concern, this system can be combined with coding, for example, using Hadamard codes or Gold codes.

1.5 Thesis Overview

In Chapter 2, the basic components of the conventional DS-SSMA with Gold codes, some of its problems and the solutions that have been applied are reviewed. An alternate, spectrally efficient system using waveshaping, its design and the constrained optimization procedure to obtain the optimized waveform will be described in Chapter 3. In addition, the theoretical Bit Error Rate (BER) for the prediction of the upper bound of the performance of the proposed system is presented. Simulation models, built using a software tool called Signal Processing Worksystem (SPW), along with its major components, functionality and implementation are presented in Chapter 4. Presented in Chapter 5 are the performances of the conventional and proposed system in AWGN, for both synchronous and asynchronous transmission mode, as well as in a Rayleigh multipath fading channel. Finally, some concluding remarks about the results and recommendations for improving the performances of the proposed system are discussed in Chapter 6.

CHAPTER 2

CONVENTIONAL DIRECT SEQUENCE SPREAD SPECTRUM MULTIPLE ACCESS(DS-SSMA)

2.1 Introduction

Spectrum is a valuable commodity. When mobile cellular radio communications was first proposed by Bell Laboratory between 1947 - 1970[15], there was considerable deliberation regarding spectrum allocation. This problem still persists today. During spring of 1992, thousands of delegates from around the world assembled in Spain for the WARC-92 to discuss frequency allocation. Evidently, efficient utilization of the radio spectrum is an international concern.

One technique that allows efficient sharing of spectrum is multiple access (MA) - a method which permits a number of users to access a common communication channel. The two common forms of MA techniques are Frequency Division Multiple Access (FDMA) and Time Division Multiple Access (TDMA). In FDMA, the allocated bandwidth is subdivided into a number of disjoint frequency bands where each band is allocated to a terminal with its own carrier frequency as shown in Fig.2.1.1. If these bands were demand assigned, then any idle band can be utilized whenever a user sends a request to transmit or receive. Otherwise, a user or terminal can only use its own allocated band! The maximum number of users that can be serviced is governed by the total available spectrum and the width of each band. A compromise needs to be made between the desire to accommodate as many users as possible and the concerns of practical filter realizations and cross-talk as the width of the band reduces. Despite these shortcomings, FDMA permits users to transmit or receive asynchronously thereby eliminating complex timing circuits.

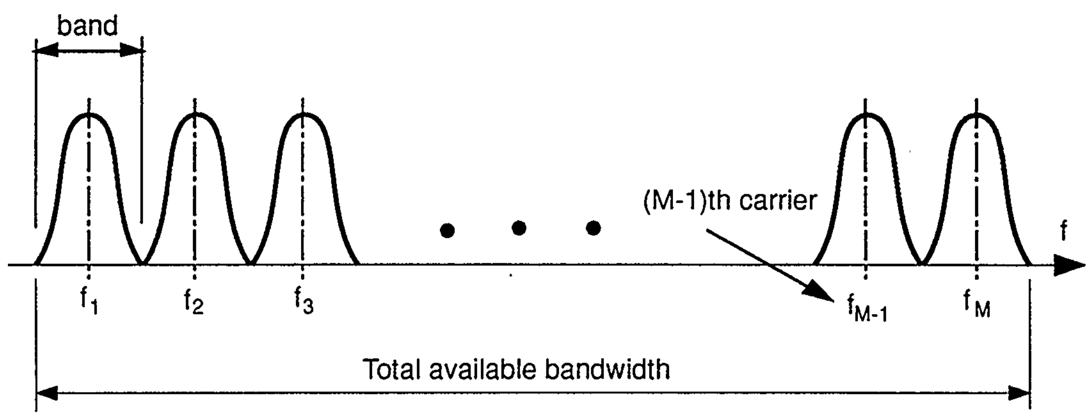

FIG.2.1.1 FDMA Format

The structure of a TDMA is shown in Fig.2.1.2. Here, a predetermined time frame is subdivided into a large number of time slots where the maximum number of terminals that can be served is determined by the size of the slot. Transmission by a terminal can only occur in its own allocated slot, utilizing the entire allocated bandwidth. Each slot is again divided into two components: data and preamble. Preamble contains all the information for the proper reception and decoding of the received signal. Even though it constitutes an overhead to the system, it is necessary for slot synchronization, carrier synchronization, bit timing and word synchronization. TDMA must deal with conflicts between serving the maximum number of terminals and reducing the complexity of the synchronization circuits.

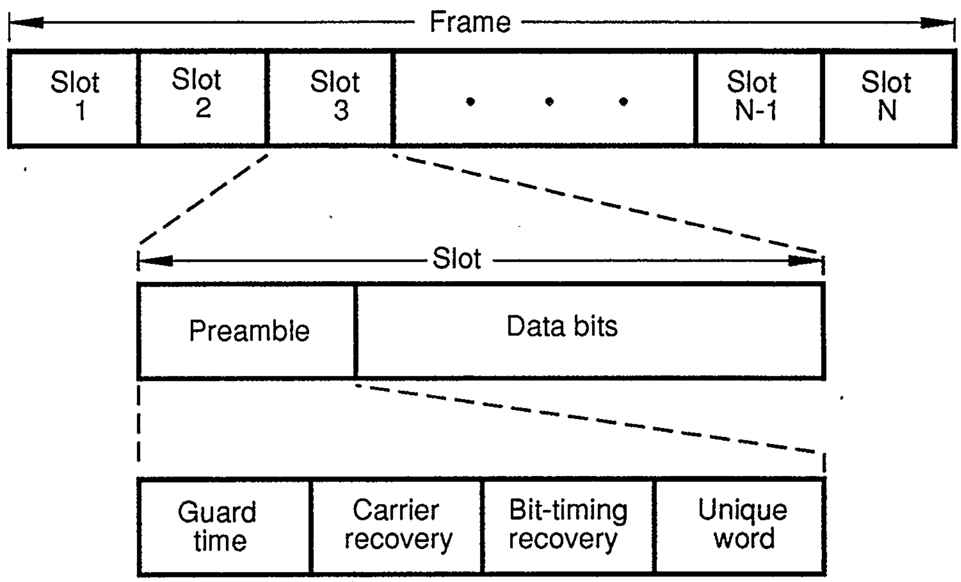

FIG.2.1.2 TDMA Format

Besides FDMA and TDMA techniques, there is a third form called Direct Sequence Spread Spectrum Multiple Access (DS-SSMA). This is a derivation of Code Division Multiple Access (CDMA) which is used extensively in military and navigational satellite communications. In Section 2.2, the conventional DS-SSMA system model and its constituents will be examined. Some of the problems associated with the conventional system will be highlighted in Section 2.3. Section 2.4 will introduce some of the measures that were applied to suppress the problems encountered with the conventional DS-SSMA system.

2.2 Model of DS-SSMA System

In DS-SSMA, there are more than one transmitter accessing one communication channel as illustrated in Fig.2.2.1. The kth receiver is only interested in the kth transmitter and all other transmitters are treated as interference.

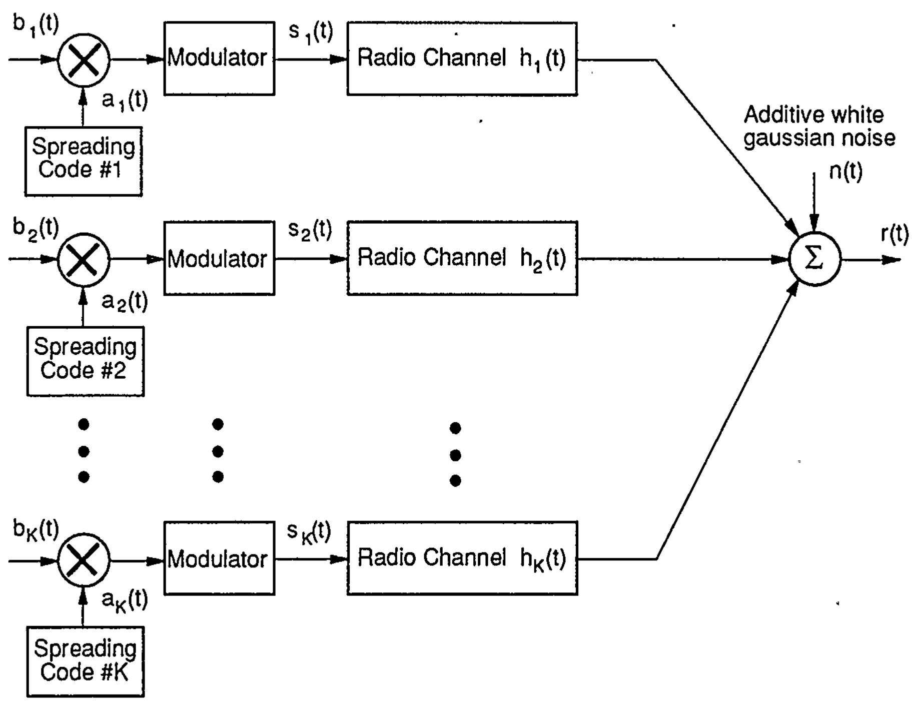

FIG.2.2.1(a) Block diagram of the transmitters of a conventional DS-SSMA system

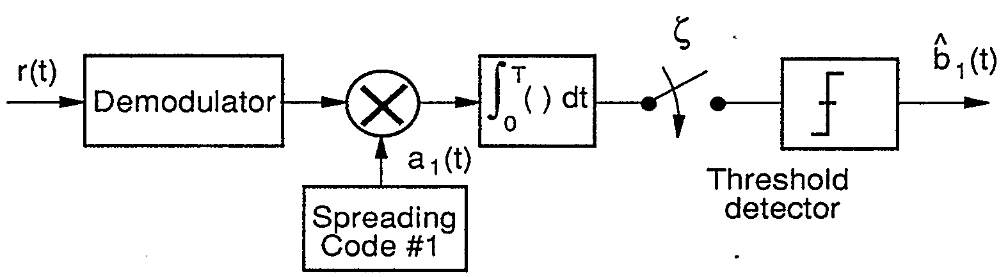

FIG.2.2.1(b) Block diagram of the receiver for user #1 of a conventional DS-SSMA system

This technique is completely different from TDMA or FDMA. Addressing of each transmitter is achieved through a unique periodic pseudo-random binary sequences. At the receiver, the desired transmission is extracted through correlation of the properly synchronized correct sequence. Transmission occurs over the entire bandwidth of the channel. With this system, the following advantages can be attained:

(a) asynchronous transmission
(b) low probability of intercept (LPI), anti-jamming
(c) narrowband interference rejection

2.2.1 Transmitter

The transmitter model of a K user DS-SSMA is shown in Fig.2.2.1(a). The complex information signal transmitted by the kth user is given by

$$b_k(t) = \sum_{j=-\infty}^{\infty} b_j^k P_T(t - jT); \qquad 1 \le k \le K \tag{2.1}$$

where b_j^k is the jth complex data symbol of the kth user, $P_T(t)$ is a rectangular waveform defined in [0,T), K is the number of users and T is the symbol duration. Each user is assigned a unique code waveform $a_k(t)$ which consists of a periodic sequence of rectangular pulses with values $\{\pm 1\}$ and duration T_c. Hence, the spreading code $a_k(t)$ can be defined as

$$a_k(t) = \sum_{l=0}^{N_c-1} a_l^k P_{T_c}(t - lT_c); \qquad 1 \le k \le K \tag{2.2}$$

where a_l^k is the l th chip of the k th user, N_c is the code period and $P_{T_c}(t)$ is a rectangular pulse in [0, T_c) with duration T_c and energy

$$\int_0^{T_c} P_{T_c}^2(t)\,dt = T_c. \tag{2.3}$$

Since $N_c = T/T_c$, there is one period of code sequence per data bit. The code period determines the performance improvement achievable and is often referred to as the processing gain[16] of the system.

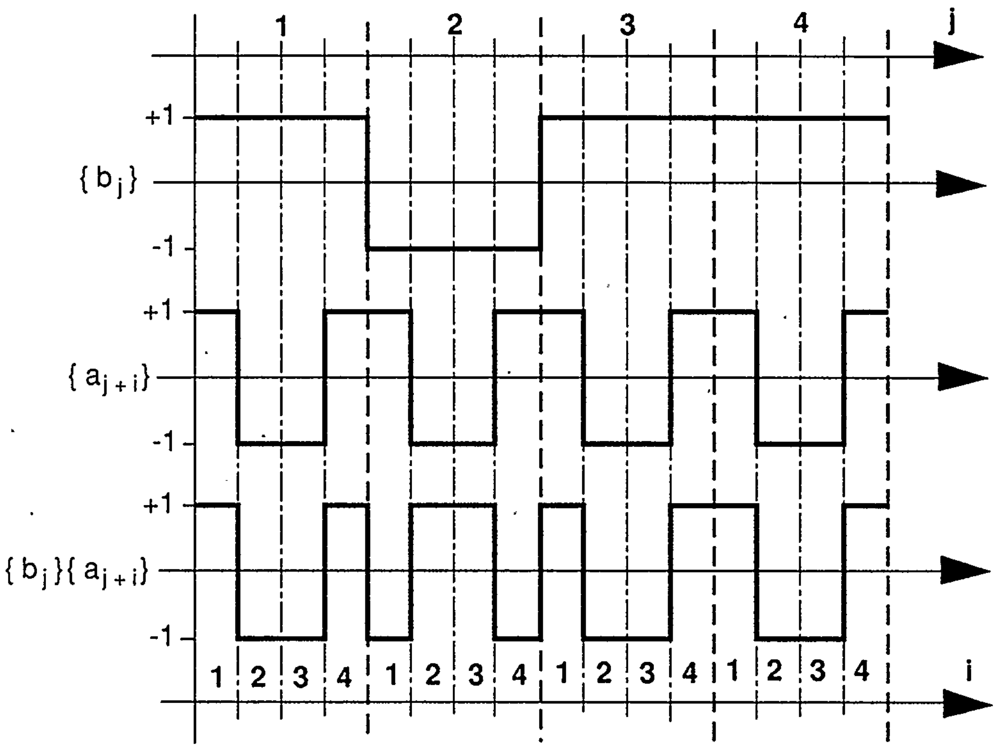

FIG.2.2.1.1 DS spreading process

Spreading of the bandwidth occurs when the information sequence { b_j }, j = 1, 2, ..., is added modulo-2 (exclusive-OR) to the pseudo-random code sequence { a_{j+i} }, i = 1, 2, ..., N_c , that is,

$$s_{j,i} = b_j \oplus a_{j+i} \tag{2.4}$$

where $\{s_{j,i}\}$ is the resulting sequence. This is equivalent to the multiplication of the two sequences together as illustrated in Fig. 2.2.1.1 for a code period N_c = 4. It should be noted that for a practical system , $N_c > 100$. After spreading, the sequence is modulated with a carrier. Thus the k th transmitted signal is given by

$$s_k(t) = \sqrt{\frac{2\,E_s}{T}}\, Re\left[\; a_k(t)\; b_k(t)\, e^{j(2\pi f_c t + \theta_k)}\right] \;;\quad 1 \le k \le K \tag{2.5}$$

where

$$E_s = \int_0^T s_k^2(t)\; dt \tag{2.6}$$

is the energy of the transmitted symbol, f_c is the common carrier frequency and θ_k is the random carrier phase distributed uniformly between 0 and 2π.

2.2.2 Pseudo-Noise (PN) Generator

The spreading codes that were employed in Fig.2.2.1 are produced from a binary shift register generator with values { ± 1 }. Ideally, this code would be an infinite sequence of equally likely random binary digits. However, this is not possible because of the infinite storage requirement at the transmitter and receiver. Hence, periodic pseudo-random codes (PN codes) with noise-like properties are often used.

One such PN code generator is shown in Fig.2.2.2.1[16]. The boxes in this figure represent the unit delays or shift registers while the circles with coefficients represent a connection if the coefficient is a "1" or no connection if the coefficient is a "0". Modulo-2 addition is performed by circles with "+". The output of the circuit is then fed back to certain stages of the shift registers. A convenient representation of the status of the feedback connections and the contents of the shift register is the use of a polynomial with octal notation. Hence, the output of a R-stage linear feedback shift register generator can be given by

$$b\ (D\ ) = \frac{a\ (D\ )}{g\ (D\ )} \tag{2.7}$$

where $a\ (D\ )$ is the initial loading of the stages of the shift registers consisting of "1"s and "0"s, except all "0"s, and $g\ (D\ )$ is the generator polynomial. Depending on the type of generator polynomial used, different codes would be generated.

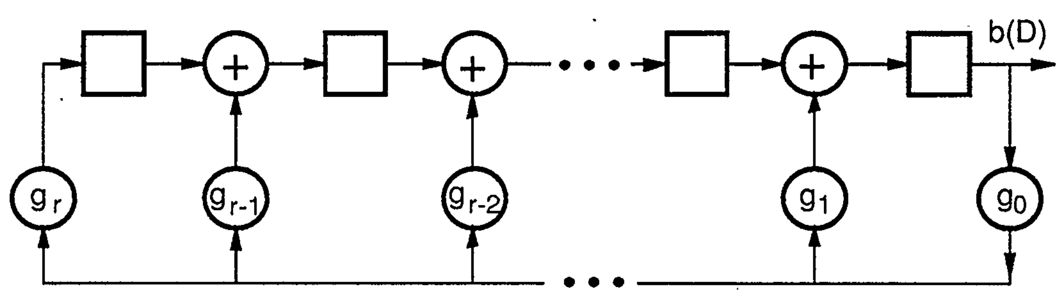

FIG.2.2.2.1 R-stage high speed linear feedback shift register generator

The binary maximal-length linear feedback shift register sequences, often referred to as the m-sequence, is one form of generator polynomial that has been studied extensively[17] because of its excellent periodic autocorrelation properties. This discrete periodic autocorrelation function of a code $b(D)$ can be defined by

$$\theta_b(k) = \frac{1}{N_c} \sum_{n=0}^{N_c - 1} a_n a_{n+k} \tag{2.8}$$

where N_c is the code period and a_n is the n th value of the code sequence with values $\{\pm 1\}$. For an m-sequence, the autocorrelation function is two-valued as illustrated in Fig.2.2.2.2 and is given by

$$\theta_b(k) = \begin{cases} 1.0 & k = l N_c \\ -\dfrac{1}{N_c} & k \neq l N_c \end{cases} \tag{2.9}$$

where l is any integer. The maximum possible period, $N_c = 2^n - 1$, obtainable with a n-stage linear feedback shift register is a characteristic of an m-sequence.

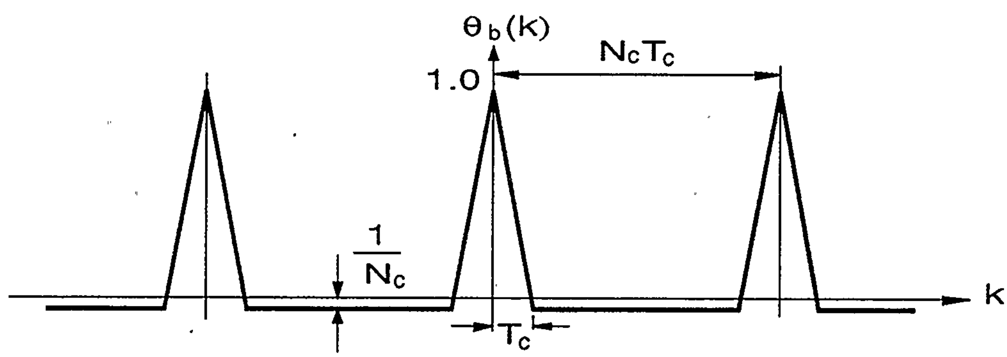

FIG.2.2.2.2 Autocorrelation function of a m-sequence

In SSMA, crosscorrelation properties are just as important as the autocorrelation properties of a sequence. Since each user is assigned a different code, then theoretically, all interfering users will not be despread at the receiver, hence causing little interference to any single user. The amount of interference generated is directly related to the crosscorrelation properties of the different spreading codes. The crosscorrelation function of two codes $b(D)$ and $b'(D)$ is given by

$$\theta_{bb'}(k) = \frac{1}{N_c} \sum_{n=0}^{N_c-1} a_n a'_{n+k} \, . \tag{2.10}$$

One set of codes, known as the Gold codes which was invented by the Magnavox Corporation in 1967, has a well-controlled crosscorrelation function. Unlike the crosscorrelation between pairs of m-sequences which may be many-valued, the crosscorrelation function of a pair of Gold codes is three-valued as given by

$$\begin{array}{l} -\frac{1}{N_c}\, t(n)\,, \\ -\frac{1}{N_c} \qquad\quad , \\ \frac{1}{N_c}\,[\,t(n)-2\,] \end{array} \tag{2.11}$$

where

$$t(n) = \begin{cases} 1 + 2^{(n+1)/2} & \text{for } n \text{ odd} \\ 1 + 2^{(n+2)/2} & \text{for } n \text{ even} \end{cases} .$$

Gold codes are generated using a pair of preferred m-sequences as illustrated in the shift register configuration of Fig.2.2.2.3. For $n = 7$, the output of the two m-sequence generators (with polynomials 211 and 217) are added modulo-2 to produce a particular class of Gold codes. The resulting $2n$-stage linear feedback shift register is not maximal-length since the period is given by $N_c = 2^n - 1$. Equivalently, the same Gold codes can be generated by taking the product of the two preferred m-sequences to give the polynomial 41567. The set of Gold codes and their initial loading conditions used throughout this thesis, often known as Auto-Optimal with Least Sidelobe Energy (AO/LSE), is extracted from [18] and summarized in Appendix A.

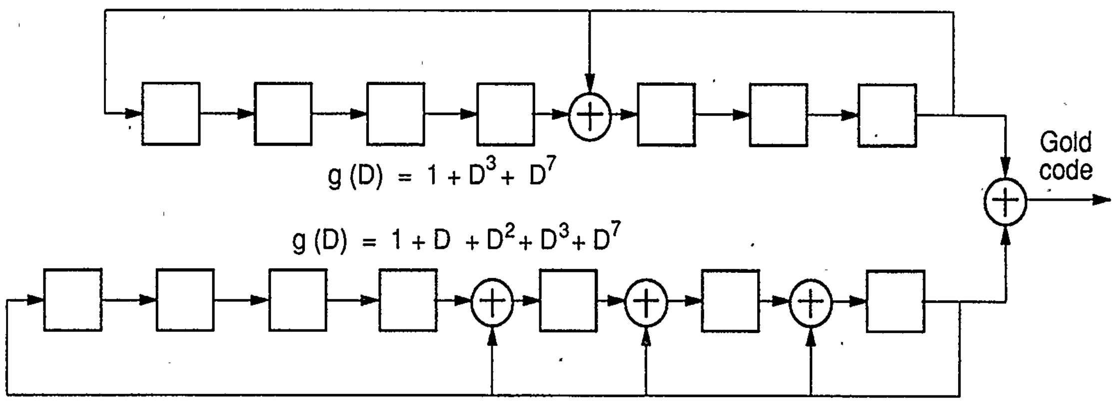

FIG.2.2.2.3 Gold Code generator with polynomial 41567

2.2.3 Indoor Wireless Channel

A received radio signal in an indoor channel is subjected to severe signal degradation because of propagation path loss, short term or multipath propagation effects and Doppler effects. Propagation path loss can be as large as 30 dB for a distance of one metre from the transmitter and a further 2 dB attenuation for each subsequent metre[19].

Multipath propagation arises when a receiver picks up several copies of a transmitted signal including the direct signal (if present), via a number of reflected paths. In fact, for an indoor environment, this may be the only mode of transmission in situations when the receiver is around a sharp corner as shown in Fig.2.2.3.1. Although it may seem that multipath propagation is sometimes beneficial, it does however cause two detrimental effects known as delay spread and multipath fading.

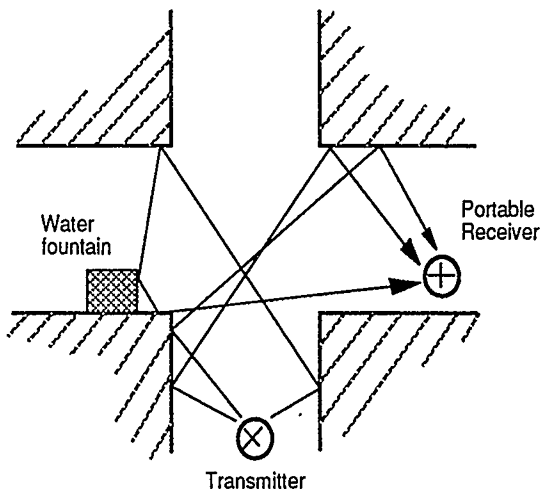

FIG.2.2.3.1 Multipath propagation

When a transmitter sends an impulse signal to the mobile unit, the received impulse signal would be spread because of the difference in arrival times of each reflected path. This phenomenon is known as delay spread[20] and is illustrated in Fig.2.2.3.2. From Fig.2.2.3.2(a), it can seen that the received discrete impulse responses are smeared to form a continuous signal with a delay spread of length Δ. To prevent intersymbol interference (ISI), the signaling rate of the transmitter is determined by the length (less than 1/Δ) of this delay spread. A typical delay envelope of an indoor channel is shown in Fig.2.2.3.2(b).

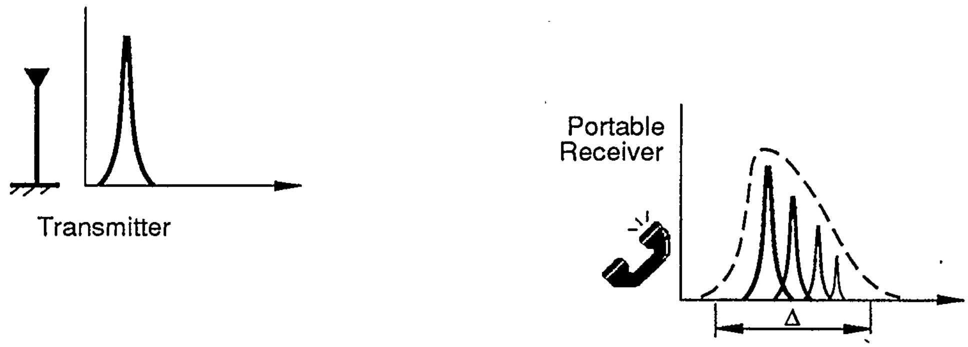

FIG.2.2.3.2(a) Illustration of delay spread

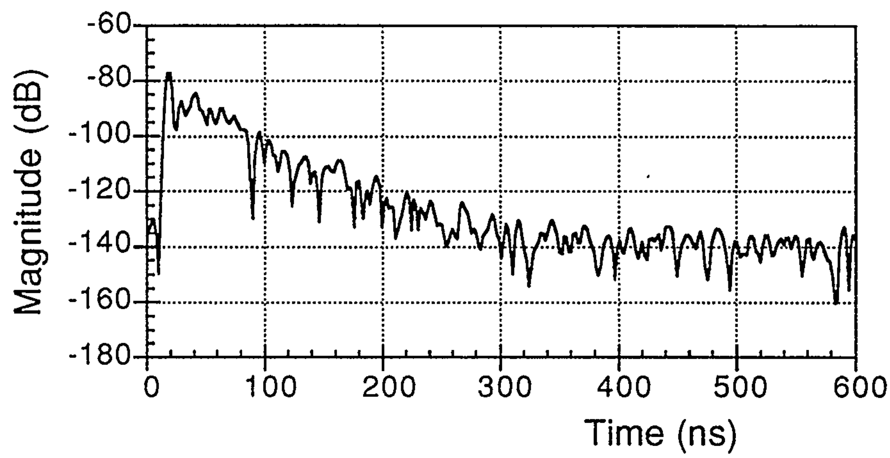

FIG.2.2.3.2(b) Typical delay spread of an indoor channel

The components due to multipath at the receiver can add up constructively to produce strong signals or destructively to produce weak signals. Destructive addition can cause severe fading of the received signal strength as shown in Fig.2.2.3.3. These fades can be as great as 30 dB and any transmission would be lost for the duration of the fade. This fading phenomenon can be described statistically by a Rayleigh distribution and hence is commonly known as Rayleigh fading.

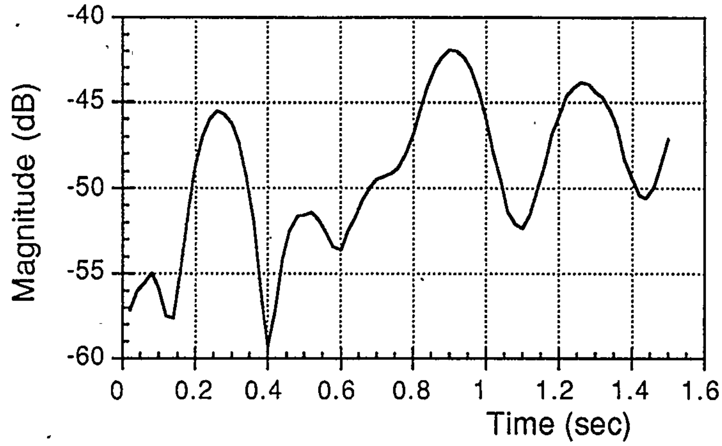

FIG.2.2.3.3 Typical received fading signal of an indoor channel with a mobile speed of 1 m/s

The Doppler effect causes a shift in the frequency of the received signal due to the movement of the mobile receiver relative to the transmitter. The speed of the mobile unit and its direction of travel with respect to the transmitter will determine the amount of Doppler shift. In an indoor channel, this effect is insignificant because of the relatively low speed of the mobile terminal.

Throughout this thesis, the indoor wireless channel will be modeled as a multipath Rayleigh fading channel. Since the bandwidth of a transmitted signal of a SSMA system is larger than the coherence bandwidth[20], defined as

$$(\Delta f)_c \approx \frac{1}{\Delta} \tag{2.12}$$

where Δ is the maximum delay spread of the multipath channel, the channel can be resolved into a number of discrete Rayleigh faded paths. The channel delay spread and the bandwidth expansion of the signal will determine the number of resolvable paths.

For the k th user, there are L Rayleigh distributed paths and each path is received at random time instants $t_{k,l}$, $l = 1, 2, ..., L$ where $t_{k,l}$ is assumed to be uniformly distributed over [0, T). To reduce ISI, the information rate is kept below the channel coherence bandwidth. Hence, the equivalent lowpass impulse response $h_k(t)$ of the channel for the k th user can be denoted as

$$h_k(t) = \sum_{l=1}^{L} \alpha_{k,l}\, \delta(t - t_{k,l})\, e^{j\phi_{k,l}} \tag{2.13}$$

where $\delta(t)$ is the Kronecker delta, $\alpha_{k,l}$ is a Rayleigh distributed path gain and $\phi_{k,l}$ is the uniformly distributed random path phase over [0, 2π). According to G. Turin[23], it will be assumed that all the parameters of all the paths are mutually uncorrelated over their specified range. Moreover, the parameters are assumed to be time invariant.

2.2.4 Receiver

The multipath channels cause all the transmitted signals to arrive at the desired receiver with unequal signal strength. Therefore, to simplify the analysis of the performance of the system, it is assumed that some form of average power control for the transmitters is in effect such that the received signal power from all users is the same. As depicted in Fig.2.2.1, the conventional SSMA receiver is of the single-user detection type, that is receiver #1 is only interested in the signal of transmitter #1 and ignores all other transmitted signals. Therefore, the received signal can be modeled as the summation of the convolution of the transmitted signals with their corresponding multipath channels. The received signal is given by

$$r(t) = \sqrt{\frac{2E_s}{T}}\, Re\left\{ \sum_{k=1}^{K} \sum_{l=1}^{L} \alpha_{k,l}\, a_k(t - t_{k,l} - \tau_k)\, b_k(t - t_{k,l} - \tau_k)\,\cdot \right.$$
$$\left. exp\left[j(2\pi f_c t + \theta_k + \phi_{k,l} - 2\pi f_c \tau_k - 2\pi f_c t_{k,l})\right]\right\} + n(t) \qquad (2.14)$$

where τ_k is the propagation time delay of the k'th signal and $n(t)$ is white Gaussian noise with a double-sided spectral density of $N_o/2$ (Watts/Hz). The time delays associated with each transmission arise because of the asynchronous transmission of the system and they are assumed to be mutually uncorrelated.

In the rest of this thesis, the receiver (denoted as #1) is assumed to be time synchronized to the first arrival of the desired signal. Therefore, the transmission delay of user #1 is ignored (ie., $\tau_1 = 0$). After demodulation of the received signal, receiver #1 decorrelates the desired signal with a code waveform given by equations (2.2) and (2.3) where in this case, $k = 1$. Therefore, the sampled signal can be expressed in terms of the equivalent complex lowpass output as

$$\xi = \sqrt{\frac{2E_s}{T}} \left\{ \alpha_{1,1} \int_0^T a_1^2(t)\, b_1(t)\, exp\left[j(\varphi_{1,1} + \Theta_1)\right] dt \right.$$
$$+ \sum_{l=2}^{L} \alpha_{1,l} \int_0^T a_1(t - t_{1,l})\, b_1(t - t_{1,l})\, a_1(t)\; exp\left[j(\varphi_{1,l} + \Theta_1\right] dt$$
$$+ \sum_{k=2}^{K} \sum_{l=1}^{L} \alpha_{k,l} \int_0^T a_k(t - t_{k,l} - \tau_k)\, b_k(t - t_{k,l} - \tau_k)\, a_1(t)\,\cdot$$
$$\left. exp\left[j(\varphi_{k,l} + \Theta_k)\right] dt \right\} + \eta \qquad (2.15)$$

where η is a sample of Gaussian noise with zero mean and variance $(N_o T/4)$, $\varphi_{k,l} = \phi_{k,l} - 2\pi f_c t_{k,l}$ and $\Theta_k = \theta_k - 2\pi f_c \tau_k$. Using equation (2.1), the above equation can be rewritten as

$$\begin{aligned}\xi = {} & \alpha_1 \sqrt{\frac{2E_s}{T}}\, b_0^1 \exp\left[j(\varphi_{1,1} + \Theta_1)\right] \\ & + \sqrt{\frac{2E_s}{T}} \sum_{l=2}^{L} \alpha_{1,l}\left[b_{-1}^1\, r_{1,1}(t_{1,l}) + b_0^1\, \hat{r}_{1,1}(t_{1,l})\right] \exp\left[j(\varphi_{1,l} + \Theta_1)\right] \\ & + \sqrt{\frac{2E_s}{T}} \sum_{k=2}^{K}\sum_{l=1}^{L} \alpha_{k,l}\left[b_{-1}^k\, r_{k,1}(t_{k,l} + \tau_k) + b_0^k\, \hat{r}_{k,1}(t_{k,l} + \tau_k)\right] \cdot \\ & \qquad \exp\left[j(\varphi_{k,l} + \Theta_k)\right] + \eta \;. \end{aligned} \tag{2.16}$$

Since all the transmitters operate with the same fixed data rate, only two symbol intervals can contribute to correlation as illustrated in Fig.2.2.4.1. This results in partial crosscorrelations between the receiver code $a_1(t)$ and the interfering codes which are defined by

$$r_{k,1}(\tau) = \int_0^{\tau} a_k(t-\tau)\, a_1(t)\, dt \tag{2.17}$$

and

$$\hat{r}_{k,1}(\tau) = \int_{\tau}^{T} a_k(t-\tau)\, a_1(t)\, dt \,. \tag{2.18}$$

The first term of equation (2.16) is valid provided that the receiver code is properly correlated with the received code sequence via the first Rayleigh faded path due to the delay lock assumption at the desired receiver. Upon close examination of equation (2.16), it can be seen that the desired signal at the output of the decorrelator is represented by the first term. Due to the different paths undertaken by the desired transmitter, replicas of the desired transmitted signal are generated and denoted by the second term. If a diversity scheme was employed, this term would be combined to the desired component to improve the decoding process. Since diversity is not the objective in this thesis, this second term is treated as self-interference. The simultaneous asynchronous transmissions of all active users of the system undergoing the different multipath propagation as the desired signal is indicated by the third term. Except for the desired signal, the second and third terms can be treated as additional noise components being added to the system which ultimately affects the symbol decision. However, if the channel was Gaussian and there was only one user, the second and third terms disappear, leaving only the desired signal and the sampled Gaussian noise.

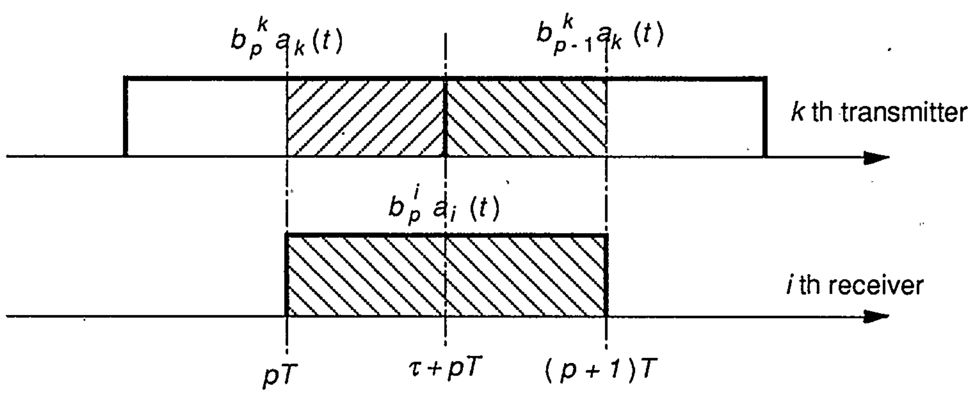

FIG.2.2.4.1 Symbol alignment for i th receiver

2.3 Problems with Conventional DS-SSMA

In the last section, we have described the application of SS to provide multiple access capability for asynchronous transmissions. However, the performance of such a system (using a simple correlator receiver) is severely limited by the crosscorrelation effects of the code sequences in a multipath Rayleigh fading indoor channel and the number of users that can be supported as shown by Kavehrad[22]. Two scenarios were examined in his work.

In case (1), the receiver terminal was stationary and hence, managed to acquire one strong non-Rayleigh faded path from the desired transmitter. Referring to equation (2.16), this situation is analogous to a dominant first term resulting in correctly decoded signals and negligible contributions from the second and third terms. This operational mode produced reasonable performance even when 10 asynchronous users were in the air resulting in only 2 dB degradation with average probability of error of 10^{-10}, at $SNR \approx 13$ dB, relative to the ideal situation (Gaussian channel). However, when there was no strong path, the performance degraded dramatically.

In case (2), the transmitter and receiver terminals were mobile and the signals arriving at the desired receiver via different paths were Rayleigh faded. Now, with only a single Rayleigh faded path in the absence of any multiple access interference, the performance was much worse than that for the first case due to a greater attenuation of the desired signal. The infamous 'near-far' problem arises when a second transmitter came on the air because the signal from the interfering transmitter was stronger at the receiver than the signal from the desired transmitter. The correlator receiver's inability to reduce the crosscorrelation effects between a pair of finite length spreading code sequences caused the interference (third term) to be significant. Kavehrad showed that a saturation in the error probability performance, in the absence of thermal noise, can be approximated by

$$\lim_{\gamma_o \to \infty} P_e \approx \frac{1}{6\, N_c} \tag{2.21}$$

where N_c is the code period and γ_o is the average signal-to-noise ratio (SNR) of the desired signal.

The same crosscorrelation effects between the interfering transmitted codes and the desired receiver code also limits the maximum number of users that can be accommodated without severe degradation in error probability performance. For the case of a set of Gold codes with $2n$ stages (where $n = 7$), the maximum number of codes (consequently, the number of users) with minimum sidelobe energy is limited to 10 [18].

2.4 Previous Work

We have seen in the last section that the principal shortcoming of a DS-SSMA system is the 'near-far' problem which arises from the conventional correlator receiver's inability to reduce the crosscorrelation effects between the desired receiver and the interfering transmitters. Although SSMA has no physical limitation in the number of user, its claim is subjective. In a scientific study, this limitation is measured in terms of the average probability of error performance and is determined by the extent of the 'near-far' effect.

Over the past few years, several researchers have devised schemes to combat or control this problem. One receiver proposed by Verdu[24] yields the optimum receiver. This is a centralized, multi-user maximum likelihood sequence detector consisting of a bank of single-user matched filters whose outputs are decoded using Viterbi algorithm. It demonstrated the ability to reduce the crosscorrelation effects resulting in a performance gain that is far superior to the conventional receiver. However, this optimum detector requires the knowledge of the signal waveforms, received energies and synchronization of the bit and phase of each active users. Such stringent requirements are very difficult to satisfy, especially in an indoor multipath fading environment. In addition, the complexity of the receiver increases exponentially with the number of users ($O(2^k)$).

An attempt to reduce the complexity of the optimum receiver resulted in a suboptimal linear detector[25] whose complexity increases linearly with the number of users. It was shown that the performance achieved with this detector approaches that of a optimum receiver. In contrast to the optimum receiver, no knowledge of the received energies is required. However, like the optimum detector, it requires the knowledge of the signature waveforms of the interfering users.

Similar to the optimum receiver is a detector based on a multi-user detection strategy using successive MA interference annihilation scheme[26]. This technique yields a performance that approaches the optimum receiver and in contrast to the optimum receiver, its complexity only varies linearly with the number of users. Again, this receiver requires the knowledge of the received energies. Although estimates can be used in the absence of exact information, studies[27] have shown that the performance deteriorates drastically if inaccurate estimates were used.

The multipath phenomenon is often treated as a nuisance which has to be suppressed. Instead, it should be seen as an opportunity for diversity reception to improve system performance. A rake receiver [23] is one such device. Signal from a transmitter arrives at a receiver via many paths and the rake receiver, consisting of a bank of correlators spanning a region of delay sufficiently wide to encompass all the significant echoes, synchronized the correlators to its respective delays and add the outputs to improve system performance. In a multiple access system, the receiver would only collect the energy of the desired transmitter and does not attempt to reduce the interference from other interfering users.

Although the single-user correlator receiver yields inferior performance, it appears to be most appropriate for many applications due to its simplicity. The motivation of this research is to develop a strategy to reduce the crosscorrelation effects (and hence the 'near-far' problem) hence optimizing or suboptimizing the conventional correlation receiver. This also implies an increase in the capacity of the system.

2.5 Summary

In this chapter, we have discussed the various MA techniques and their major differences. A model of the DS-SSMA system was presented and detailed descriptions of the transmitter, PN generator, indoor wireless channel and receiver were provided. Although the conventional DS-SSMA system offers several advantages over other MA schemes, it suffers from the 'near-far' problem and limited capacity. To improve this 'near-far' resistance, several solutions were briefly introduced. However, due to their complexities and large bandwidth requirement, alternative schemes should be investigated, which instigated this research.

CHAPTER 3

ALTERNATE SYSTEM

3.1 Introduction

In the previous chapter, we have identified some of the problems associated with the conventional DS-SSMA system that yield an inferior average error probability performance which in turn, limit the capacity of the system. To reduce or control these problems, several receivers were introduced. However, these receivers are impractical in an indoor wireless channel due to their large bandwidth requirements and complexities, which increases either exponentially or linearly with increasing number of users in the system.

The objective of this research is to develop an optimal or suboptimal receiver using waveshaping. This structure exploits the simplicity of the single-user correlation receiver which, would produce a far superior error probability performance than that of the conventional receiver. Details of the modified system are presented in Section 3.2. A theoretical average probability of error for the optimal receiver is shown in Section 3.3. In Section 3.4, the selection of the transmitter waveforms and the formulation of the optimization problem to obtain the receiver waveforms, based upon the reduction of the average error probability, are described. Finally, in Section 3.5, a plan to evaluate the system performance is presented.

3.2 Modified DS-SSMA system

The basic components of the modified system is very similar to the conventional system. Unlike the conventional system, each user of the modified system is assigned a pair of unique signature waveforms, one for the transmitter and the other for the receiver. These waveforms differ greatly from the rectangular waveforms. By having an additional degree of freedom (unique waveforms), the system has a potential for increasing the capacity of the system. Reduction or control of the 'near-far' effect is achieved through the optimal or suboptimal selection of the pair of unique waveforms.

3.2.1 Transmitter

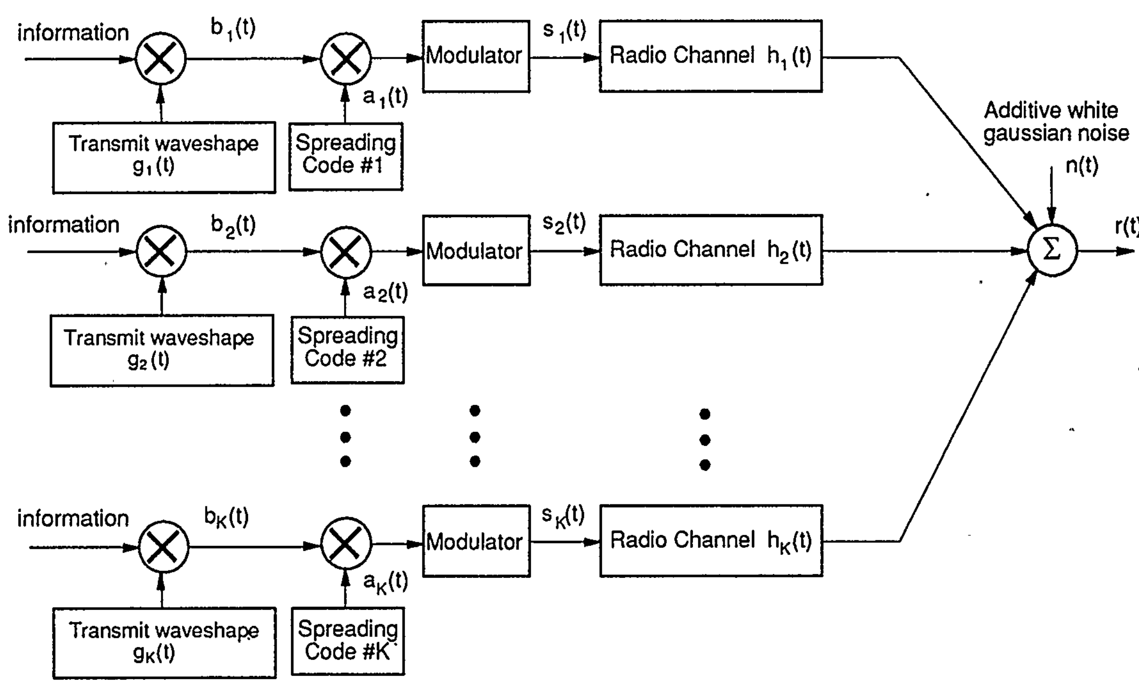

FIG.3.2.1.1 Transmitter of a modified DS-SSMA system

The transmitter of the modified DS-SSMA with waveshaping is shown in Fig.3.2.1.1. Comparing this model to that of Fig.2.2.1(a), the only difference is the block containing the unique transmit waveform. Hence, slight modification to equation (2.1) results in

$$b_k(t) = \sum_{j=-\infty}^{\infty} b_j^k g_k(t) \quad ; \qquad 1 \leq k \leq K \tag{3.1}$$

where b_j^k is the j th complex data symbol of the k th user, K is the number of users and $g_k(t)$ is the k th unique transmit waveform defined in [0,T). The energy of this waveform is denoted by

$$\int_0^T g_k^2(t)\, dt = T. \tag{3.2}$$

Since the remainder of the transmitter model remains the same, the unique spreading waveform $a_k(t)$ and the energy in equations (2.2) and (2.3) are valid and are restated here by

$$a_k(t) = \sum_{l=0}^{N_c-1} a_l^k P_{T_c}(t - lT_c)\,; \qquad 1 \leq k \leq K$$

and

$$\int_0^{T_c} P_{T_c}^2(t)\, dt = T_C\,,$$

respectively. It should be noted that the unique code sequence { a_l^k } of length N_c is not limited to the Gold codes and is optional, providing an additional level of security to the system. After carrier modulation, the k th transmitted signal can be given by equations (2.5) and (2.6) where the information signal $b_k(t)$ is replaced, respectively, by equations (3.1) and (3.2).

3.2.2 Multipath channel

To make a fair comparison between the error probability performance of the conventional and that of the modified DS-SSMA systems, the same multipath Rayleigh fading channel described in Section 2.2.3 will be used.

3.2.3 Receiver

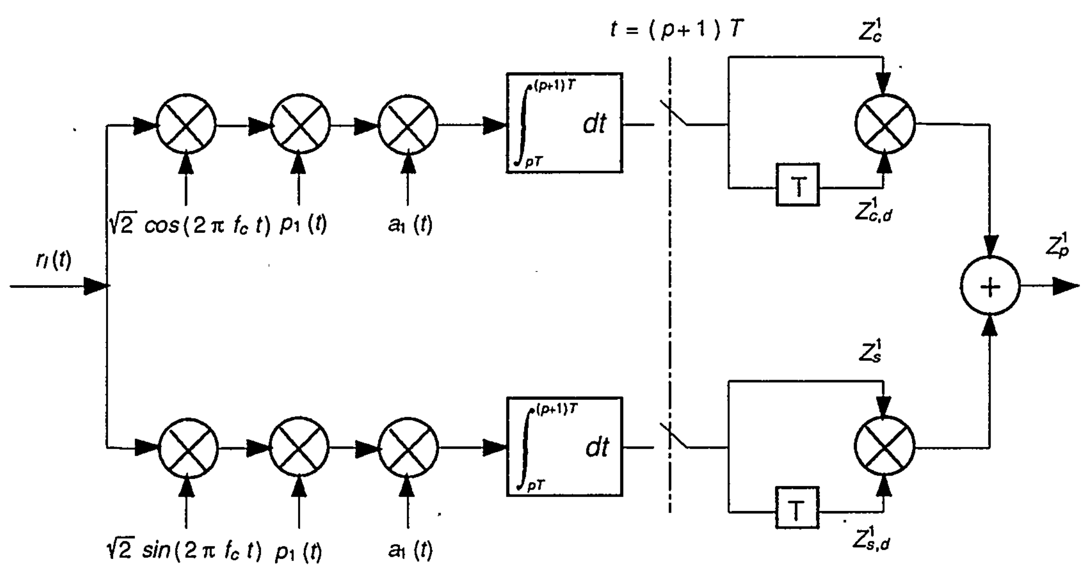

FIG.3.2.3.1 Noncoherent DQPSK receiver of the inphase branch for user #1

An optimum implementation of a noncoherent DQPSK of the inphase branch for the modified DS-SSMA system is shown in Fig.3.2.3.1. It should be noted that for DQPSK demodulation, an additional branch which is similar to the inphase branch would be required. For simplicity, only one branch will be discussed. In this analysis, it is assumed that the received signal power from all the users is the same and the receiver is of the single-user detection type, similar to that in Section 2.2.4. The only difference between this receiver and that of Fig.2.2.1(b) is the optimized receiver waveform $p_1(t)$ for receiver #1. At the sampling instant, the lowpass output of the integrator of the inphase branch for an asynchronous system can be expressed as

$$Z_c^1 = D_c^1 + \sqrt{\frac{2E_s}{T}}\, I_c^1 + \eta_c \tag{3.3}$$

where η_c is the sampled Gaussian noise with zero mean and variance

$$Var(\eta_c) = \frac{N_o}{2} \int_0^T p_1^2(t)\, dt\,. \tag{3.4}$$

The desired signal component D_c^1 is defined by

$$D_c^1 = \sqrt{\frac{2E_s}{T}}\, \alpha_{1,1}\, b_0^1 \int_0^T g_1(t)\, p_1(t) \cos\left(\varphi_{1,1} + \Theta_1\right) dt, \tag{3.5}$$

and because only two bit intervals can contribute to the correlation, as shown in Fig. 2.2.4.1, I_c^1 is given by

$$I_c^1 = \begin{cases} \sum\limits_{l=2}^{L} \alpha_{1,l}\left[b_{-1}^1\, r_{1,1}(\tau_{1,l}) + b_0^1\, \hat{r}_{1,1}(\tau_{1,l})\right] \cos\left(\varphi_{1,l} + \Theta_1\right), & k=1 \\ \sum\limits_{k=2}^{K} \sum\limits_{l=1}^{L} \alpha_{k,l}\left[b_{-1}^k\, r_{k,1}(\tau_{k,l}) + b_0^k\, \hat{r}_{k,1}(\tau_{k,l})\right] \cos\left(\varphi_{k,l} + \Theta_k\right), & k \neq 1 \end{cases}, \tag{3.6}$$

respectively. The phases $\varphi_{k,l}$ and Θ_k remain as those defined in Section 2.2.4 whereas the Rayleigh distributed gain $\alpha_{k,l}$ can be found in Section 2.2.3. Equation (3.5) implies that the receiver code at the desired receiver is delay-locked to the transmit code via the first Rayleigh faded path. The first term of equation (3.6) arises from the various delayed versions of the desired transmitter (#1), whereas the second term is caused by the multiple access interference from the k th transmitted signal. In addition, without loss of generality, the arguments of $r_{k,i}$ and $\hat{r}_{k,i}$ are considered to be modulo T since the symbol interval of interest is [0,T). Equivalently, the sampled lowpass output of the integrator for the quadrature branch Z_s^1 is obtained in a similar manner.

Similar to Fig.2.2.4.1, the bit alignment at the desired receiver between a pair of consecutive data (b_{-1}^k, b_0^k) produces two partial crosscorrelation functions. These are expressed by

$$r_{k,i}(\tau_{k,l}) = \int_0^{\tau_{k,l}} a_k(t-\tau_{k,l})\, a_i(t)\, g_k(t-\tau_{k,l})\, p_i(t)\, P_T(t+T-\tau_{k,l})\, dt \tag{3.7}$$

and

$$\hat{r}_{k,i}(\tau_{k,l}) = \int_{\tau_{k,l}}^{T} a_k(t-\tau_{k,l})\, a_i(t)\, g_k(t-\tau_{k,l})\, p_i(t)\, P_T(t-\tau_{k,l})\, dt. \tag{3.8}$$

The receiver waveform $p_1(t)$ is selected to optimally reduce the self and multiple access interferences, thereby improving the system performance. The output of the quadrature branch is defined by equations (3.3), (3.4), (3.5) and (3.6) where cos(.) are replaced by - sin(.). To obtain $Z_{c,d}^1$ and $Z_{s,d}^1$, replace b_0^k by b_1^1 in equation (3.5) and (b_{-1}^k, b_0^k) by (b_0^k, b_1^k) in equation (3.6). The detection statistic of the receiver for the inphase branch given by

$$Z_p^1 = Z_c^1 Z_{c,d}^1 + Z_s^1 Z_{s,d}^1 \quad , \tag{3.9}$$

is compared to a zero threshold to form an estimate $\hat{b}_0^1$ of the transmitted bit which must be differentially decoded. Similar expressions can be obtained for the quadrature arm since the optimum DQPSK demodulator is symmetrical.

3.3 Average probability of error analysis

If the inphase branch output statistics Z_c^1, $Z_{c,d}^1$, Z_s^1 and $Z_{s,d}^1$ of the DQPSK demodulator as described earlier are conditionally Gaussian random variables when conditioned on Θ_k, $\varphi_{k,l}$, $\alpha_{k,l}$ and $\tau_{k,l}$, it is known [28, 29] that the average probability of error P_e^1 for receiver #1 can be expressed as

$$P_e^1 = \frac{1}{2}\left(1 - \frac{\left(\tilde{\sigma}_c^1\right)^2}{\left(\sigma_c^1\right)^2}\right) exp\left(-\frac{\left(D_c^1\right)^2 + \left(D_s^1\right)^2}{2\left(\sigma_c^1\right)^2}\right) \tag{3.10}$$

where D_c^1 and D_s^1 are the desired terms of the inphase and quadrature components of the inphase branch, respectively. The second moments in equation (3.10) are defined by

$$\left(\sigma_c^1\right)^2 = Var\left\{Z_c^1\right\} \quad \text{and} \quad \left(\tilde{\sigma}_c^1\right)^2 = Cov\left\{Z_c^1, Z_{c,d}^1\right\}. \tag{3.11}$$

Often in the analysis of DS-SSMA system, it is assumed that the interference is approximately Gaussian. According to the central limit theorem, if there are sufficient independent random variables or a moderately large number of users, this assumption is appropriate. This is the case in a multiple access system with multipath propagation. Therefore, using the Gaussian approximation of the interference, the average probability of error can be expressed as [28, 29]

$$\overline{P}^{G}_{e,1} = \frac{1}{2}\left(1 - \frac{\tilde{v}_1}{v_1}\right) exp\left(- \frac{1}{2\, v_1}\right), \quad 1 \le i \le K. \tag{3.12}$$

The normalized second moments $\tilde{v}_1$ and v_1 are defined by

$$v_1 = \sum_{k=1}^{K} \sigma^2_{k,1} + 2\,\frac{Var\left\{N^1_c\right\}}{E_b} \tag{3.13}$$

and

$$\tilde{v}_1 = \sum_{k=1}^{K} \tilde{\sigma}^2_{k,1} \tag{3.14}$$

respectively, where

$$\sigma^2_{k,1} = Var\left\{ r_{k,1}\left(\tau_{k,1}\right)\right\} + Var\left\{ \hat{r}_{k,1}\left(\tau_{k,1}\right)\right\} \tag{3.15}$$

and

$$\tilde{\sigma}^2_{k,1} = Cov\left\{ r_{k,1}\left(\tau_{k,1}\right)\hat{r}_{k,1}\left(\tau_{k,1}\right) \right\}. \tag{3.16}$$

Taking into account the self interference of the desired transmitter caused by the multipath propagation, the second moments can be rewritten as

$$\sigma^2_{k,1} = \sigma^2_{1,1}\,(\textit{self interference}) + \underset{k\neq 1}{\sigma^{\,2}_{k,1}}\;(\textit{multiple access interference}) \tag{3.17}$$

and

$$\tilde{\sigma}^2_{k,1} = \tilde{\sigma}^2_{1,1}\,(\textit{self interference}) + \underset{k\neq 1}{\tilde{\sigma}^{\,2}_{k,1}}\;(\textit{multiple access interference}) \tag{3.18}$$

where they can be further expanded into

$$\begin{aligned} \sigma^2_{k,1} = {} & \sum_{l=2}^{L} \overline{\alpha^2_{1,l}} \left\{ E\left[r^2_{1,1}\left(\tau_{1,l}\right)\right] + E\left[\hat{r}^2_{1,1}\left(\tau_{1,l}\right)\right] \right\} \\ & + \sum_{k=2}^{K} \sum_{l=1}^{L} \overline{\alpha^2_{k,l}} \left\{ E\left[r^2_{k,1}\left(\tau_{k,l}\right)\right] + E\left[\hat{r}^2_{k,1}\left(\tau_{k,l}\right)\right] \right\} \end{aligned} \tag{3.19}$$

and

$$\begin{aligned} \tilde{\sigma}^2_{k,1} = {} & \sum_{l=2}^{L} \overline{\alpha^2_{1,l}} \left\{ E\left[r_{1,1}\left(\tau_{1,l}\right)\hat{r}_{1,1}\left(\tau_{1,l}\right)\right] \right\} \\ & + \sum_{k=2}^{K} \sum_{l=1}^{L} \overline{\alpha^2_{k,l}} \left\{ E\left[\, r_{k,1}\left(\tau_{k,l}\right)\hat{r}_{k,1}\left(\tau_{k,l}\right)\right] \right\}. \end{aligned} \tag{3.20}$$

The variance of the Rayleigh gain of the l th path of the k th transmitter is denoted by $\overline{\alpha^2_{k,l}}$. When the spreading code $a_k(t)$ is not used, the partial crosscorrelation functions are given by

$$r_{k,i}\left(\tau_{k,l}\right) = \int_0^{\tau_{k,l}} g_k\left(t-\tau_{k,l}\right)\, p_i(t)\; dt \tag{3.21}$$

and

$$\hat{r}_{k,i}(\tau_{k,l}) = \int_{\tau_{k,l}}^{T} g_k(t-\tau_{k,l})\; p_i(t)\; dt. \tag{3.22}$$

The exact expressions for the variance and covariance of the partial correlation functions are listed in Appendix C. Note that the reduction of the average error probability (equation 3.12) necessitates the minimization of the normalized second moment v_1 (equation 3.13), which is related to the partial crosscorrelation functions (equation 3.15).

3.4 Selection of signature waveforms

In the previous section, it was shown by equation (3.12) that the average probability of error performance can be improved if the desired receiver waveform was selected optimally such that it reduced the partial crosscorrelation effects caused by the multipath propagation and other interfering user. Description of the choice of the transmit and receiver waveforms and the formulation of the optimization process for the receiver are given in the following sections. Note that once the transmit waveforms are selected and the receiver waveforms have been optimized, they remain fixed and in particularly for the receiver, no provision is made for the optimization process to be adaptive.

3.4.1 Transmitter waveforms

The waveforms selected for each transmitter must satisfy three requirements:

(i) distinguishability,
(ii) normalized energy and
(iii) minimal bandwidth.

Note that criterion (i) is necessary to achieve multiple access capability and criterion (iii) is one of the key factors in the modified DS-SSMA system. One way to distinguish the various transmitters is to ensure that all the transmit waveshapes are orthogonal [28] and for all $k \neq i$ signals, the criterion is given by

$$\sum_{k=1}^{K} \int_0^T g_i(t)\, g_k(t)\; dt \;=\; \delta_{k,\,i}\,, \qquad i = 1, 2, \ldots, K \tag{3.23}$$

where $\delta_{k,i}$ is the Kronecker delta. The transmit waveform $g_k(t)$ is unique in [0, T) and has normalized energy defined by

$$\int_0^T g_k^2(t)\; dt \;=\; 1, \qquad 1 \leq k \leq K. \tag{3.24}$$

For mathematical tractability, the two most appropriate definitions for specifying bandwidth are (i) the second moment bandwidth and (ii) the minimum out-of-band bandwidth [28]. Definition (i) produces a waveform which is a linear combination of half-period sinusoids, whereas definition (ii) results in a linear combination of prolate spheroidal wavefunctions. These two classes of waveforms satisfy the above requirements provided a suitable orthonormal matrix is selected. To facilitate practical implementation of the transmitter, the optimal transmit waveshape (using either definitions) for the k th user based upon a linear combination of half-period sinusoids is used and is given by

$$g_k(t) = \sqrt{\frac{2}{MT}} \sum_{l=1}^{M} g_{k,l} \sin\left(\frac{\pi l t}{T}\right), \quad M = 2^n \,,\; 0 \le t \le T \tag{3.25}$$

where $g_{k,l}$ is the element in the k th column and l th row of a Hadamard matrix. An arbitrary large number of transmit waveforms can be used since $N = M = 2^n$, n = 1, 2, ... This recursive generation is given by

$$G_M = \begin{bmatrix} G_{M-1} & G_{M-1} \\ G_{M-1} & -G_{M-1} \end{bmatrix}, \quad M = 2^n, \; n = 1, 2, ... \tag{3.26}$$

where $G_o = 1$.

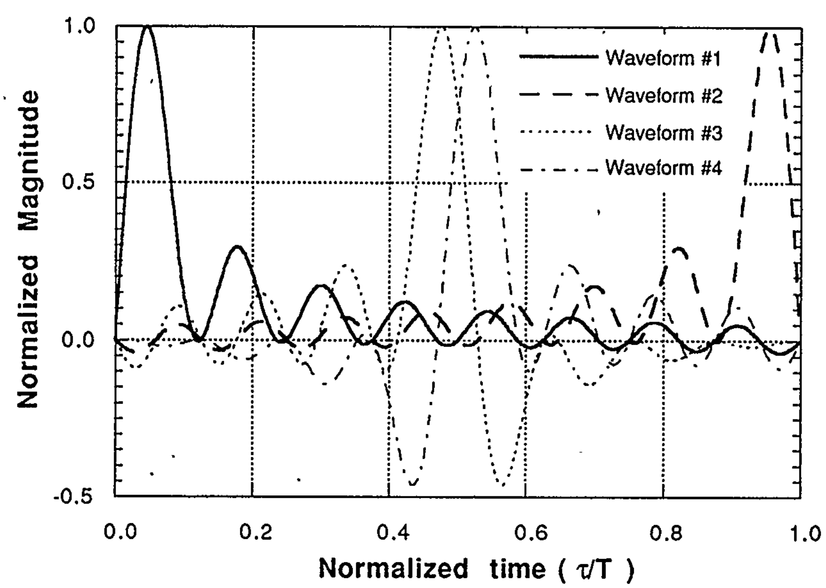

FIG.3.4.1.1 Transmit waveform characteristics for $M = 16$

A plot of some of the typical transmit waveforms for $M = 16$ is presented in Fig.3.4.1.1 where each user utilizing one of these waveforms has its own unique characteristics. It can be seen that waveforms #1 and #2 are similar in shape, the difference being one is the time delayed and phase reversed version of the other. The same is true for waveforms #3 and #4. This implies that pairs of waveforms will have identical spectral densities and therefore become non-distinguishable in the frequency domain. When subjected to multipath effects, one of the pair of similar waveforms may be time delayed and phase reversed such that they are now identical in the time domain. Because there is no distinction in both the frequency and time domains, they cannot be resolved. To avoid this, the transmit waveshapes are divided into two groups: one group of $M/2$ odd-numbered waveforms and the remaining $M/2$ even-numbered waveforms. Each group can be transmitted in different time slot or frequency band. Alternatively, the two groups can be combined by assigning two orthogonal codes.

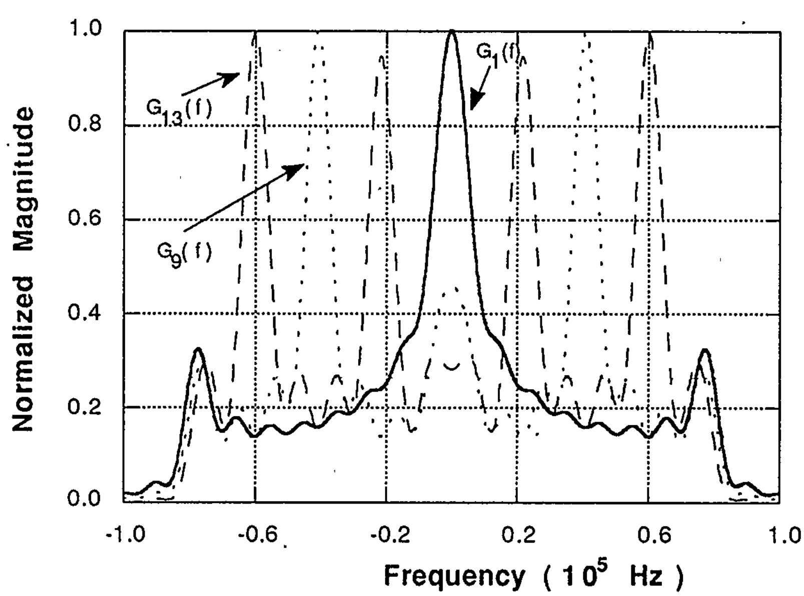

FIG.3.4.1.2 Transmit waveform spectra for $M = 16$

One advantage of using these transmit waveforms is that they are spectrally efficient, as illustrated in Fig.3.4.1.2 for R = 9600 bits/sec. The waveforms themselves also introduce some degree of spreading which can be given by $(M+3)/2T$ where $T=1/R$. Note that this expression gives the null-to-null spectral bandwidth. As the size of the Hadamard matrix increases (also increases the number of users), the spectral occupancy (normalized with respect to R) also increases, which can be seen from Fig.3.4.1.3.

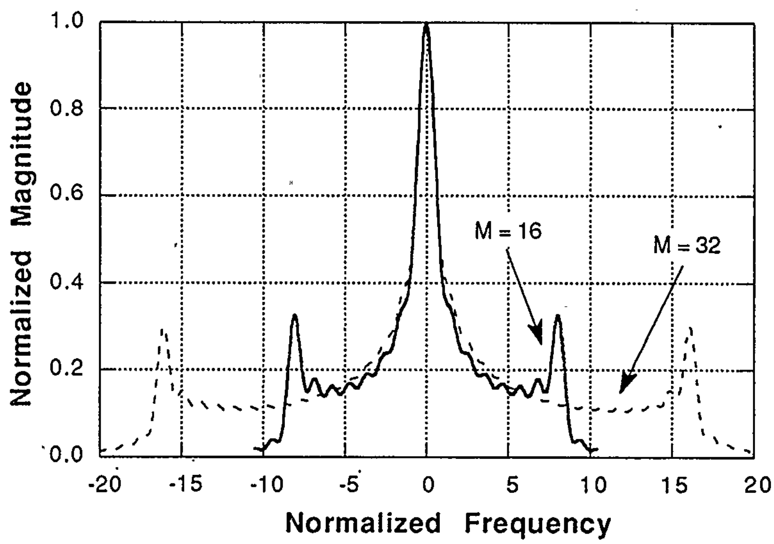

FIG.3.4.1.3 Effect of increasing the size of Hadamard matrix

3.4.2 Receiver waveforms

In a synchronous system, a receiver can extract the desired signal without interference from other transmitters because all the transmit waveforms and the codes retain their orthogonality. So the decorrelating waveform $p_i(t)$ at the receiver is identical to the transmit waveform $g_i(t)$. However, when transmission is asynchronous, orthogonality of all transmit waveforms can no longer be maintained due to the different propagation time delays at the desired receiver. Destruction of the orthogonality is further aggravated in a multipath environment.

To facilitate practical implementation, let the decorrelating waveform $p_i(t)$ be of the same form as the transmit waveform $g_k(t)$, that is,

$$p_i(t) = \sqrt{\frac{2}{MT}} \sum_{l=1}^{M} p_{i,l} \sin\left(\frac{\pi l t}{T}\right), \qquad M = 2^n \tag{3.27}$$

where $p_{i,l}$ is the element of the i th column and l th row of an (M x M) matrix. Recalling that the BER performance is improved by reducing the partial correlations, the problem of selecting $p_i(t)$ can be formulated as follows: given the number of users K and the transmit waveforms $g_k(t)$, the elements $p_{i,l}$ are selected as the solution to the constrained optimization problem:

$$\begin{aligned} &\textit{Minimize}: && \sum_k \left\{ E\left[r_{k,i}^2(\tau) \right] + E\left[\hat{r}_{k,i}^2(\tau) \right] \right\}, \\ &\textit{subjected to}: && \int_0^T g_i(t)\, p_i(t)\, dt = 1 \qquad \text{and} \\ & && -A \le p_{i,l} \le A \end{aligned} \tag{3.28}$$

for $1 \le i \le K$, $1 \le k \le K$ and $1 \le l \le M$. A is any arbitrary value selected so as to limit the optimization subspace. However, limiting the subspace results in a suboptimal solution. The above problem is convex[28] because the objective function is quadratic and the constraint functions are linear in $p_{i,l}$, respectively. Therefore, the existence of a solution is assured.

To obtain a suboptimal solution to this constrained nonlinear optimization problem we employ a commercial, numerical software package called GINO (**G**eneral **IN**teractive **O**ptimizer)[30]. This is an interactive version of GRG2 (Generalized Reduced Gradient). The GRG algorithm used was first developed by Jean Abadie in the late 1960's and later refined by Leon Lasdon of the University of Texas at Austin and Allen Waren of the Cleveland State University.

The optimization problem can be entered interactively or through a file interface and must be of the following form [31]:

$$\begin{aligned} &\textit{minimize or maximize :} && f_k(x) \\ &\textit{subject to :} && lb(n+i) \le f_i(x) \le ub(n+i) \\ & && \qquad i = 1, 2, \ldots\ldots, m \\ & && \qquad i \ne k \\ & && lb(i) \le x_i \le ub(i) \\ & && \qquad i = 1, 2, \ldots\ldots, n \end{aligned} \tag{3.29}$$

The objective function f_k ,which may be linear or nonlinear, is real-valued and x is a vector of n real-valued variables while the remaining (m -1) functions are either equality or inequality constraints. Bounds, both lower and upper, can be placed on the variables and are handled separately from the constraint functions.

Initially, the user supplies a program to compute the functions f_i which, in turn, is computed for the given vector x . In addition, the user also specifies the upper and lower bounds as well as other parameters such as the initial starting point and the maximum number of iterations required to reach an optimal solution within certain tolerances. Then GRG automatically calculates the first partial derivatives of each function f_i with respect to each x_i variable using either the forward or central finite difference approximation. Next, the program operates in two phases. Phase I optimization is started if the initial point supplied does not satisfy all f_i constraints. During this optimization, the Phase I objective function consists of an optional fraction of the true objective and the sum of the constraint violations and the process may terminate with either a feasible or infeasible solution status. An infeasible solution may suggest that the optimization is caught in the local minimum of the Phase I objective function or too large of the true objective was specified and that the problem may actually have feasible solutions. If this is the case, rerun the optimization with a different starting point or reduce the fraction of the true objective. Using the feasible solution of Phase I or a user supplied starting point which is feasible, Phase II attempts to optimize the true objective function. The optimization terminates if the necessary conditions for optimality, called the Karush-Kuhn-Tucker conditions are satisfied and produces a summarized output.

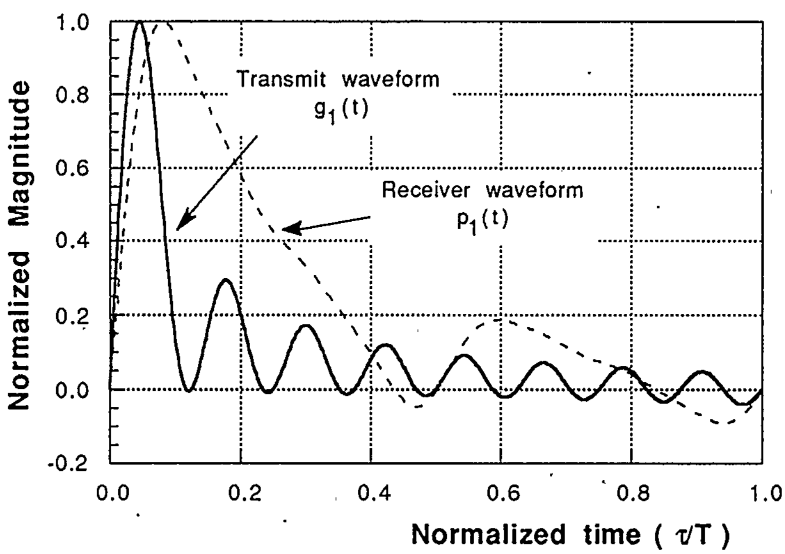

FIG.3.4.2.1 Optimized waveform characteristics for user #1

Listed in Tables B.2 and B.3 are the transmit and receiver codes, respectively. Although the optimized receiver column vector codes retain the same sign as their respective counterparts for the transmit codes, they are no longer orthogonal. This comes as no surprise because the receiver waveforms have been designed to counteract the multipath and crosscorrelations effects instead of maintaining orthogonality. It also implies that the optimized receiver waveform would differ from the transmit waveform as illustrated in Fig.3.4.2.1 for user #1.

3.5 Simulation strategy

Phase I of this project involves the building and verification of a computer model capable of simulating the digital signal transmission in a conventional, single-user Direct Sequence Spread Spectrum system as depicted in Fig. 2.2.1. The system performance, measured by the average bit error rate, is first determined and verified for an ideal Gaussian channel. This result is then used as a benchmark against which the performances of a conventional system (Gold codes) with multiple access in both a Gaussian and an indoor wireless channel, and that of the proposed system.

Phase II consists of building and simulating the modified system by simple replacement of the Gold codes with the Hadamard codes and inclusion of waveshaping. The receiver waveform is not optimized and is an exact replica of the desired transmit waveform. System performance is evaluated for a Gaussian and an indoor wireless channel with different propagation time delay and multipath delay spread.

Phase III is similar to Phase II except that the receiver waveform is optimized and different from the transmit waveform. System performances are evaluated under the same conditions as those of Phase II.

Phase IV involves the simulation of the modified system with waveshaping but no spreading codes. Similar to the system in Phase III, the receiver waveform is optimized and is different from the transmit waveform. The same conditions as those of Phase II are used to evaluate the system performances and in addition, the effect of the size of the Hadamard matrix on error performance are also examined.

The final phase entails the evaluation of the theoretical average probability of error performance for the modified system in Phase IV. These results are then compared with the simulations to verify its function as a prediction tool. It offers an easy and quick route for assessing the system performances under different operating conditions without undergoing the slow and computationally intensive simulation process.

3.6 Summary

An alternative to the DS-SSMA system which uses waveshaping instead of Gold codes is presented. A theoretical average error probability for the proposed system is shown. Details of the design of the transmit waveforms, formulation of the constrained optimization problem to obtain the receiver waveforms and the procedures required for the numerical optimizer, GINO, are described. Finally, a plan is drawn to compare the various systems performances.

CHAPTER 4

COMPUTER MODEL FOR SIMULATIONS

4.1 Introduction

In communications, it is very common to represent each component of a system design, from the transmitter to the receiver as functional block in a signal flow diagram format without being consumed by the details of the activities of each block. This allows an engineer to achieve dramatic time and productivity improvement in system design. One such software package chosen for the simulations of the various systems described in the previous chapter is the **Signal Processing WorkSystem™ (SPW™)** from Comdisco Systems Incorporated which runs on a DECstation 3100 with Ultrix Worksystem V4.1. It is a powerful integrated software package that provides all the tools required to graphically and interactively capture, simulate, test and implement a wide range of Digital Signal Processing (DSP) algorithms and communications systems designs.

4.2 SPW architecture

The architecture of SPW is shown in Fig.4.2.1. A system design is schematically captured using the Block Diagram Editor (BDE), one component of the SPW, as a hierarchical signal flow block diagram. The various blocks of the design can be selected and combined from the Function Block Library which contains an extensive set of DSP function blocks, the BOSS™ (Block Oriented System Simulator) Communications Library which includes 200 communications-oriented blocks or blocks created by the user whose function is determined by the written source code (C or FORTRAN). Simulation is run directly from BDE based on the block diagram and input signals, and no simulation codes need to be written.

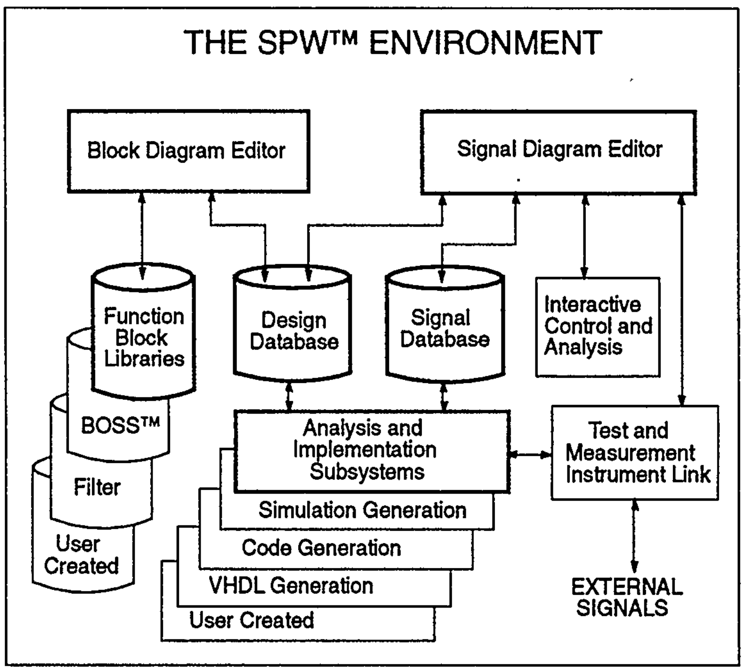

FIG.4.2.1 SPW architecture

The other major component of SPW is the Signal Display Editor (SDE) through which the visual results of the simulation is available. It supports multiple-window display of signals, provides powerful spectral analysis and correlation capabilities, contains extensive communications systems analysis methods and facilitates import/export of ASCII signal files between SPW format and other programs. Through the Test and Measurement Instrument Link, any outside signals (possibly real-time), via the GPIB (General Purpose Interface Board) can be used to test and simulate a system design. In addition, SPW provides several paths for hardware implementation which include the Code Generation System™ (CGS™) for chip programming (eg., TMS320C30), the VHDL (an IEEE standard language Std 1076 for designing and documenting digital systems) Design System™ (VDS™) for PCB (Printed Circuit Board) and ASIC (Applications Specific Integrated Circuit) implementations and the Hardware Design System™ (HDS™), a fixed point precision design aid for DSP and communications systems, ASICs, PCBs and new DSP chip architecture.

4.3 Simulation systems

In the signal flow diagram of BDE, each physical hardware block representation is translated into software routines that performs its specific discrete time signal processing function. The blocks can be multi-level deep, using blocks from the standard libraries or custom-coded for a specialized function. This modular approach to design makes BDE extremely flexible to changes in design and the multiple windows and graphical user interface makes it a very user friendly design tool.

Four basic simulation systems are built : (i) the conventional DS-SSMA system using the Gold codes, (ii) the proposed system using Hadamard codes and unoptimized waveshaping, (iii) the proposed system using Hadamard codes and sub-optimal waveshaping and finally (iv) the system with only sub-optimal waveshaping (ie., no spreading codes). The functional modules of each block are described in the next few sections.

4.3.1 Conventional DS-SSMA

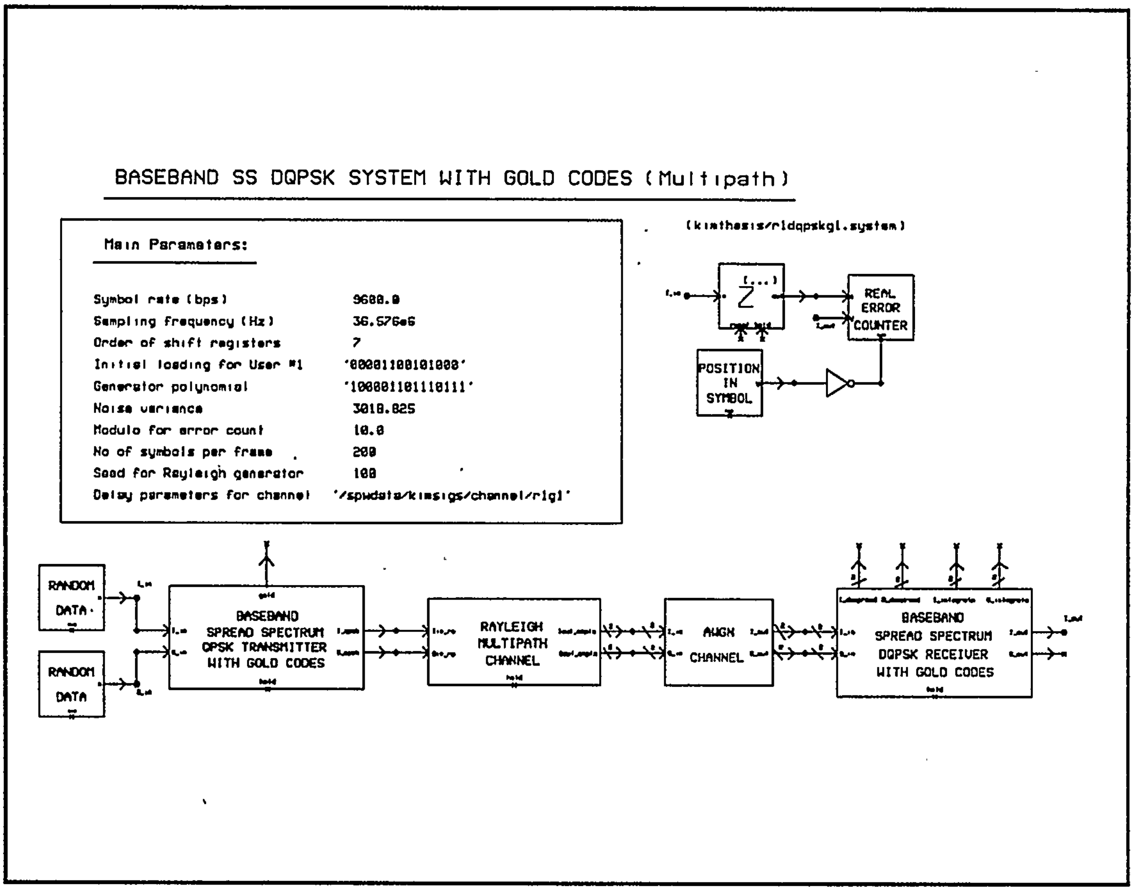

FIG.4.3.1.1 BDE block diagram of the conventional DS-SSMA system using Gold codes

The BDE implementation of the conventional DS-SSMA system using Gold codes can be seen from Fig.4.3.1.1. Following the direction of the signal flow diagram, the first block representing the data source transmits binary values {0 and 1} over the communication link which could be a wireline or an indoor radio environment. Required parameters are the symbol rate (bps) and the sampling frequency (samples/secs). Throughout this thesis, all systems are designed with the same data throughput and are fixed at R = 9600 bits/secs. The sampling frequency is chosen such that it can sample the chips sufficiently and not lose the smearing effect caused by the multipath delay spread without placing undue burden on the system processing. In addition, the output of the random data block is made equally likely.

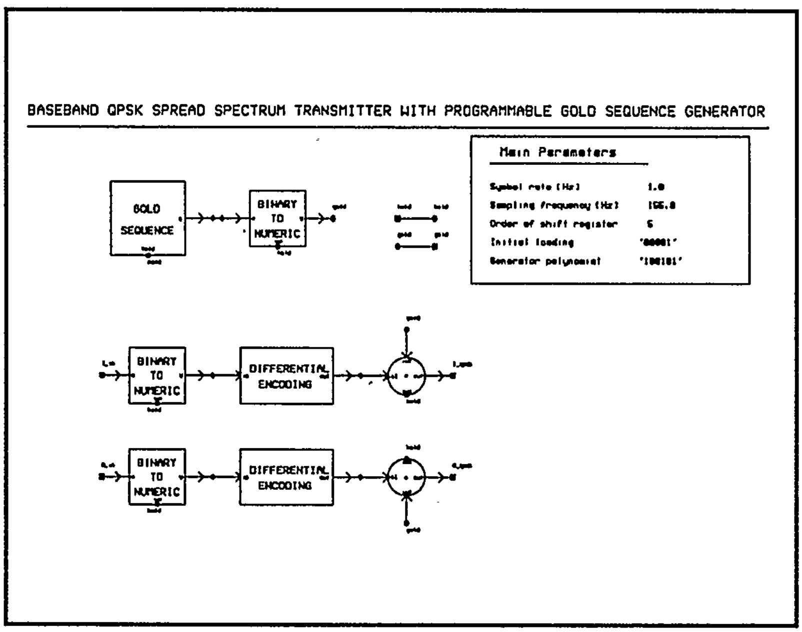

FIG.4.3.1.2 BDE expansion of the baseband equivalent of the differentially encoded QPSK modulator with Gold codes

The next block is the baseband equivalent of the differentially encoded QPSK modulator with Gold codes whose expanded version is shown in Fig.4.3.1.2. Data is fed through the inphase and quadrature branches of the modulator where the binary values are converted into { ± 1 } by the 'BINARY TO NUMERIC' block and then differentially encoded. This encoding block is custom-coded whose function is described by the written C source code. Similarly, the 'GOLD SEQUENCE' block is also user created and is based on the Gold code generator of Fig.2.2.2.3.

GOLD SEQUNECE GENERATOR BLOCK PARAMETERS

MAIN PARAMETERS:

Feed through type	ALL_FEED_THROUGH
Symbol rate (Hz)	1.0
Sampling frequency (Hz)	155.0
Order of shift register	5
Initial loading of shift register	'00001'
Generator polynomial	'100101'

FIG.4.3.1.3 BDE parameter screen for the custom-coded Gold Sequence block

As with any custom-coded block, it is possible to change its behavior by replacing the values of the parameters associated with that block as shown in

Fig.4.3.1.3. Instead of changing any parameter values at the bottom-most level, BDE allows the export of parameters from the lowest level to the top-most level. So if there was any changes at the system level, it is immediately reflected in all the blocks that contains the parameter. The Gold code generator is fully programmable and determined completely by the shift registers order, the generator polynomial and the initial loading conditions of the shift registers (taken from Appendix A). This system is designed to operate in a 1.5 MHz band with a sequence period $N_c = 127$ and R = 9600 bps where the occupied bandwidth is $BW_{ss} \approx N_c R = 1.22$ MHz. Note that in BDE, connectors (invisible wires) can be used to connect modules together and hence reduce confusion arising from the numerous interconnecting wires.

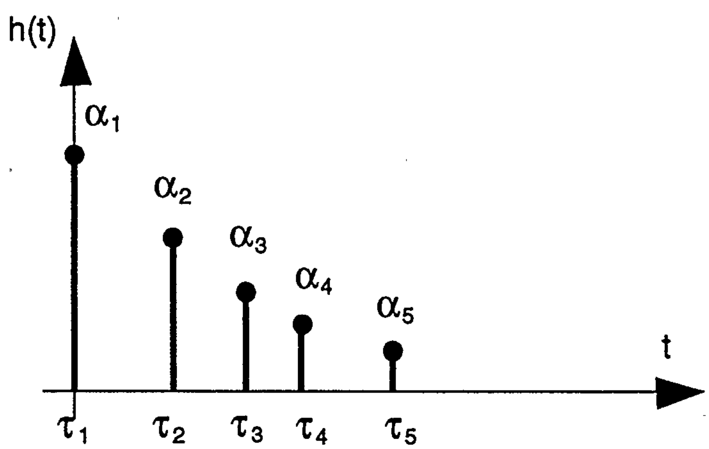

FIG.4.3.1.4 Model of the Rayleigh multipath channel

After modulation and spreading, the data passes through a 'RAYLEIGH MULTIPATH CHANNEL' block which is modeled as a filter having discrete impulses at specified delays as shown in Fig.4.3.1.4. In addition, except for the first impulse, each impulse has a phase associated with it. An impulse represents a path and the first path is assumed to have the strongest signal. The number of paths and the absolute locations of the impulses (secs) are user-specified through a file and chosen[19] to emulate a real indoor channel characteristics. Excess delay spread profiles of T/64 ($\approx$ 1600 nsecs) and T/256 ($\approx$ 410 nsecs) are selected and each profile has six equally spaced paths of intervals 320 nsecs and 82 nsecs, respectively. The magnitude of each path is Rayleigh distributed with $\sigma^2 = 1$ and except for the first path, subsequent paths are further attenuated by an exponential function. Assuming that data is transmitted in a burst mode, that is in a frame, a new set of magnitudes and phases is re-generated to simulate a dynamic channel. Several other options are available and can be seen from the parameter screen in Fig.4.3.1.5.

RAYLEIGH MULTIPATH CHANNEL BLOCK PARAMETERS

Main Parameters:

Feed_through type	ALL_FEED_THROUGH
Symbol rate (bps)	9600.0
Sampling frequency (Hz)	4876800.0
Delay spread input file	'/spw/spwdata/kimsigs/input1'
Number of symbols per frame	100
Seed value for random generator	10
Type of normalization:	'c'
'c' for constant	
'd' for decaying	
Single path in delay profile (y/n)	'n'
if yes, enter magnitude	0.8
I/O vectors	Iout_cmplx,Qout_cmplx
Iout_cmplx vector length	2
Qout_cmplx vector length	2

FIG.4.3.1.5 BDE parameter screen for the Rayleigh multipath channel block

The impulse response profile of a channel can be represented by a single-number called the rms delay spread τ_{rms}, defined as [32]

$$\tau_{rms} = \sqrt{\left[\frac{\sum_{k=0}^{L-1} \alpha_k^2 [\tau_k - \tau_0 - \bar{\tau}]^2}{\sum_{k=0}^{L-1} \alpha_k^2} \right]} \tag{4.1}$$

where the mean excess delay $\bar{\tau}$ is given by

$$\bar{\tau} = \frac{\sum_{k=0}^{L-1} \alpha_k^2 [\tau_k - \tau_0]}{\sum_{k=0}^{L-1} \alpha_k^2}. \tag{4.2}$$

It provides a measure of the multipath delay spread and indicates the potential for intersymbol interference[33, 34].

White Gaussian noise whose power is controlled by the variance is added to the output of the channel before entering the receiver. An expanded view of the receiver block is shown in Fig.4.3.1.6. The receiver demodulator implementation is based on the optimum demodulator described in Section 3.2.3. The two branches of the demodulator are identical: one for the inphase and the other for the quadrature component. Received signal is first despread with the code sequences having the same initial loading condition and generator polynomial as that of the desired transmitter. Correlation and sampling are achieved with the 'INTEGRATE & DUMP' block. A train of impulses, with an interval of T, generated from the delta and 'POSITION IN SYMBOL' blocks provides the bit timing information to the 'reset' input of the 'INTEGRATE & DUMP' block. Other timing circuits include 'tdl_dly' and 'start' which delays processing for a certain period and triggers connected blocks when it is active, respectively. The outputs of the numerous 'MAKE COMPLEX' blocks can be connected to the 'SIGNAL SINK' blocks where the simulation results can be viewed in SDE for diagnostics and analysis purposes.

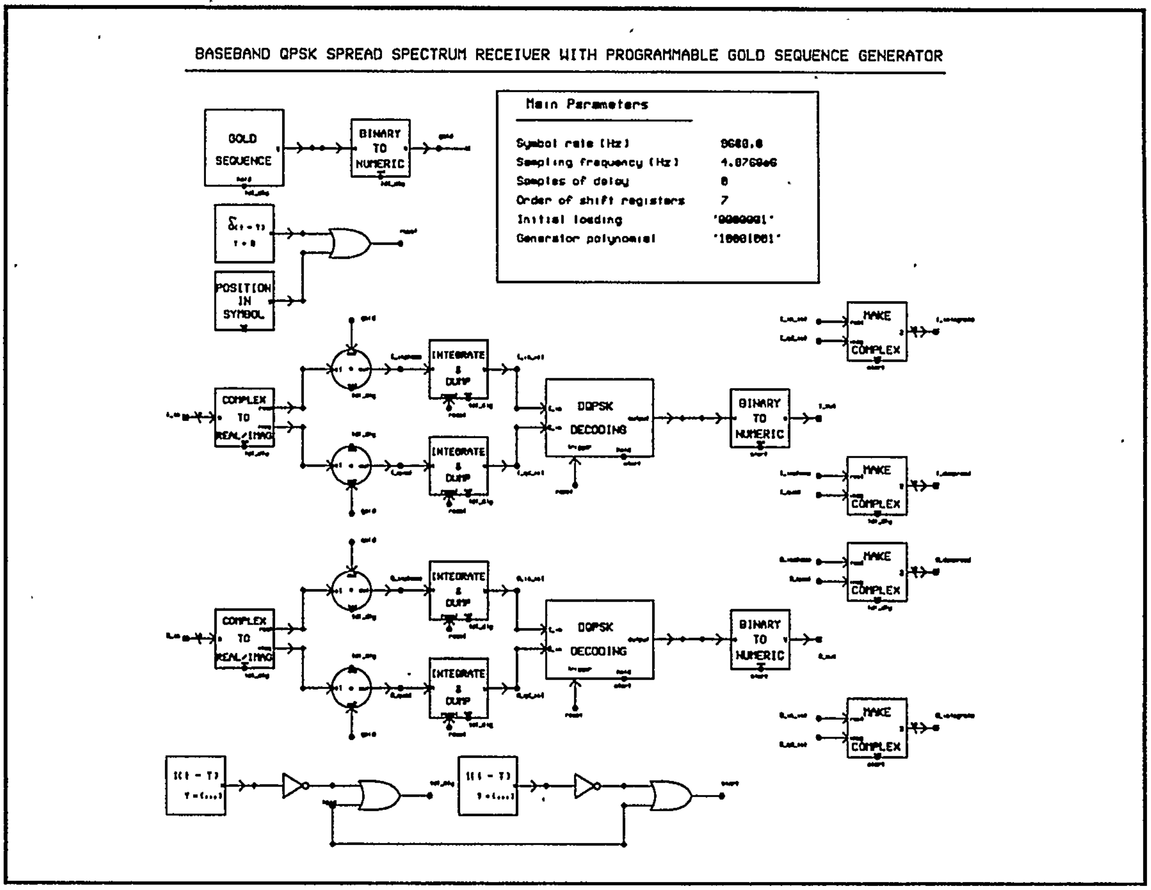

FIG.4.3.1.6 BDE expanded view of the baseband equivalent of the Spread Spectrum DQPSK receiver with Gold codes

One commonly used indicator of the performance of a system is the Bit Error Rate (BER) which is defined as

$$P_e = \frac{\text{Number of bits that are in error}}{\text{Total number of transmitted bits}} . \qquad (4.3)$$

This function is accomplished by the 'REAL ERROR COUNTER' block in Fig.4.3.1.1 which compares the output decisions of one branch of the receiver with the transmitted data of the same branch and counts the data that are in error. Before any comparison can be made, the transmitted data has to be delayed by an appropriate amount. A parameter in the block permits the results to be printed to a file in SPW once every *X* number of transmitted bits and updates the error probability. For a multiple access system, additional user can be easily accommodated using the same data source and transmitter blocks described earlier but each being assigned with a different loading condition.

4.3.2 Hadamard codes and unoptimized waveshaping

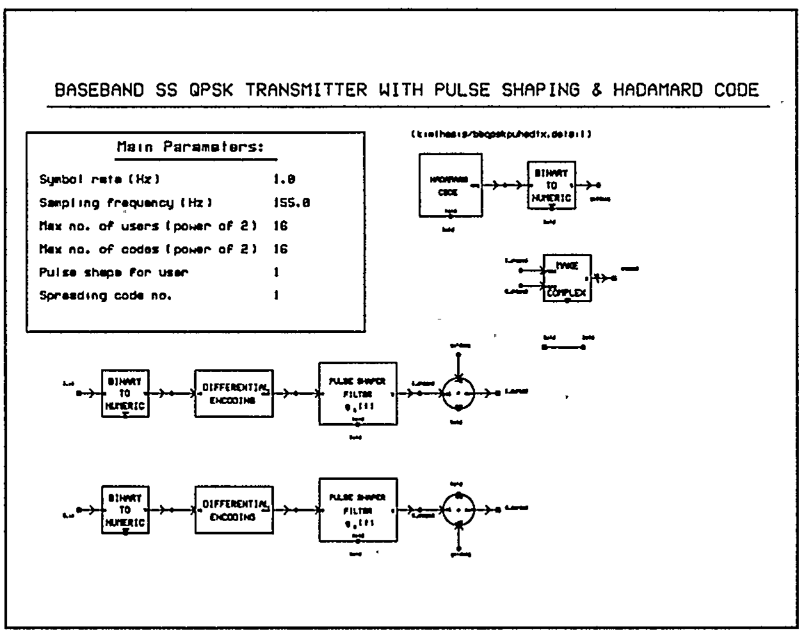

FIG.4.3.2.1 BDE expanded view of the baseband equivalent QPSK transmitter with pulse shaping and Hadamard codes

To build this new system is easy and straightforward. It involves replacement of the transmitter and receiver blocks in Fig.4.3.1.1 with a new transmitter and receiver block, respectively. Parameters associated with the replaced blocks are substituted with a completely new set. The remaining components consisting of the channels, error count and data source remain unchanged. An expanded view of the new transmitter block is shown in Fig.4.3.2.1. Instead of using Gold sequences to spread the encoded data as described in Section 4.3.2, the data is first spread using the transmit waveform and then followed by the Hadamard codes. These blocks are custom-coded and specified by the size and the column number of the Hadamard matrix. Spectral occupancy of the system is given by

$$BW_{SH} \approx \frac{N(M+3)R}{2} \tag{4.4}$$

where M and N are the maximum size of the Hadamard codes and the transmit waveforms, respectively. For $N=16$ and $M=16$, the system bandwidth $BW_{SH} \approx 1.46$ MHz is within the allocated frequency band. With this system, there is a potential for increasing the maximum number of users over the conventional DS-SSMA system. The transmit waveforms are divided into $M/2$ odd-numbered group and $M/2$ even-numbered group where each group of waveforms is assigned to a unique Hadamard code $c_i(t)$, $i = 1, 2, ..., N$. Therefore, the total possible number of users is $K = MN = 256$.

The exploded view of the new receiver block is shown in Fig.4.3.2.2. Comparing with the receiver block of Fig.4.3.1.6, the difference is that the received data is first despread with the Hadamard codes and then followed by the unoptimized waveform which is an exact replica of the transmit waveform. All the timing circuits, optimum demodulators and provisions for signal analysis and diagnostics remain unchanged.

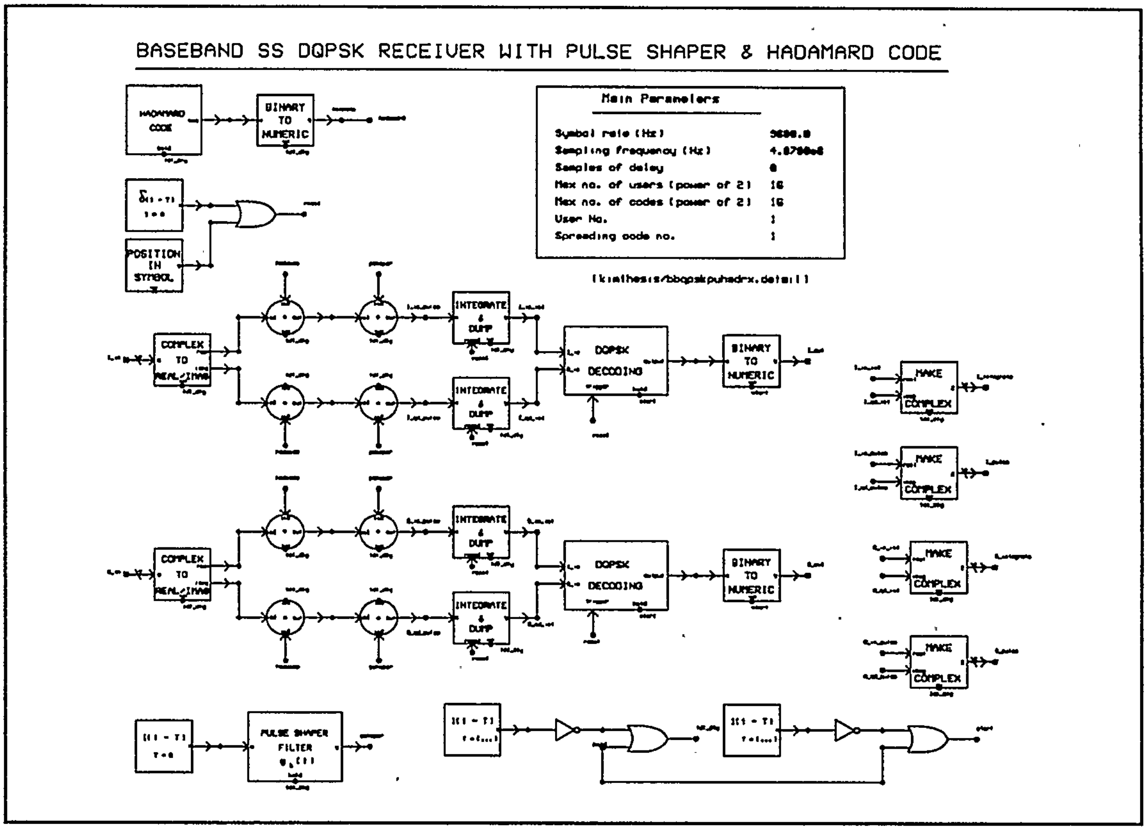

FIG.4.3.2.2 BDE expanded view of the baseband equivalent DQPSK receiver with unoptimized waveshaping and Hadamard codes

4.3.3 Hadamard codes and sub-optimal waveshaping

The transmitter block of this system remains unchanged whereas the receiver block requires some minor modification. From Fig.4.3.3.1, the 'PULSE SHAPER FILTER' block has been replaced by the 'RX PULSE SHAPER FILTER' block. Functionally, the two blocks are identical. However, this new block produces a new despreading waveform that is different from the transmit waveform. It requires a code, obtained from the solution to the constrained optimization problem, which is specified as a file with its appropriate path to be operable. The codes for different optimized receiver waveform are listed in Table B.3. The remaining parameters are identical to the old block and are shown in Fig.4.3.3.2.

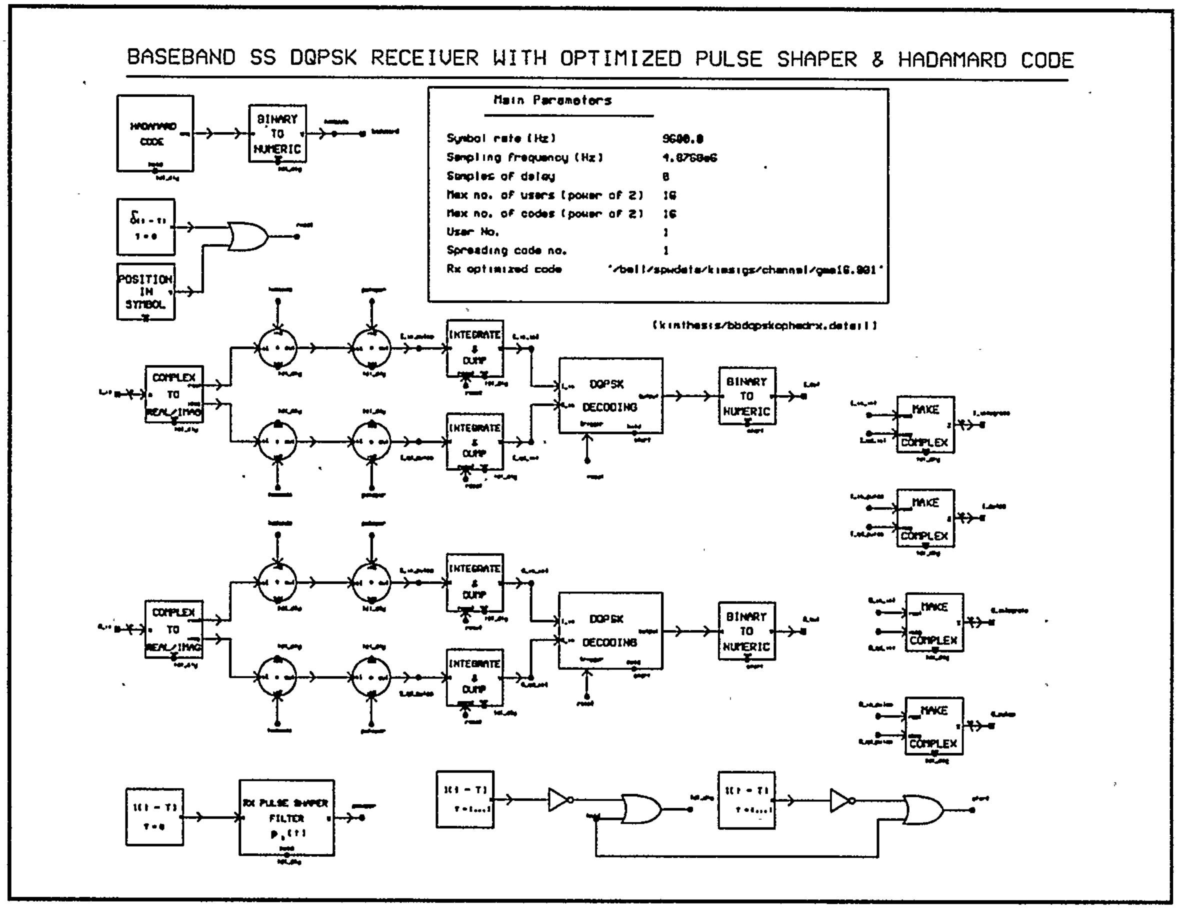

FIG.4.3.3.1 BDE expanded view of the baseband equivalent DQPSK receiver with sub-optimal waveshaping and Hadamard codes

RX PULSE SHAPER FILTER BLOCK PARAMETERS

MAIN PARAMETERS:

Feed through type	ALL_FEED_THROUGH
Sampling frequency (Hz)	3.5e9
Symbol rate (Hz)	9600.0
Max no. of users (power of 2)	16
Desired user ocde filename	'/spwdata/kimsigs/code/p1'
First input sample time (sample)	0

FIG.4.3.3.2 BDE parameter screen for the Rx Pulse Shaper filter block

4.3.4 Sub-optimal waveshaping

Using the same design approach adopted in Section 4.3.2, the new transmitter block is shown in Fig.4.3.4.1. In this exploded view, everything remains similar to that of Fig.4.3.2.1 except for the missing Hadamard code block. As for the receiver block which is displayed in Fig.4.3.4.2, there is no Hadamard code and once again, the receiver waveform is completely different from the transmit waveform. Parameters required to specify this optimized receiver waveform are the same as that shown in Fig.4.3.3.2.

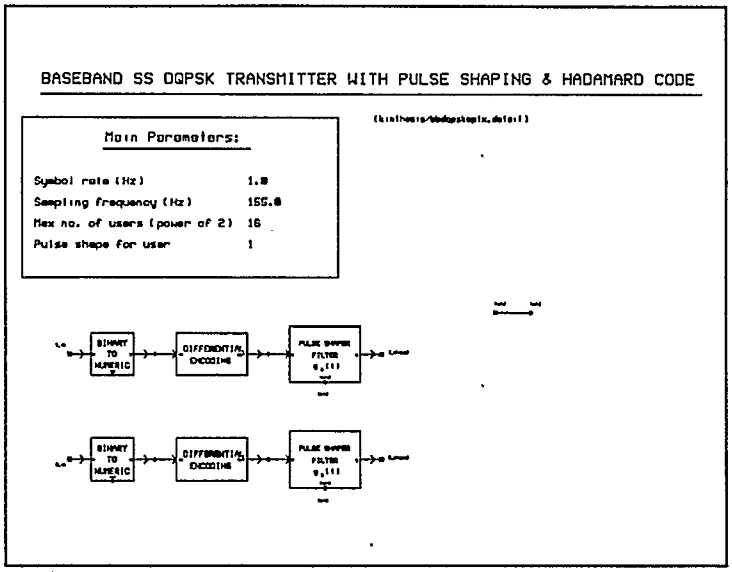

FIG.4.3.4.1 BDE expanded view of the baseband equivalent QPSK transmitter with waveshaping

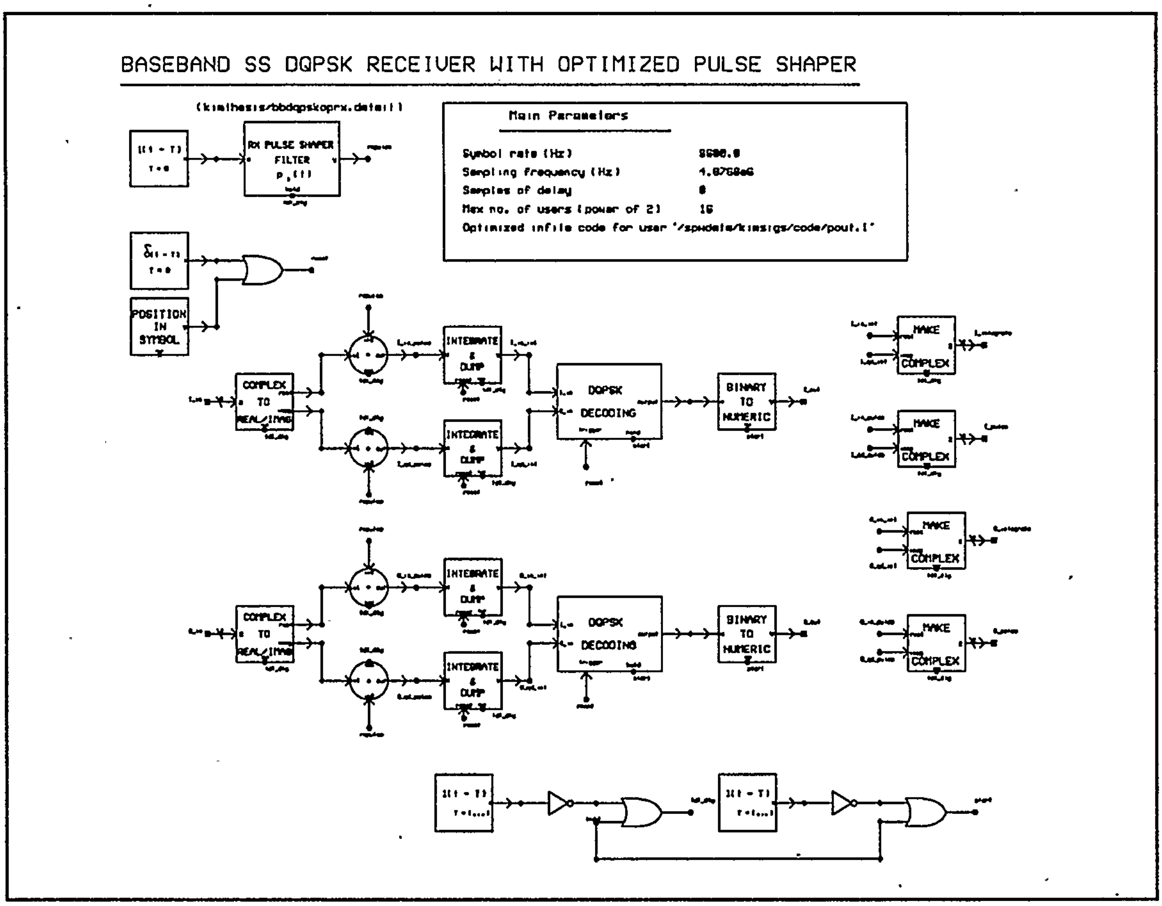

FIG.4.3.4.2 BDE expanded view of the baseband equivalent DQPSK receiver with optimized waveshaping

4.4 Summary

A software package called SPW was chosen to build simulation models to evaluate the various system performances. It is a powerful software design tool that can interactively and graphically capture a schematic diagram of a system design and then test and simulate the system without writing any codes. Its major components, functionality and implementation of the various proposed simulation systems were presented.

CHAPTER 5

RESULTS & DISCUSSION

5.1 Introduction

In the last chapter, four basic simulation systems were presented and for convenience, will be denoted as follows:

System A - conventional DS-SSMA with Gold codes
System B - Hadamard codes and unoptimized waveshaping
System C - Hadamard codes and sub-optimal waveshaping
System D - only sub-optimal waveshaping.

These systems were designed to operate with a data rate $R = 9600$ bps and in an allocated spectral band of 1.5 MHz. System A, utilizing a sequence period $N_c = 127$, has a null-to-null spectral occupancy of approximately 1.22 MHz and is limited to a maximum of 10 users[18] due to the AO/LSE condition. Systems B and C, where the size of the Hadamard codes is $M = 16$ and the number of transmit waveforms is $N = 16$, both occupy approximately a 1.46 MHz band (see equation 4.4). In contrast to system A, systems B and C yield a total possible number of 256 users (see Section 4.3.2). Note that with Hadamard codes, systems B and C have an additional level of security. The most spectrally efficient model is system D, where for a Hadamard matrix size of 16 and 32, the null-to-null occupied bandwidth is approximately 91.3 kHz and 168.0 kHz (see Section 3.4.1), respectively.

This chapter first presents some simulation results for the above systems in a Gaussian channel for synchronous transmission. Then the systems performances are determined for asynchronous transmission with different transmission delays and number of interfering users. In the case of a multipath channel, performances are determined for different multipath delay spread profiles and multiple access interference. Finally, a theoretical BER is used to predict the upper bound of the performance of system D.

5.2 Performances in Gaussian channel

To establish the accuracy and validity of the four models, simulation results for these systems are generated for the case of a single user with DQPSK modulation and compared with known results[21]. Even though the simulation models are wideband systems, the performances (BER) should be identical to that of a narrowband DQPSK modulated system in Additive White Gaussian Noise (AWGN). After the establishment of the benchmarks, the four systems performances are examined for synchronous and asynchronous transmissions with different number of users and propagation time delays.

5.2.1 Synchronous transmission

The BER performance curve, as explained in Chapter 4, is obtained by comparing the number of bits coming out of the receiver that are in error with the total number of transmitted bits. To obtain a high level of confidence interval for the BER evaluation, a commonly used rule of thumb to determine the total number of transmitted bits is given by

$$\textit{Total no. of transmitted bits} \approx \frac{100}{P_e} \tag{5.1}$$

where P_e is the average probability of error for a given signal-to-noise ratio (SNR). Computation time is also reduced since fewer number of bits can be transmitted at low SNR values. A smoother BER curve can be obtained by averaging the error curve for a number of runs (say, 10). However, due to the drastic increase in the processing time, only one run is conducted for each error curve. The increase in processing time is a result of large oversampling required for the implementation.

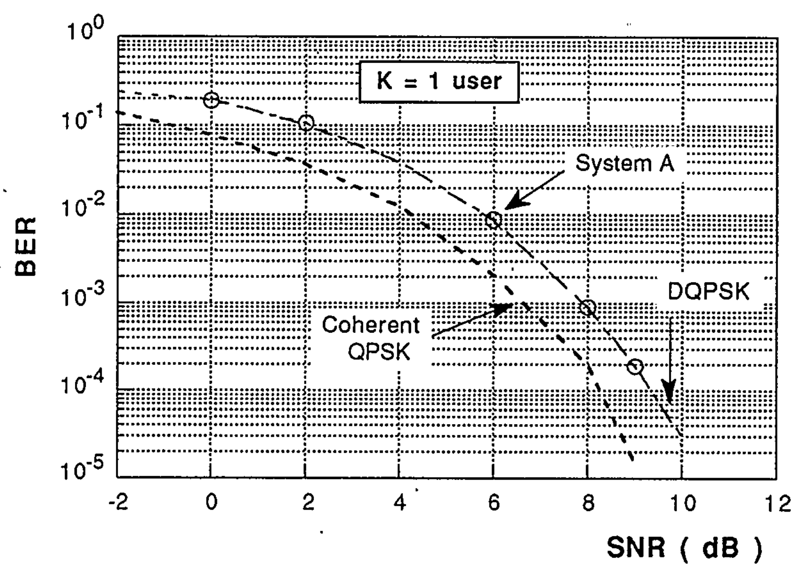

FIG.5.2.1.1(a) BER performance of system A in AWGN for K = 1

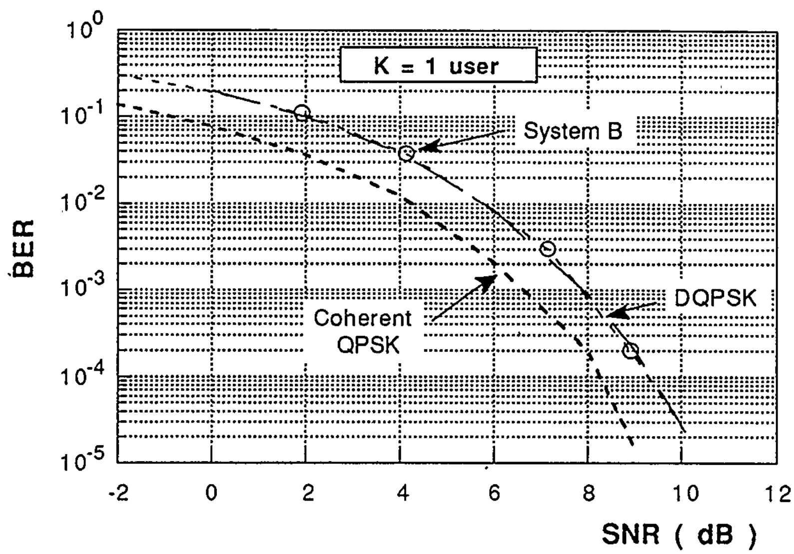

FIG.5.2.1.1(b) BER performance of system B in AWGN for K = 1

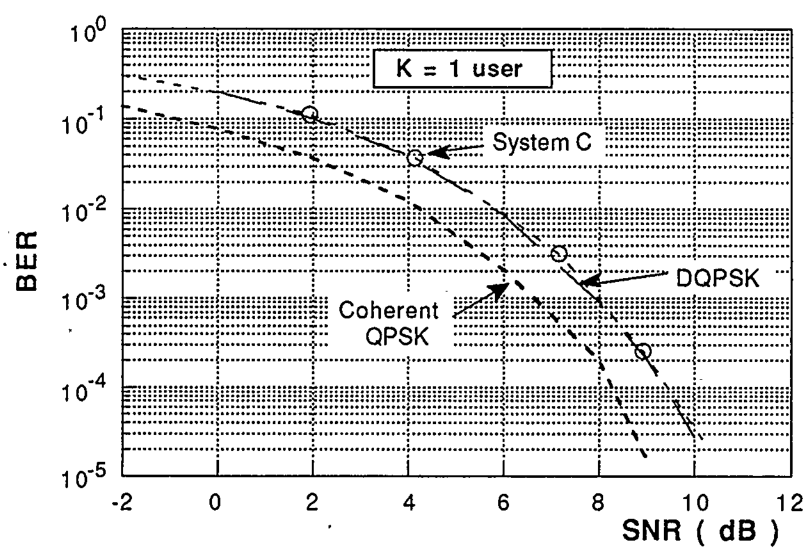

FIG.5.2.1.1(c) BER performance of system C in AWGN for K = 1

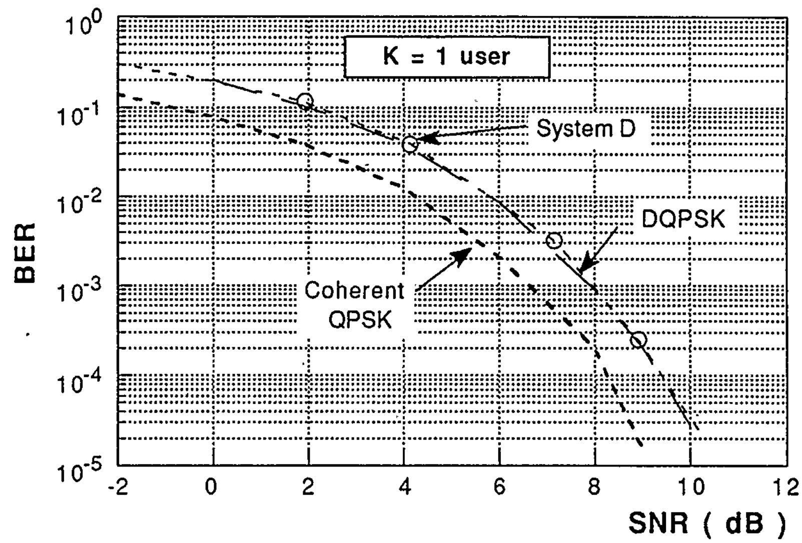

FIG.5.2.1.1(d) BER performance of system D in AWGN for K = 1

Performances of the four systems, for a single user , $K = 1$, in AWGN are shown in Figs.5.2.1.1(a)-(d). Error curve for the coherent QPSK demodulation was extracted from Proakis[21] and it represents the best possible performance attainable. Results obtained for the four systems compare well with the DQPSK demodulation scheme (also from [21]). In addition, these results exhibit similar performances and therefore verify the accuracy of the computer models.

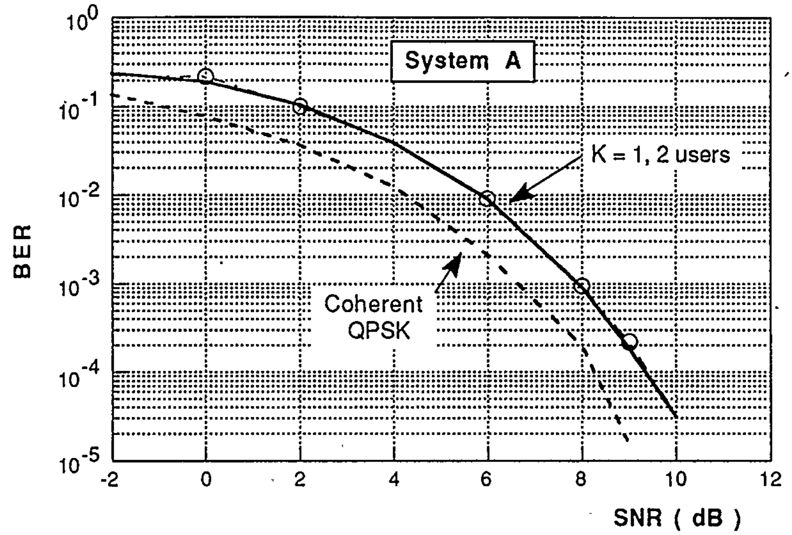

FIG.5.2.1.2(a) BER in AWGN with multiple access for synchronous system A

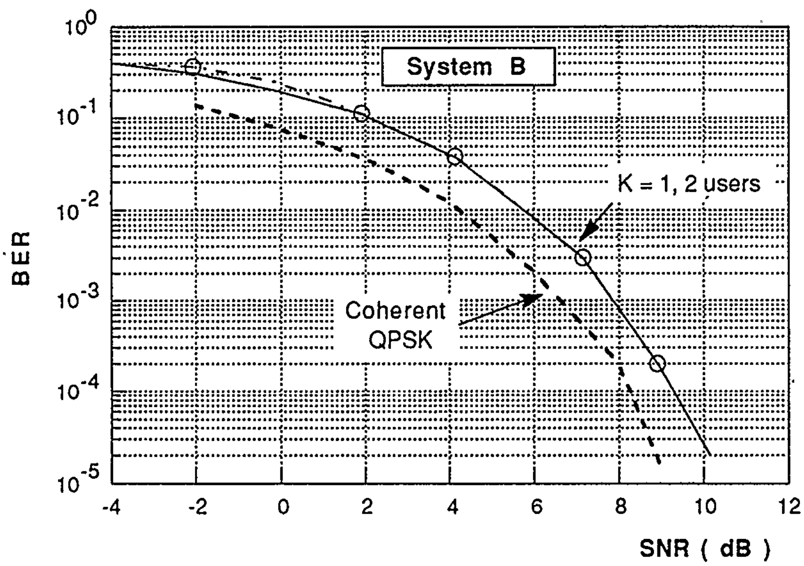

FIG.5.2.1.2(b) BER in AWGN with multiple access for synchronous system B

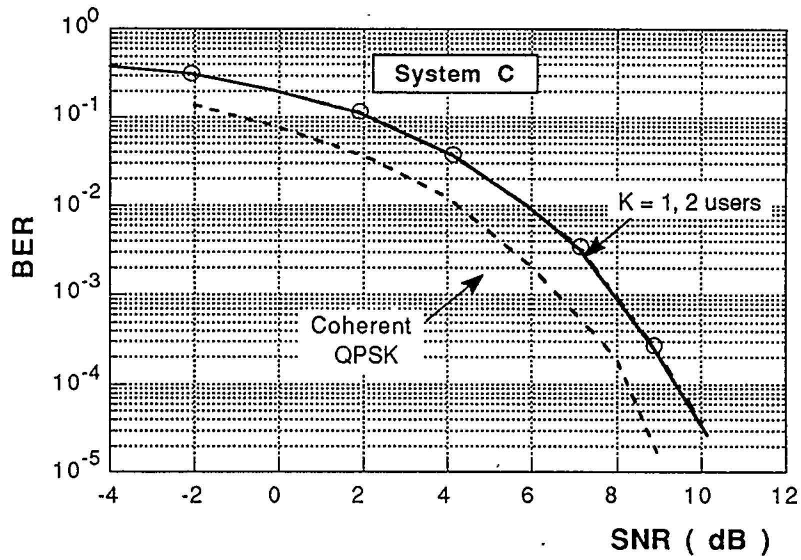

FIG.5.2.1.2(c) BER in AWGN with multiple access for synchronous system C

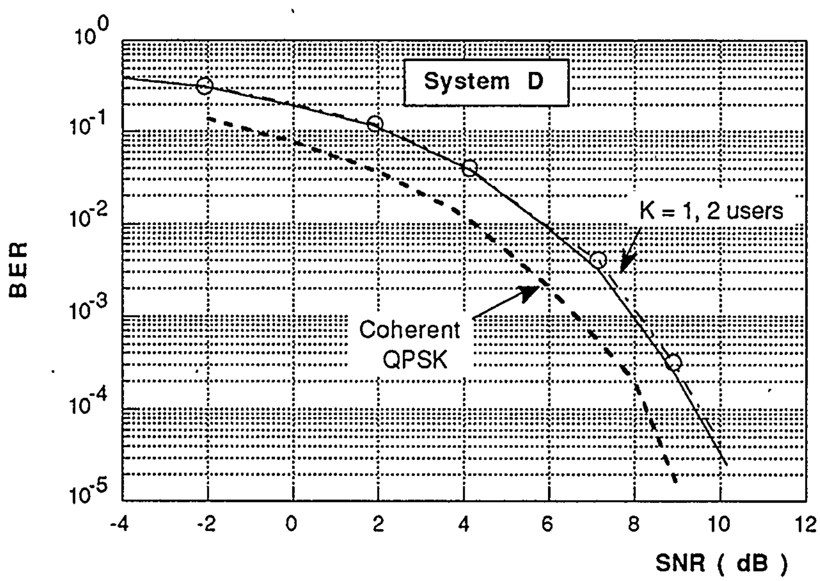

FIG.5.2.1.2(d) BER in AWGN with multiple access for synchronous system D

In a synchronized multiple access system with AWGN, there is no performance degradation, as illustrated in Figs.5.2.1.2(a) - (d), when the second transmitter becomes active. This phenomena occurs because the crosscorrelation effects between the desired receiver and the interfering transmitter is minimal when transmissions are synchronous. It also implies that no degradation would occur as more users are added to the systems. This is true for systems B, C and D with up to 256 active transmitters because the transmit waveforms and codes are orthogonal. For system A, however, the number of Gold codes with insignificant crosscorrelations is much less than 127. Beyond about 10 active transmitters, performance starts to degrade for A. If we define bandwidth efficiency η as

$$\eta = \frac{\textit{Number of users}}{\textit{Bandwidth occupancy}} \quad \text{users / MHz} \tag{5.2}$$

then $\eta_A < 104$ users/MHz, $\eta_{B,C} \approx 175$ users/MHz and $\eta_D \approx 190$ users/MHz (for M = 32). The most bandwidth efficient is system D while B and C are slightly less bandwidth efficient due to the tradeoff caused by the use of Hadamard codes for additional security. Despite the tradeoff, B and C are more bandwidth efficient than that of A. Hence, in applications where bandwidth is scarce (for example, the low-frequency band 30 kHz - 300 kHz and the medium-frequency band 300 kHz - 3 MHz[38]), the use of waveshaping is more attractive than that of DS-SSMA. Potential applications would be in fire, smoke and burglar alarms. A large number of sensors, placed at different locations in a floor of a building, transmit to a central transceiver which in turn, can be connected to a central station. The sensors can be battery powered as they operate with very low power. Since each sensor has its own identification, the transceiver can easily locate the source of trouble.

5.2.2 Asynchronous transmission

In an asynchronous multiple access system, the transmissions by all the users are not synchronized. This can result in partial crosscorrelation effects between the desired receiver and the interfering transmitters. Failure to reduce these partial crosscorrelations by the desired receiver causes a degradation in the BER performances. The following two sections examine this performance degradation under the effects of multiple access and variation in the maximum propagation time delay.

5.2.2.1 Effect of multiple access

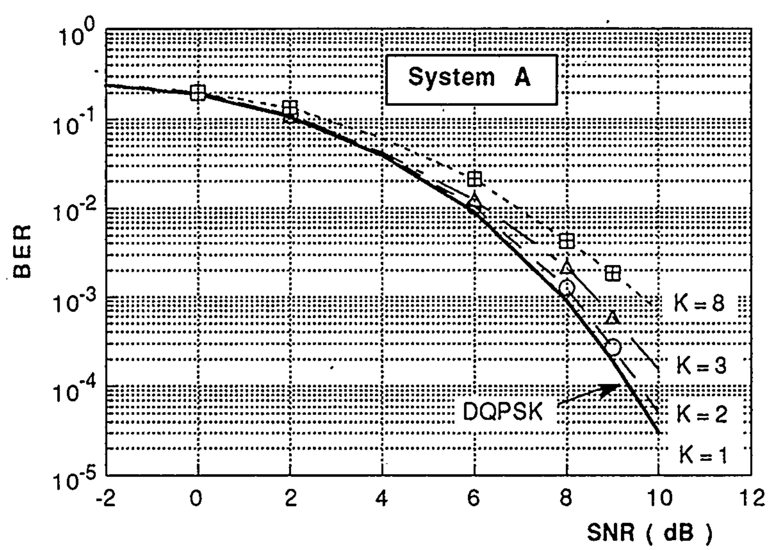

FIG.5.2.2.1.1 Effect of multiple access on BER performance in AWGN for system A .

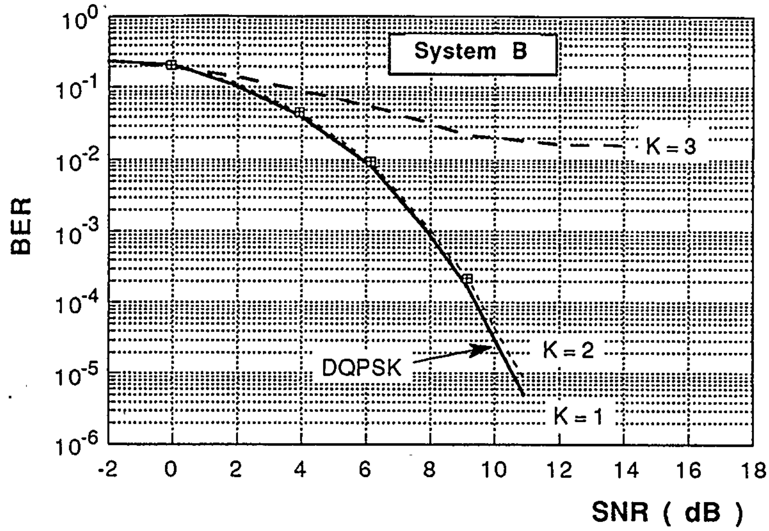

FIG.5.2.2.1.2 Effect of multiple access on BER performance in AWGN for system B

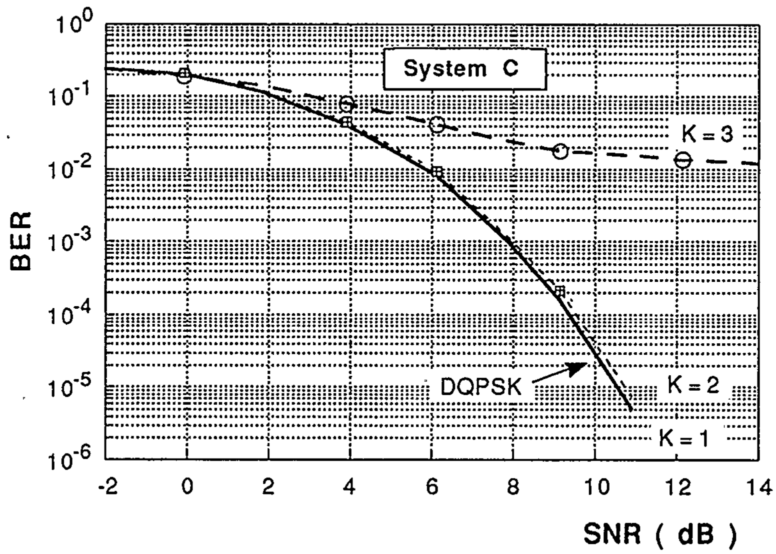

FIG.5.2.2.1.3 Effect of multiple access on BER performance in AWGN for system C

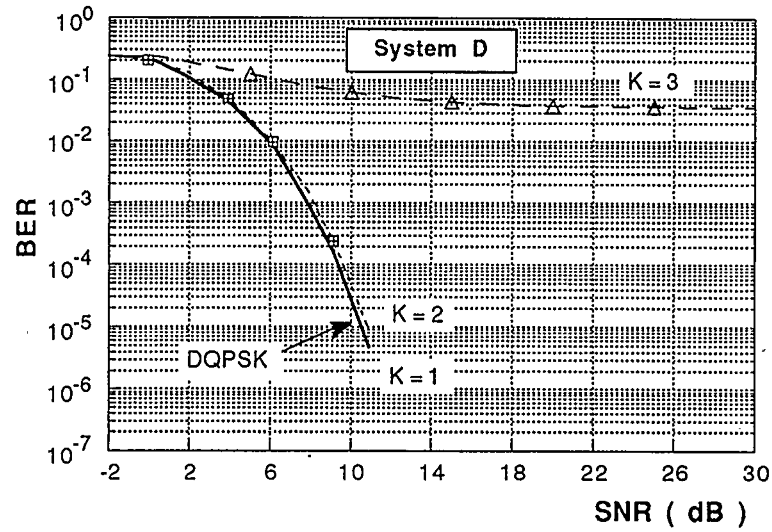

FIG.5.2.2.1.4 Effect of multiple access on BER performance in AWGN for system D

By propagation time delay, we mean the relative time of arrival of an interfering signal relative to the desired signal, measured as a fraction of the symbol duration (τ / T). In this section, the random variable τ is set such that $\frac{\tau}{T} \in [0,1]$, for each interferer of the four systems to facilitate examination of the effects of multiple access. Since the data is assumed to be transmitted in a burst mode, a new τ is generated for each frame (200 symbols) of each interferer and they are independent and uncorrelated. Fig.5.2.2.1.1 shows the BER performance of system A in AWGN. The performance of a single-user case is similar to that of the conventional DQPSK system. However, when a second transmitter is active, the system performance deteriorates slightly at high SNR. This scenario contrasts with that in the synchronous case where there is no performance degradation. As more users are added to the system, the multiple access interferences become more severe, causing a performance degradation of at least an order of magnitude (10^{-1}) between $K=1$ and $K=8$ users at $SNR=10$ dB.

Similar performance degradation, caused by an additional user to the single-user case, can be seen in system B which is shown in Fig.5.2.2.1.2. For $K=2$ users, system B exhibits slight performance degradation at high SNR and compares favorably with that of system A in Fig.5.2.2.1.1. However, when the third user is active, the BER performance deteriorates rapidly and saturates before the SNR reaches 12 dB. This implies that with an increase in signal power, no gain in performance is achieved.

System C exhibits similar performance degradation for $K=2$ users, as seen from Fig.5.2.2.1.3 and it compares well with that of system A. Once again, similar to system B of Fig.5.2.2.1.2, the BER performance deteriorates rapidly and saturates at $P_e \approx 0.015$ for $SNR=12$ dB when the third user becomes active. We note that the performance improvement over the unoptimized receiver waveform of system B is marginal. This is because of the limitations of the numerical optimizer, GINO, which restricts a wider optimization search space to yield a much more reduced objective function.

Illustrated in Fig.5.2.2.1.4 is the BER performance of system D in AWGN. The desired receiver waveform used is identical to that of system C, except for the missing Hadamard codes. For $K=2$ users, it exhibits similar performance as that of systems A, B and C. When the third user transmits, the performance deteriorates rapidly and saturates at $P_e \approx 0.04$ for $SNR=16$ dB. This is once again due to the limitations of GINO.

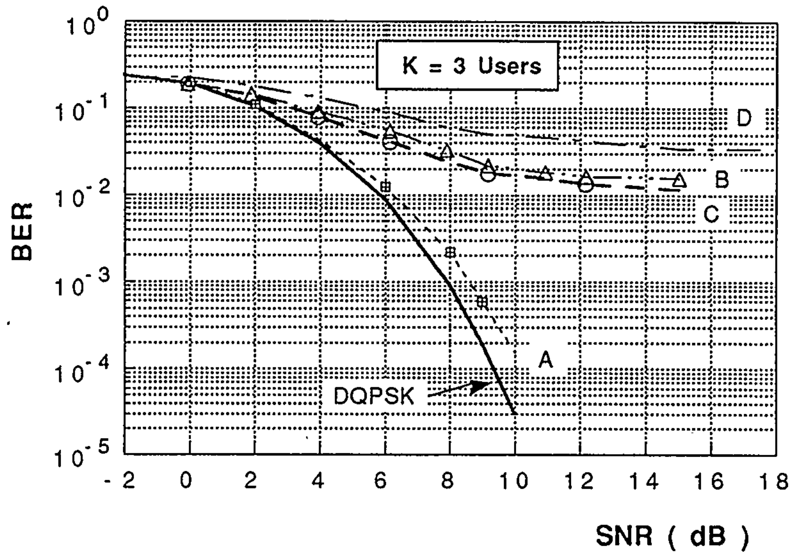

FIG.5.2.2.1.5 Comparison of the BER performances in AWGN for systems A, B, C and D for K = 3 users

A comparison of the systems performances for $K = 3$ users is shown in Fig.5.2.2.1.5. Because the desired receiver is not optimized, system B performs poorly in comparison to system A. System C, despite having its receiver waveform optimized, performs only slightly better than that of system B. System D has the worst performance. A remedy is to reformulate the objective function to include the Hadamard (or any suitable) codes for the selection of the receiver waveform. The limitations of GINO can be overcome by using a more powerful numerical system, like MINOS, which can handle a much wider optimization search space and larger number of variables. System A exhibits the best performance because the Gold codes selected are optimized for asynchronous operation. Note, however, that the number of users for such Gold codes of length $N_c = 127$, is limited to 10.

5.2.2.2 Effect of propagation time delay

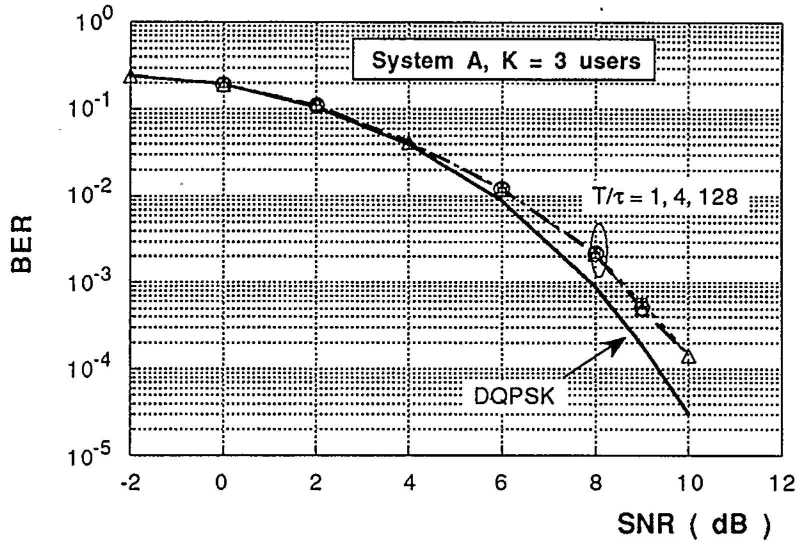

FIG.5.2.2.2.1 Effect of propagation time delay on BER performances of system A in AWGN for K = 3 users

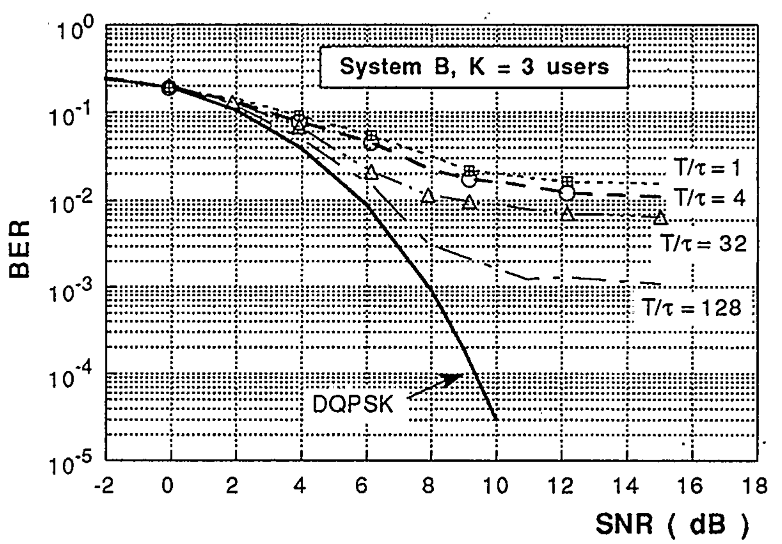

FIG.5.2.2.2.2 Effect of propagation time delay on BER performances of system B in AWGN for K = 3 users

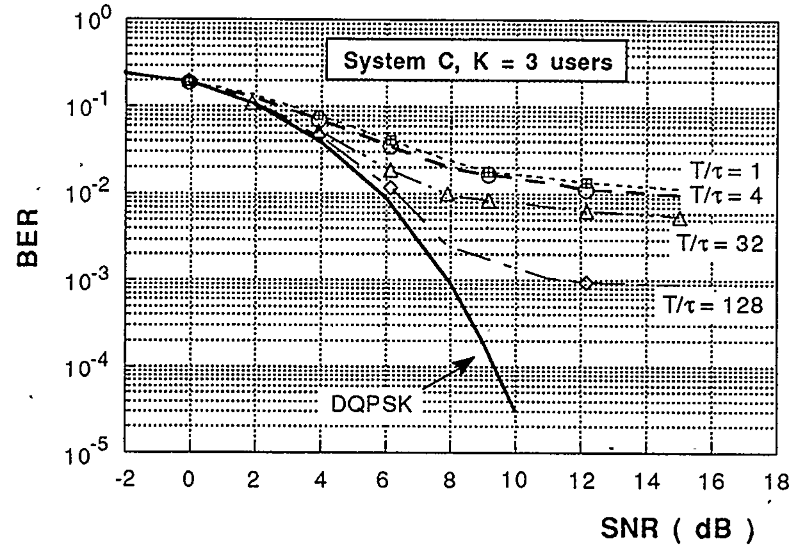

FIG.5.2.2.2.3 Effect of propagation time delay on BER performances of system C in AWGN for K = 3 users

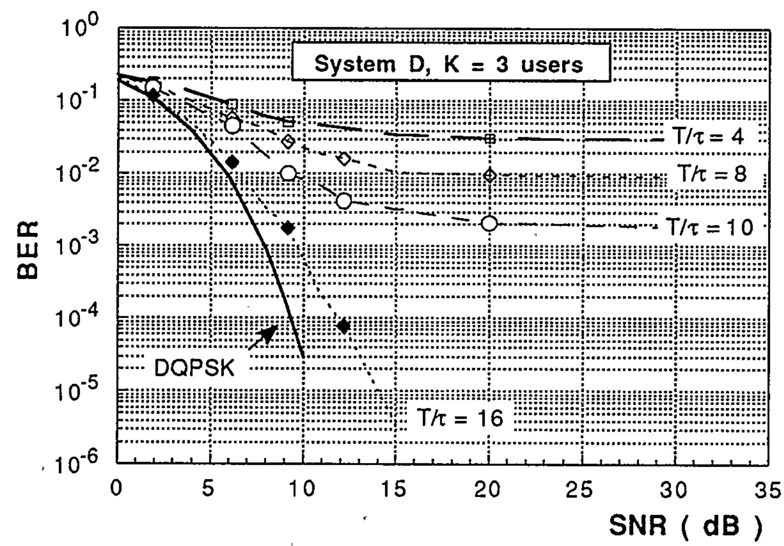

FIG.5.2.2.2.4 Effect of propagation time delay on BER performances of system D in AWGN for K = 3 users

This study is to determine the range of propagation time delays for which the systems performances are considered reasonably good and for which synchronization is not necessary. For simplicity and clarity sake, this delay is denoted as its inverse in the figures. System B shows that the BER performance is highly dependent on this time delay factor, as illustrated in Fig.5.2.2.2.2 for K = 3 users. As the maximum propagation time delay decreases, the system performance improves. Similar dependence on the maximum propagation time delay can be observed from Figs.5.2.2.2.3 and 5.2.2.2.4 for systems C and D, respectively. The use of sub-optimal waveform for C results in only slight performance improvement over B. To operate systems B and C with a $P_e < 10^{-3}$, without synchronization, the symbol rate ($R = 1/T$) should be reduced so that the delay factor is $T/\tau > 128$. On the other hand, system D exhibits the best performance (among B, C and D) and can easily achieve $P_e < 10^{-3}$ with relative delay of $T/\tau > 12$. This superior performance of system D over that of B and C indicates the need for the Hadamard codes to be optimized jointly with the receiver waveform or alternatively, the use of other optimized codes (eg. Gold codes) in conjunction with the receiver waveform. In applications where the relative delays are small or some form of synchronization can be maintained, system D performance can surpass that of A, with a potential to accommodate up to 256 users as compared to about 10 users for A.

Comparison between the simulated and theoretical BER performances of system D (M=16) in AWGN, for $K = 3$ users, is illustrated in Fig.5.2.2.2.5. The theoretical BER prediction compares favourably with the simulated results and as such, it can be used as a reasonable and quick estimate of the upper bound of the system performances without undergoing the computationally intensive operation of the simulated process.

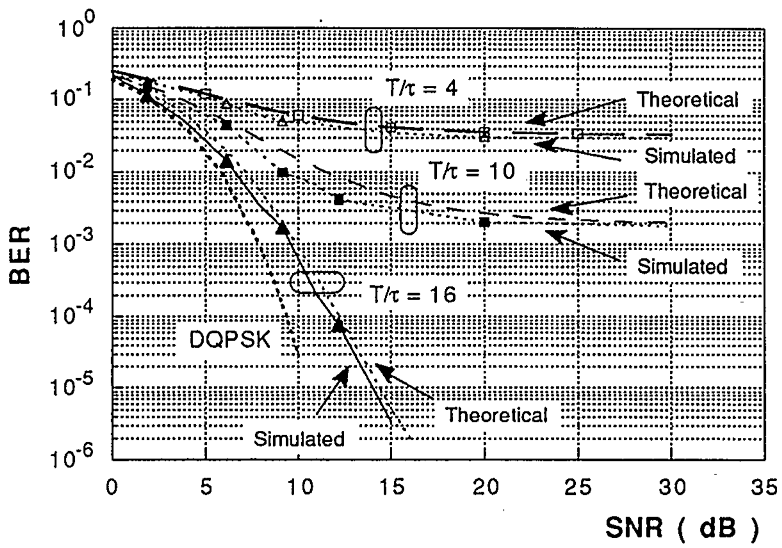

FIG.5.2.2.2.5 Comparisons of the simulated and theoretical BER performances of system D in AWGN for K = 3 users

Fig.5.2.2.2.6 shows the varying degree of dependency, for the four systems, on the maximum propagation time delay for $SNR = 12$ dB and $K = 3$ users. The proposed system and its variants are highly dependent on the maximum propagation time delay. Systems B and C have comparable degree of dependency, except that system C saturates with a lower BER than that of system B. This slight improvement is attributed to the sub-optimal receiver waveform used for system C. Due to its smaller spreading bandwidth, system D, for $\tau/T > 0.1$, saturates with a much higher BER than that of systems B and C. However, for $\tau/T < 0.1$, system D shows dramatic performance improvement as compared to $\tau/T < 0.05$ for systems B and C. This implies that system D can operate at a reasonably low BER with less severe synchronization requirements than that of systems B and C. Results indicate that the modified system has a potential for achieving better performance than that of the A if synchronization of the transmitters can be attained within 0.05 to 0.1 of the symbol period. In applications where the transmitters and receivers are stationary, eg., a fire alarm sending message to a central receiver, this synchronization requirement can be easily satisfied.

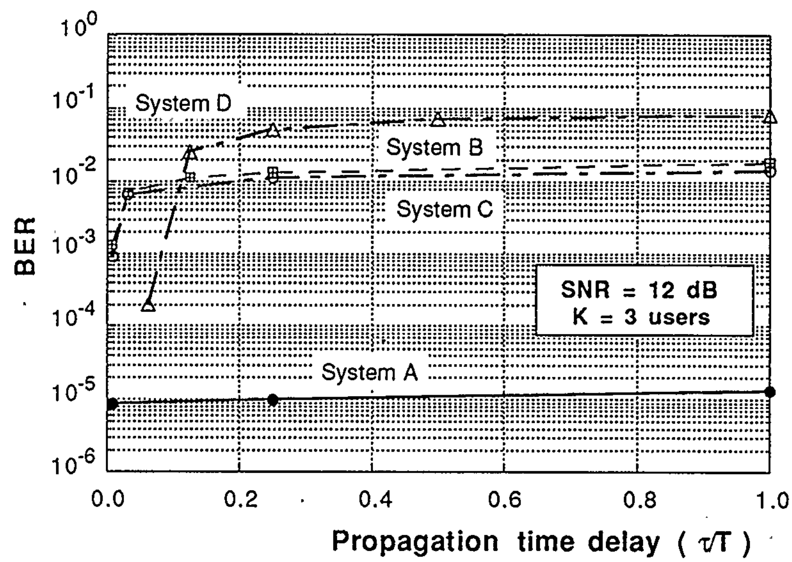

FIG.5.2.2.2.6 Comparisons of the BER performances as a function of the maximum propagation time delay for systems A, B, C and D in AWGN for SNR = 12 dB and K =3 users

5.3 Performances in multipath channel

The Rayleigh distributed multipath channel used in the simulations is based on the model described in Fig.4.3.1.4 where the locations of each impulses, in seconds, is specified in a file. Six equally spaced paths and two maximum delay spread profile of T/64 (≈ 1600 nsecs) and T/256 (≈ 410 nsecs) were chosen to represent a typical channel characteristics [19] which translate into τ_{rms} value of 180 nsecs and 45 nsecs, respectively, using equations 4.1 and 4.2.. In a flat fading channel, there is only one Rayleigh distributed path and it is assumed that the path delay is known and the phase shift due to Doppler spread, changes slowly.

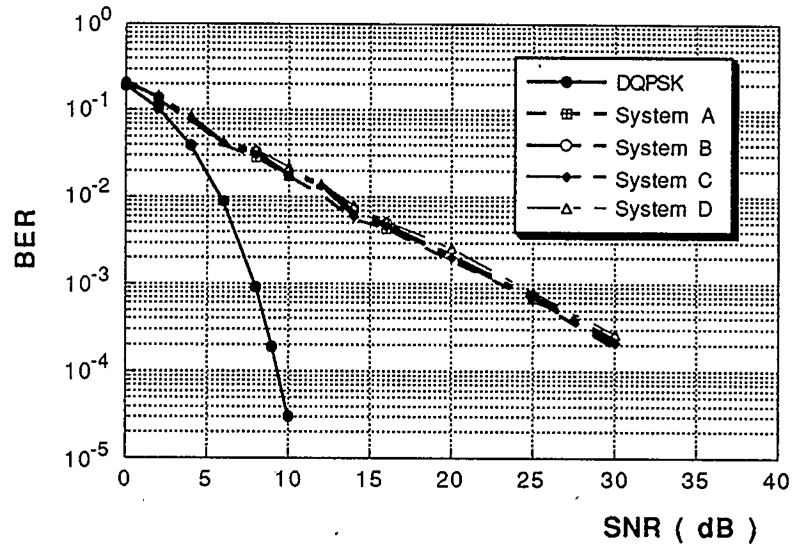

FIG.5.3.1 BER performances of the four systems in Rayleigh flat fading channel

The BER performances of the four systems in a Rayleigh flat fading channel for one user is shown in Fig.5.3.1. All four systems performances deteriorate in such a channel and they have comparable results. These form the reference for comparison of performances in the case of a multiple access system undergoing a Rayleigh frequency selective channel.

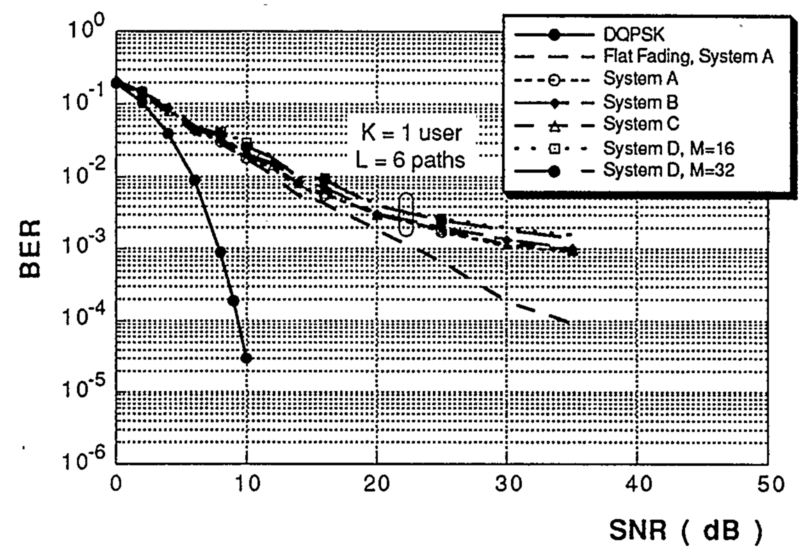

FIG.5.3.2 BER performances of the four systems for K =1 user and L = 6 paths in Rayleigh frequency selective fading channel

Fig.5.3.2 shows the BER performances of the four systems in a Rayleigh frequency selective fading channel for K = 1 user, L = 6 paths and a maximum delay spread profile of T/256 seconds. All four systems exhibit comparable performances. Due to the small delay spread profile (< 0.01 T), the reflections of the desired signal have little destructive effects at low SNR. Thus, they deteriorate like a flat fading channel. At higher SNR values, the reflections become significant, thereby causing the systems performances to saturate at about SNR = 30 dB with $P_e \approx 0.001$. Hence, in the absence of multiple access interference, these receivers are susceptible to self-interference caused by the multipath propagation. If the energies of these reflected paths were used constructively instead of being treated as interferences[22,23], that is diversity in the form of a Rake receiver, the performances would improve.

Since their bandwidth occupancies are approximately equal ($\approx$ 1.5 MHz), systems A, B and C have comparable performances. The use of optimized waveform for system C does not result in drastic improvement over that of B because of the sub-optimal results from the constrained optimization process. Even though system D requires only a marginal bandwidth expansion which is only about 17.5 times (for M = 32) larger than the data bandwidth as compared to 156 times for the Gold codes, its performance is only slightly worse than A, B and C. A larger bandwidth in a frequency selective fading channel is desirable because certain frequency components of the signal would experience fade and hopefully, sufficient energy would be left to reconstruct the signal thereby providing reasonable performance. This limited bandwidth expansion can be overcome by increasing the size of the Hadamard matrix of system D, as seen by the slight improvement from M = 16 to M = 32. However, matrix size beyond 32 was not attempted because GINO has a limitation on the size of the search space and variables.

The effects of multiple access interference on BER performances in a Rayleigh frequency selective fading channel are shown in Figs.5.3.3(a), 5.3.3(b), 5.3.3(c) and 5,3.3(d) for systems A, B, C and D, respectively, for L = 6 paths and a maximum delay spread profile of T/256 seconds. Simulation is performed only for a maximum of 2 users due to the computationally intensive process. Performance degradation for the single-user case is due to the self-interferences from the six paths. When two users are active, in addition to the self-interferences of the desired transmitters, multiple copies of the interfering transmitters cause further deterioration of the systems performances.

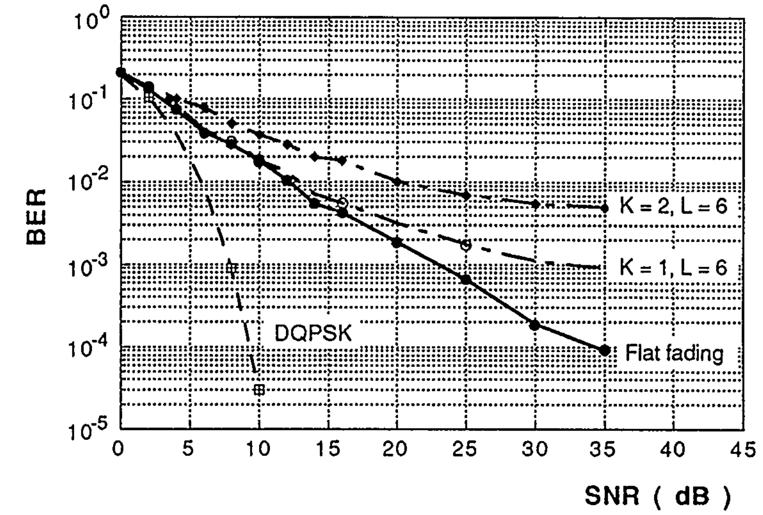

FIG.5.3.3(a) Effect of multiple access interference on BER performance of system A for L = 6 paths in Rayleigh fading channel

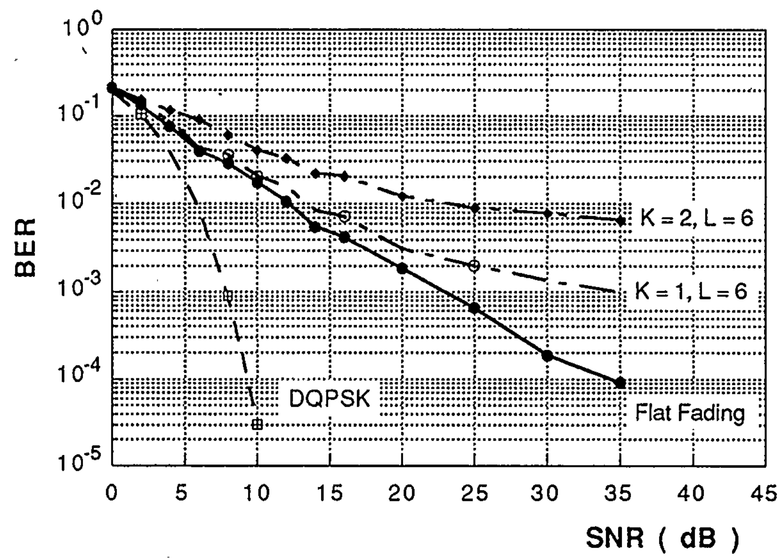

FIG.5.3.3(b) Effect of multiple access interference on BER performance of system B for L = 6 paths in Rayleigh fading channel

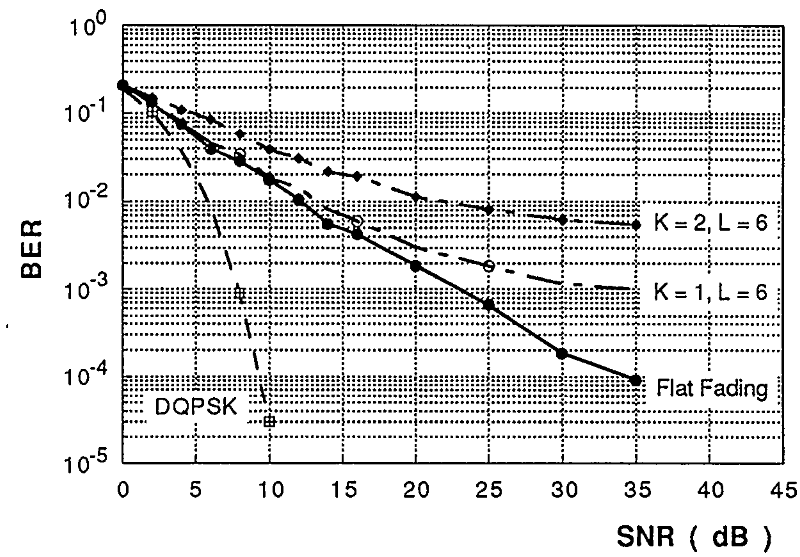

FIG.5.3.3(c) Effect of multiple access interference on BER performance of system C for L = 6 paths in Rayleigh fading channel

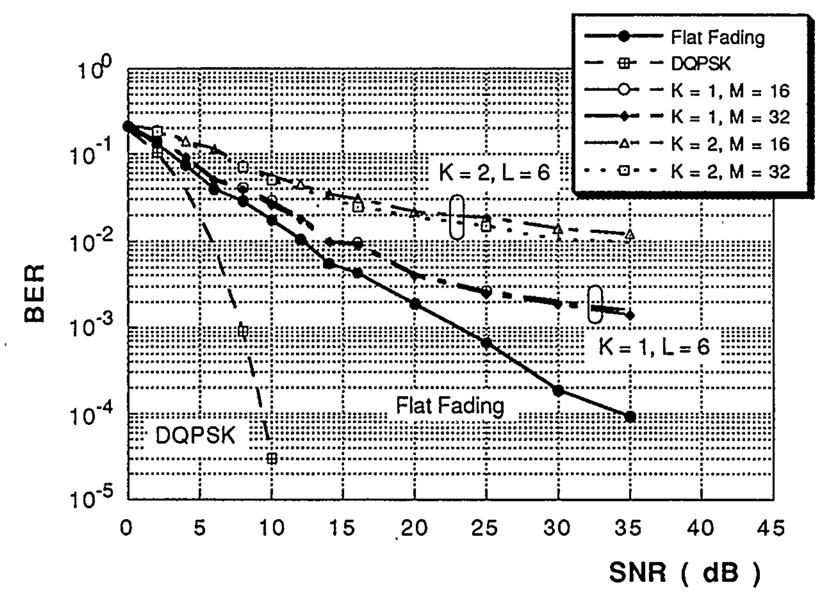

FIG.5.3.3(d) Effect of multiple access interference on BER performance of system D for L = 6 paths in Rayleigh fading channel

The multiple access interference due to the second user causes varying degree of performance degradation, as shown in Fig.5.3.4, in a Rayleigh fading channel with delay spread profile of T/256 seconds. Although the Gold codes possess the AO/LSE property, the performance of system A is almost identical to those of B and C and only slightly better than that of D. Systems B and C performances are comparable to that of A, primarily because of their similar bandwidth occupancies. Once again, system D exhibits a slightly worse performance when a second user is activated, attributed largely to the insufficient bandwidth expansion and the sub-optimal constrained optimization solution. Similar to the single-user case as in Fig.5.3.2, a slight performance improvement is obtained by increasing the size of the Hadamard matrix, up to a possible size of M = 256 with bandwidth of approximately 1.24 MHz and K = 128 users.

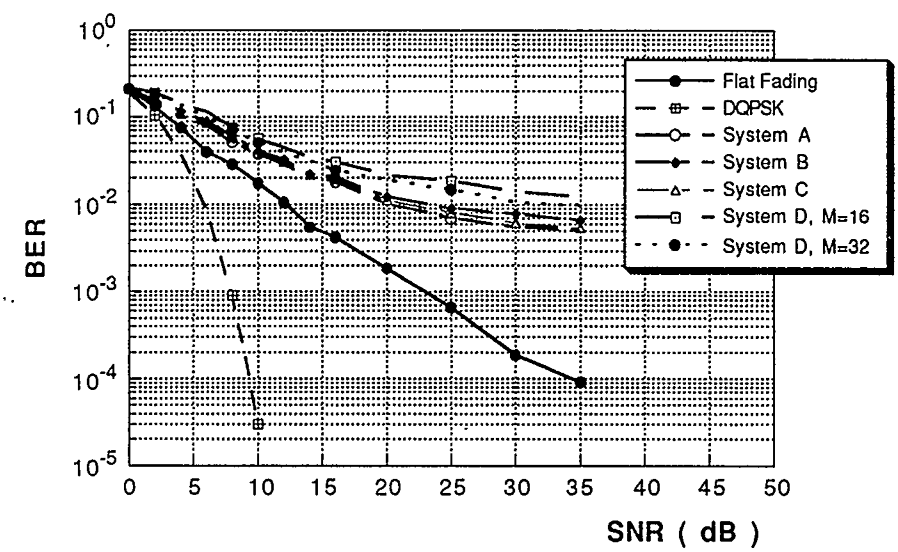

FIG.5.3.4 Comparison of the BER performances of the four systems for K = 2 users and L = 6 paths in Rayleigh fading channel

Fig.5.3.5(a) shows the effect of maximum delay spread on the BER performance of system A for K = 2 users, L = 6 paths and M = 16 in a Rayleigh fading channel. There is no appreciable difference in performances for delay spread profiles of T/64 and T/256 seconds suggesting an independence of the channel characteristics and also implies that the Gold codes used are more resilient to the changes in the channel characteristics. However, B, C and D are slightly dependent on the channel delay spread profile, as shown in Figs.5.3.5(b), 5.3.5(c) and 5.3.5(d), respectively. As alluded earlier, this dependency is attributed to the unoptimized receiver waveform for system B, sub-optimal waveform for system C and finally, a combination of inadequate bandwidth expansion and sub-optimal waveform for system D. Recent studies and analysis have shown that these channel profiles may need some form of diversity or equalization for better performances [35, 36]. In these three systems (B, C and D), as the delay spread decreases from T/64 to T/256, the BER performance improves. This implies that τ_{rms} also decreases, thereby suggesting the suitability of these systems for small and medium-size office buildings [37]. The theoretical BER curve, as shown in Fig.5.3.5(d), provides a reasonable estimate of the simulated results and can be used as a convenient tool to predict the upper bound of the system performances under different conditions. Note that the factor β of the theoretical results attempts to emulate the effects of the maximum delay spread profile by varying the amount of energy within a fraction of the symbol duration in the evaluation of the variances and covariances (Appendix C).

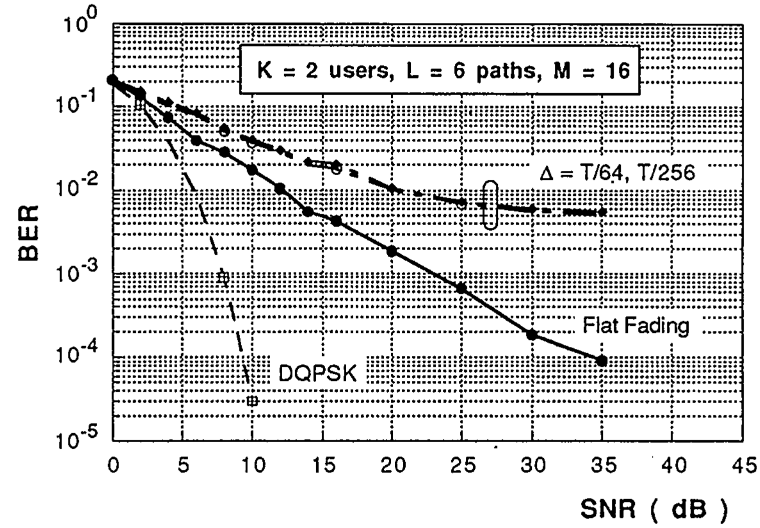

FIG.5.3.5(a) Effect of maximum delay spread profile on BER performances of system A for K = 2 users, L = 6 paths and M = 16 in Rayleigh fading channel

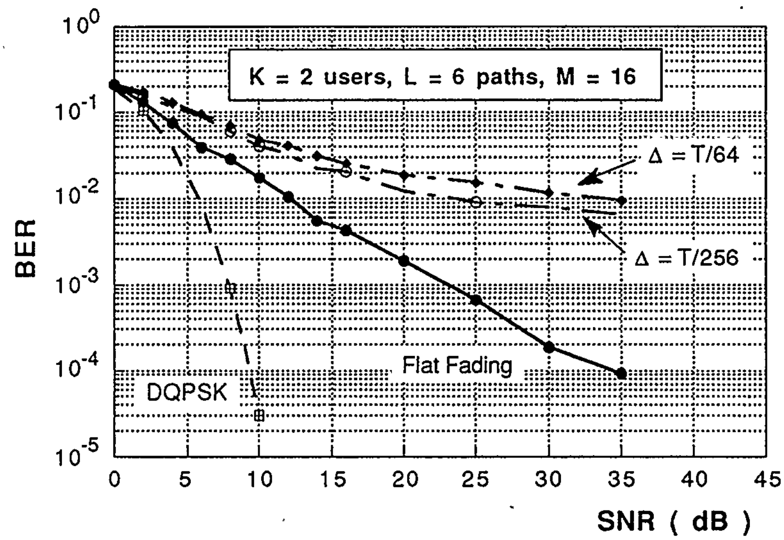

FIG.5.3.5(b) Effect of maximum delay spread profile on BER performances of system B for K = 2 users, L = 6 paths and M = 16 in Rayleigh fading channel

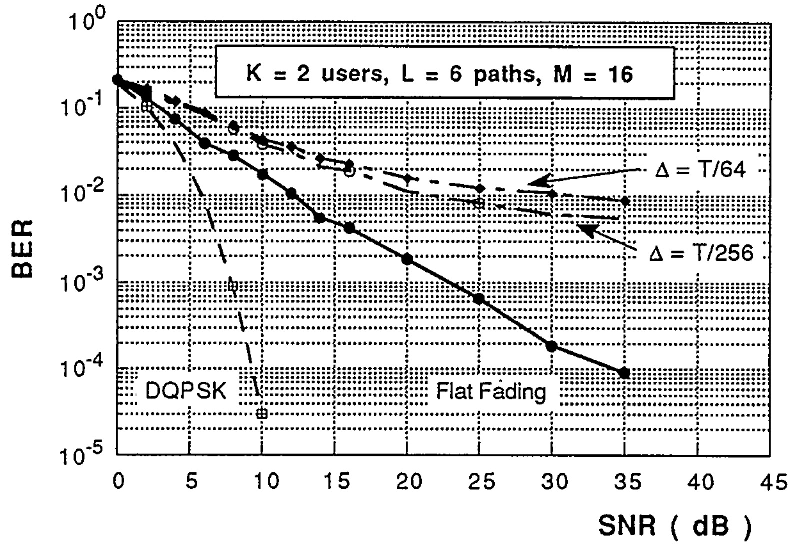

FIG.5.3.5(c) Effect of maximum delay spread profile on BER performances of system C for K = 2 users, L = 6 paths and M = 16 in Rayleigh fading channel

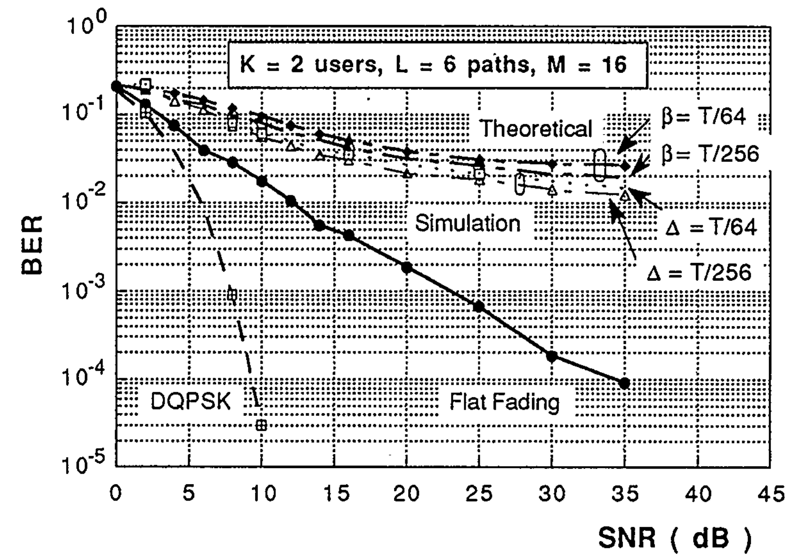

FIG.5.3.5(d) Effect of maximum delay spread profile on the theoretical and simulated BER performances of system D for K = 2 users, L = 6 paths and M = 16 in Rayleigh fading channel

5.4 Summary

Simulation results for the four models are presented for both synchronous and asynchronous transmissions under the effect of multiple access interference in AWGN channel. The sensitivity of the systems to varying transmission delays are also examined for asynchronous transmission. For the case of a multipath channel, performances are determined for different delay spread profiles and multiple access interference. Finally, the suitability of the theoretical average error probability to predict the upper bound of system D is also presented.

CHAPTER 6

CONCLUSIONS

6.1 Simulation model

Computer models for four systems, namely, (a) a conventional DS-SSMA system using Gold codes, (b) an unoptimized system with Hadamard codes, (c) a sub-optimized receiver waveform system with Hadamard codes and (d) a sub-optimized waveshape system with no spreading codes, were successfully built using a highly integrated and powerful software design tool called SPW. It permits a system design to be captured schematically and then tested and simulated without writing any codes, thereby achieving dramatic time and productivity improvement. Any modifications to the design can be easily accommodated since it adopted a modular approach to system design. In addition, user-created blocks can be incorporated into the design where no such functions are available in the standard library. Despite such features, the simulation process can be time consuming because of the brute force technique employed to evaluate the BER performances of the models. This problem is further compounded by the large number of oversamples (due to the large bandwidth of the system) involved in the simulation process.

6.2 Constrained optimization results

The objective function for the optimization process is designed to reduce the energy of the sum of the partial crosscorrelation functions while maintaining the autocorrelation peak to be unity. This formulation is a condition for minimizing the average probability of error. Solution to this constrained optimization problem is achieved using a nonlinear optimizer called GINO. During the optimization process, it is found necessary to limit the search space for the optimal solution because GINO has a limitation on the number and size of variables. This results in a sub-optimal solution.

6.3 Simulation results

For synchronous transmission in an AWGN channel, all four systems exhibits performances identical with that of DQPSK demodulation system. The modified system and its variant (ie., using waveshaping) are more bandwidth efficient than that of the conventional system. This is a critical factor in the low-frequency and medium-frequency band where the bandwidth available is scarce, thereby making the proposed system an attractive alternative to the conventional system.

For asynchronous transmission in an AWGN channel, performance depends upon the maximum relative delays of the interfering signals. For relative delays of up to 0.1 of the symbol period, system D (with no codes) exhibit the best performance of the three systems (B, C and D). Systems B and C perform well only for relative delays up to 0.05 of the symbol period. Although system C uses sub-optimal waveform, its performance improvement over B is only marginal. Further improvement can be obtained by using more suitable codes, for instance Gold codes instead of Hadamard codes, in conjunction with the waveforms. Alternatively, the optimization problem should be formulated to include Hadamard codes for the selection of the receiver waveform. In applications where the relative delays are small or synchronization can be established to within 0.05 to 0.1 of the symbol period (eg. stationary transmitters and receivers), the proposed systems can accommodate up to 256 potential users compared to about 10 users for system A, within the same allocated bandwidth.

In the case of a single-user undergoing a Rayleigh fading multipath channel, the four systems saturate with comparable performances, thereby necessitating the use of a diversity receiver to improve performances. When subjected to multiple access interferences, all systems show comparable performances where D is only slightly worse than A, B and C. However, D being the most bandwidth efficient, has the potential for obtaining better performance than that of A by increasing the size of the Hadamard matrix and consequently, the number of users (potentially, 128 users for D as compared to 10 users for A) while satisfying the bandwidth limitation. In addition, D would be insensitive to the channel characteristics and hence, suitable for a wider variety of indoor environment. Additional improvements to D can be obtained by using a more powerful numerical optimizer to yield an optimal waveform. Similarly for system C, it has the potential to surpass the performance of A through the use of a better optimizer and optimized codes, accommodating up to 256 users as opposed to 10 users for A.

6.4 Recommendations for future work

In this research, unoptimized Hadamard codes were used in conjunction with waveshaping. For some applications, the resulting system exhibits a superior performance in terms of BER, bandwidth and multiple access capability. To further extend the usefulness of such a system to other applications, the following approaches are recommended: (a) use optimized codes, like Gold codes or search for new ones and (b) include the Hadamard codes in the objective function and jointly optimize the receiver waveforms and the codes. Improvement in the optimization results can be obtained by using a much more powerful and expensive non-linear numerical optimizer, MINOS. Once these are done, the improvements to the proposed system performances can then be investigated.

REFERENCES

[1] R. A. Scholtz, "The Origins of Spread-Spectrum Communications," *IEEE Trans. on Comm.*, vol. com-30, pp. 882-853, May 1982.

[2] N. Wiener, Extrapolation, Interpolation, and Smoothing of Stationary Time Series with Engineering Applications. Cambridge, MA: M.I.T. Press, 1949.

[3] J. M. Whittaker, Interpolatory Function Theory (Cambridge Tracts in Mathematics and Mathematical Physics, no. 33). New York: Cambridge Univ. Press, 1935.

[4] E. T. Whittaker, "On the functions which are represented by the expansions of the interpolation theory," *Proc, Roy. Soc. Edinburgh*, vol. 35, pp. 191-194, 1915.

[5] J. McNamee, F. Stenger, and E. L. Whitney, "Whittaker's cardinal function in retrospect," *Math. Comput.*, vol. 25, pp. 141-154, Jan. 1971.

[6] A. J. Jerri, "The Shannon sampling theorem - Its various extensions and applications: A tutorial review," *Proc. IEEE*, vol. 65, pp. 1565-1596, Nov. 1977.

[7] R. V. L. Hartley, "The transmission of information," *Bell Syst. Tech. J.*, vol. 7, pp. 535-560, 1928.

[8] H. Nyquist, "Certain topics in telegraph transmission theory," *AIEE Trans.*, vol. 47, pp. 617-644, Apr. 1928.

[9] V. A. Kotelnikov, "Carrying capacity of 'ether' and wire in electrical communications" (in Russian), *Papers on Radio Communications 1st All-Union Conv. Questions of Technical Reconstruction of Communications*, All-Union Energetics Committee, USSR, pp. 1-19, 1933.

[10] C. E. Shannon, "Communication in the presence of noise," *Proc. IRE*, vol. 37, pp. 10-21, Jan. 1949.

[11] D. Gabor, "Theory of communication," *J. Inst. Elec. Eng. (London)*, vol. 93, part 3, pp. 429-457, Nov. 1946.

[12] R.L. Pickholtz, D.L. Schilling and L.B. Milstein, "Theory of Spread-Spectrum Communications - A Tutorial," *IEEE Trans. on Comm.*, vol. com-30, pp. 855-884, May 1982.

[13] D.L. Schilling, L.B. Milstein, R.L. Pickholtz, M. Kullback and F. Miller, "Spread Spectrum for Commercial Communications," *IEEE Comm. Mag.*, pp. 66-78, April 1991.

[14] D.L. Schilling, R.L. Pickholtz and L.B. Milstein, "Spread Spectrum goes commercial," *IEEE Spectrum*, pp. 40-45, Aug. 1990.

[15] G. Calhoun, <u>Digital Cellular Radio</u>, Artech House Inc., Norwood MA, 1988.

[16] R.E. Ziemer and R.L. Peterson, <u>Digital Communications and Spread Spectrum Systems</u>, Macmillian Publishing Company, New York, 1985.

[17] D.V. Sarwate and M.B. Pursley, "Crosscorrelation Properties of Pseudorandom and Related Sequences," *Proc. IEEE*, Vol. 68, No. 5, pp. 593-619, May 1980.

[18] M.B. Pursley and H.F.A. Roefs, "Numerical Evaluation of Correlation Parameters for Optimal Phases of Binary Shift-Register Sequences," *IEEE Trans. on Comm.*, Vol. com-27, No. 10, pp. 1597-1604, October 1979.

[19] G.D. Morrison, "A Frequency Domain Measurement System for Indoor Ultrahigh frequency radio propagation studies," M.Sc thesis, Dept. of Elec. & Compu. Engg., Univ. of Calgary, Dec. 1991.

[20] W.C.Y. Lee, Mobile Communications Engineering, McGraw-Hill Inc., 1982.

[21] J.G. Proakis, Digital Communications, New York: McGraw-Hill Inc., 1983.

[22] M. Kavehrad, "Performance of Nondiversity Receivers for Spread Spectrum in Indoor Wireless Communications," *AT & T Tech. J*, Vol. 64, pp. 1181-1210, Jul-Aug 1985.

[23] G. Turin, "Introduction to Spread-Spectrum Anti-Multipath Techniques and Their Application to Urban Digital Radio," *Proc. IEEE*, Vol. 68, pp. 328-353, Mar 1980.

[24] S. Verdu, "Minimum Probability of Error for Asynchronous Gaussian Multiple-Access Channels," *IEEE Trans. on Information Theory*, Vol. IT-32, No. 1, pp. 85-96, Jan 1986.

[25] R. Lupas and S. Verdu, "Near-far resistance of multiuser detectors in asynchronous channels," *IEEE Trans. on Comm.*, Vol. Com-38, No. 4, pp. 496-508, Apr 1990.

[26] M.K. Varansi and B. Aazhang, "Multistage detection in asynchronous code-division multiple-access communications," *IEEE Trans. on Comm.*, Vol. 38, No. 4, pp. 509-519, Apr 1990.

[27] S. Verdu, "Optimum multi-user signal detection," *Ph. D dissertation*, Dep. Elec. Comp. Eng., Univ. Illinois, Urbana-Champaign, 1984.

[28] A.B. Sesay[1], P.C. Yip[2] and K.M. Wong[2], "Waveform Division Multiple -Access," *to appear in IEE Proc. of Comm., Speech and Vision*, [1]TRLabs and Dept. of Elect. and Compu. Engg., Univ. of Calgary, Alberta and [2]Comm. Research Lab., Dept. of Elect. and Compu. Engg., McMaster Univ, Hamiltion.

[29] E. Geraniotis, "Performance of noncoherent direct-sequence spread-spectrum multiple-access," *IEEE J. Selected Areas in Comm.*, Vol. SAC-3, pp. 687-694, August 1985.

[30] J. Liebman, L. Ladson, L. Schrage and A. Waren, MODELING AND OPTIMIZATION WITH GINO, The Scientific Press, South San Francisco CA, 1986.

[31] L. Ladson and A. Waren, GRG2 USER'S GUIDE, Jan. 1986.

[32] P.A. Bello, "Characterization of randomly time-variant linear channels," *IEEE Trans. on Comm. Syst.*, Vol. CS-11, Dec 1963.

[33] W.C. Jakes, Microwave Mobile Communications, Wiley, New York, 1974.

[34] M.J. Gans, "A power-spectral theory of propagation in the mobile radio environment," *IEEE Trans. on Vehicular Technology*, Vol. VT-21, pp. 27-38, Feb. 1972.

[35] T.A. Sexton and K. Pahlavan, "Channel modeling and adaptive equalization of indoor radio channels," *IEEE Journal on Selected Areas in Comms.*, Vol. JSAC-5, pp. 128-137, Feb. 1987

[36] S.J. Howard and K. Pahlavan, "Performance of a DFE modem evaluated from measured indoor radio multipath profiles," *Proceedings of ICC'90*, Altanta, GA., April 16-19, 1990.

[37] A.A.M. Saleh, R.A. Valenzuela, "A statistical model for indoor multipath propagation," *IEEE Journal on Sel. Areas in Comms.*, Vol. SAC-5, No. 2, PP. 128-137, Feb. 1987..

[38] P.K. Enge, D.V. Sarwate, "Spread-Spectrum Multiple-Access Performance of Orthogonal Codes: Linear Receivers," *IEEE Trans. on Comms.*, Vol. Com-35, No. 12, pp. 1309-1318, December 1987.

APPENDIX A

The optimal gold sequences of period 127 with different initial loading conditions for a generator polynomial 41567 (or '100 001 101 110 111' in binary notation) [18] that are used in the simulations are listed below.

No	Octal Notation	Binary Notation
1	01450	00 001 100 101 000
2	15167	01 101 001 110 111
3	17160	01 101 001 110 000
4	33112	11 011 001 001 010
5	35576	11 101 101 111 110
6	05573	00 101 101 111 011
7	03665	00 011 110 110 101
8	15665	01 101 110 110 101
9	00005	00 000 000 000 101
10	00144	00 000 001 100 100

APPENDIX B

Listed in Table B.1 are the values of A, the upper and lower bounds for the optimized codes $p_{i,l}$ (for M = 16) as described in Section 3.3.2, which are used in the constrained optimization process to produce the optimized codes. To locate the bounds, look for the element in the i th column which is indicated by the number at the top of the table and the l th row.

Table B.1 Bounds for the constraints for optimizing codes (M =16)

#1	#2	#3	#4	#5	#6	#7	#8	#9	#10	#11	#12	#13	#14	#15	#16
± 20	±0.5	± 20	±0.5	±0.5	±0.5	±0.2	±0.5	± 20	±0.5	±0.5	± 20	±0.5	±0.5	±0.5	± 20
± 20	±0.5	± 20	± 20	±0.5	±0.5	±0.2	± 20	± 20	± 20	±0.5	± 20	±0.5	± 20	±0.5	± 20
± 20	±0.5	± 1.0	± 20	±0.5	± 20	± 20	± 20	±0.5	±0.5	± 20	± 20	± 20	± 20	± 20	± 20
± 20	±0.5	± 1.0	± 20	±0.5	± 20	± 20	± 20	±0.5	± 20	± 20	± 20	± 20	± 20	± 20	± 20
± 1.0	±0.5	± 20	± 20	± 20	± 20	± 20	± 20	± 20	±0.5	± 20	± 20	± 20	± 20	± 20	± 20
± 1.0	±0.5	± 20	± 1.0	± 20	± 20	± 20	± 20	± 20	± 20	± 20	± 20	± 20	± 20	± 20	±0.5
± 1.0	±0.5	± 1.0	± 1.0	± 20	±0.5	± 20	± 20	± 20	± 20	± 20	± 20	± 20	± 20	± 1.0	±0.5
± 1.0	±0.5	± 1.0	±0.5	± 20	±0.5	± 20	± 20	± 20	±0.5	± 20	± 20	± 20	± 20	± 1.0	± 20
±0.3	± 20	± 20	±0.5	± 20	±0.5	±0.2	± 1.0	± 20	±0.5	± 1.0	± 20	±0.5	± 20	±0.5	±0.5
±0.3	± 20	± 20	± 1.0	± 20	±0.5	±0.2	±0.5	± 20	± 20	± 1.0	±0.5	±0.5	±0.5	±0.5	±0.5
±0.3	± 20	± 1.0	± 1.0	±0.5	±0.5	±0.5	±0.5	±0.5	±0.5	±0.5	±0.5	±0.5	±0.5	±0.5	±0.5
±0.3	± 20	± 1.0	±0.5	±0.5	± 1.0	±0.5	± 1.0	±0.5	±0.5	±0.5	± 20	±0.5	±0.5	±0.5	±0.5
±0.1	± 20	±0.2	±0.5	±0.5	± 1.0	±0.5	±0.5	±0.5	± 1.0	±0.2	±0.5	± 20	±0.5	±0.5	±0.5
±0.1	± 20	±0.2	± 1.0	±0.5	±0.5	±0.5	±0.5	±0.5	±0.5	±0.2	±0.5	± 20	±0.5	±0.5	±0.5
±0.1	± 20	± 1.0	± 1.0	±0.5	±0.5	±0.5	±0.5	±0.5	± 1.0	±0.5	±0.5	±0.5	±0.5	±0.5	±0.5
±0.1	± 20	± 1.0	±0.5	±0.5	±0.5	±0.5	±0.5	±0.5	±0.5	±0.5	±0.5	±0.5	±0.5	±0.5	±0.5

Table B.2 Codes for transmit waveforms

#1	#2	#3	#4	#5	#6	#7	#8	#9	#10	#11	#12	#13	#14	#15	#16
1	1	1	1	1	1	1	1	1	1	1	1	1	1	1	1
1	-1	1	-1	1	-1	1	-1	1	-1	1	-1	1	-1	1	-1
1	1	-1	-1	1	1	-1	-1	1	1	-1	-1	1	1	-1	-1
1	-1	-1	1	1	-1	-1	1	1	-1	-1	1	1	-1	-1	1
1	1	1	1	-1	-1	-1	-1	1	1	1	1	-1	-1	-1	-1
1	-1	1	-1	-1	1	-1	1	1	-1	1	-1	-1	1	-1	1
1	1	-1	-1	-1	-1	1	1	1	1	-1	-1	-1	-1	1	1
1	-1	-1	1	-1	1	1	-1	1	-1	-1	1	-1	1	1	-1
1	1	1	1	1	1	1	1	-1	-1	-1	-1	-1	-1	-1	-1
1	-1	1	-1	1	-1	1	-1	-1	1	-1	1	-1	1	-1	1
1	1	-1	-1	1	1	-1	-1	-1	-1	1	1	-1	-1	1	1
1	-1	-1	1	1	-1	-1	1	-1	1	1	-1	-1	1	1	-1
1	1	1	1	-1	-1	-1	-1	-1	-1	-1	-1	1	1	1	1
1	-1	1	-1	-1	1	-1	1	-1	1	-1	1	1	-1	1	-1
1	1	-1	-1	-1	-1	1	1	-1	-1	1	1	1	1	-1	-1
1	-1	-1	1	-1	1	1	-1	-1	1	1	-1	1	-1	-1	1

In Table B.2, the elements are the codes $g_{k,l}$ of the Hadamard matrix (size M = 16) where the k th transmitter is indicated by the column number while the index l points to the l th row.

Table B.3 Codes for optimized received waveforms

#1	#2	#3	#4	#5	#6	#7	#8	#9	#10	#11	#12	#13	#14	#15	#16
2.574	0.500	1.243	0.500	0.500	0.500	0.200	0.500	1.468	0.500	0.500	1.232	0.500	0.500	0.500	1.702
2.576	-0.500	1.243	-1.916	0.500	-0.500	0.200	-1.694	1.469	-1.879	0.500	-1.233	0.500	-1.661	0.500	-1.703
2.623	0.500	-1.000	-1.637	0.500	2.244	-2.024	-1.460	0.500	0.500	-1.758	-1.255	1.474	1.434	-2.244	-1.734
2.626	-0.500	-1.000	1.639	0.500	-2.246	-2.026	1.462	0.500	-1.893	-1.760	1.257	1.475	-1.435	-2.247	1.736
1.000	0.500	1.271	1.807	-1.823	-2.252	-2.031	-1.466	1.502	0.500	1.765	1.260	-1.480	-1.439	-2.252	-2.056
1.000	-0.500	1.273	-1.000	-1.826	2.257	-2.035	1.469	1.505	-1.900	1.769	-1.262	-1.483	1.442	-2.257	0.500
1.000	0.500	-1.000	-1.000	-1.829	-0.500	2.038	1.471	1.506	1.904	-1.771	-1.264	-1.484	-1.444	1.000	0.500
1.000	-0.500	-1.000	0.500	-1.835	0.500	2.046	-1.476	1.511	-0.500	-1.777	1.270	-1.490	1.449	1.000	-2.069
0.300	1.376	1.281	0.500	1.837	0.500	0.200	1.000	-1.515	-0.500	-1.000	-1.468	-0.500	-1.695	-0.500	-0.500
0.300	-1.384	1.289	-1.000	1.850	-0.500	0.200	-0.500	-1.523	1.925	-1.000	0.500	-0.500	0.500	-0.500	0.500
0.300	1.386	-1.000	-1.000	0.500	0.500	-0.500	-0.500	-0.500	-0.500	0.500	0.500	-0.500	-0.500	0.500	0.500
0.300	-1.405	-1.000	0.500	0.500	-1.000	-0.500	1.000	-0.500	0.500	0.500	-1.500	-0.500	0.500	0.500	-0.500
0.100	1.407	0.200	0.500	-0.500	-1.000	-0.500	-0.500	-0.500	-1.000	-0.200	-0.500	1.526	0.500	0.500	0.500
0.100	-1.465	0.200	-1.000	-0.500	0.500	-0.500	0.500	-0.500	0.500	-0.200	0.500	1.589	-0.500	0.500	-0.500
0.100	1.326	-1.000	-1.000	-0.500	-0.500	0.500	0.500	-0.500	-1.000	0.500	0.500	0.500	0.500	-0.500	-0.500
0.100	-2.249	-1.000	0.500	-0.500	0.500	0.500	-0.500	-0.500	0.500	0.500	-0.500	0.500	-0.500	-0.500	0.500

Table B.3 lists the results of the constrained optimization process for M = 16. The optimized codes $p_{i,l}$ is obtained by locating the element in the i th column (indicated by the number at the top of the table) and the l th row.

APPENDIX C

The variances and covariance needed for the evaluation of the Gaussian approximation for the average probability of error are listed below. Using equations (3.21) and (3.22) as the starting point, the partial crosscorrelation functions are

$$r_{k,i}(\tau) = \begin{cases} \frac{1}{M}\sum_{l=1}^{M} g_{k,l}\, p_{i,l}\left[\frac{\tau}{T}\cos\left(\frac{\pi l \tau}{T}\right) - \frac{1}{\pi l}\sin\left(\frac{\pi l \tau}{T}\right)\right], & l = m \\ \frac{1}{M}\sum_{l=1}^{M}\sum_{m=1}^{M} g_{k,l}\, p_{i,m}\frac{2}{\pi\left(m^2 - l^2\right)}\left[l\sin\left(\frac{\pi m \tau}{T}\right) - m\sin\left(\frac{\pi l \tau}{T}\right)\right], & l \neq m \end{cases} \tag{C.1}$$

and

$$\hat{r}_{k,i}(\tau) = \begin{cases} \frac{1}{M}\sum_{l=1}^{M} g_{k,l}\, p_{i,l}\left[\left(1 - \frac{\tau}{T}\right)\cos\left(\frac{\pi l \tau}{T}\right) + \frac{1}{\pi l}\sin\left(\frac{\pi l \tau}{T}\right)\right], & l = m \\ \frac{1}{M}\sum_{l=1}^{M}\sum_{m=1}^{M} g_{k,l}\, p_{i,m}\frac{2}{\pi\left(m^2 - l^2\right)}\left[-l\sin\left(\frac{\pi m \tau}{T}\right) + b\sin\left(\frac{\pi l \tau}{T}\right)\right], & l \neq m \end{cases} \tag{C.2}$$

where

$$b = m\cos(\pi m)\cos(\pi l) \tag{C.3}$$

and the indices (l and m) are integers. The size of the Hadamard matrix is denoted by M. Variances of the partial crosscorrelation function are obtained using

$$Var\left\{r_{k,i}(\tau)\right\} = \frac{1}{\beta T}\int_0^{\beta T} r_{k,i}^2(\tau)\ dt \tag{C.4a}$$

and

$$Var\left\{\hat{r}_{k,i}(\tau)\right\} = \frac{1}{\beta T}\int_0^{\beta T} \hat{r}_{k,i}^2(\tau)\ dt \tag{C.4b}$$

while the covariance is evaluated using

$$Cov\left\{\ r_{k,i}(\tau)\,\hat{r}_{k,i}(\tau)\ \right\} = \frac{1}{\beta T}\int_0^{\beta T} r_{k,i}(\tau)\,\hat{r}_{k,i}(\tau)\,dt\,. \tag{C.5}$$

The factor β is a fraction of the symbol duration.

The products of the crosscorrelation functions indicated by equations (C.4a) and (C.4b) result in four summations whose indices are denoted by *a*, *b*, *c* and *d*. Therefore, the variance of equation (C.4a) when subjected to the conditions $(a = b)$ and $(c = d)$ gives

$$Var\left\{r_{k,i}(\tau)\right\} = \frac{1}{\beta M^2}\sum_{a=1}^{M}\sum_{c=1}^{M} g_{k,a}\,g_{k,c}\,p_{k,a}\,p_{k,c}\{A - B - C + D\}$$

where

$$\begin{aligned} A = &\frac{1}{\pi^3 (a-c)^3}\left[\pi^2(a-c)^2\,\beta^2 sin\,\pi\,\beta\,(a-c) - 2sin\,\pi\,\beta\,(a-c) + 2\pi\beta(a-c)cos\,\pi\,\beta\,(a-c)\right] \\ &+\frac{1}{\pi^3 (a+c)^3}\left[\pi^2(a+c)^2\,\beta^2 sin\,\pi\,\beta\,(a+c) - 2sin\,\pi\,\beta\,(a+c) + 2\pi\beta(a+c)cos\,\pi\,\beta\,(a+c)\right], \end{aligned}$$

$$B = \frac{1}{2\,\pi^3 c\,(c\,-a)^2}\left[\sin \pi\beta(c-a) - \pi\beta(c-a)\cos \pi\beta(c-a)\right]$$
$$+\ \frac{1}{2\,\pi^3 c\,(c\,+a)^2}\left[\sin \pi\beta(c+a) - \pi\beta(c+a)\cos \pi\beta(c+a)\right]\ ,$$

$$C = \frac{1}{2\,\pi^3 a\,(a\,-c)^2}\left[\sin \pi\beta(a-c) - \pi\beta(a-c)\cos \pi\beta(a-c)\right]$$
$$+\ \frac{1}{2\,\pi^3 a\,(a\,+c)^2}\left[\sin \pi\beta(a+c) - \pi\beta(a+c)\cos \pi\beta(a+c)\right]\ ,$$

$$D = \frac{1}{2\,\pi^3 a\,c}\left[\frac{\sin \pi\beta(a-c)}{(a\,-c)} - \frac{\sin \pi\beta(a+c)}{(a\,+c)}\right]\ . \qquad \text{..... (C.6)}$$

Note that equation (C.6) is valid for $(a \neq c)$. A similar expression can be obtained to account for the singularities when $(a = c)$. When none of the indices are equal, that is, $[(a \neq b),(c \neq d),(a \neq c),(b \neq d)]$, the variance of (C.4a) is given by

$$Var\{r_{k,i}(\tau)\} = \frac{1}{\beta M^2}\sum_{a=1}^{M}\sum_{b=1}^{M}\sum_{c=1}^{M}\sum_{d=1}^{M} g_{k,a}g_{k,c}p_{k,b}p_{k,d}\ \frac{4}{\pi^2(b^2-a^2)(d^2-c^2)}\{A-B-C+D\}$$

where

$$A = \frac{ac}{2\pi}\left[\frac{\sin \pi\beta\,(b-d)}{(b-d)} - \frac{\sin \pi\beta\,(b+d)}{(b+d)}\right]\ ,$$

$$B = \frac{ad}{2\pi}\left[\frac{\sin \pi\beta\,(b-c)}{(b-c)} - \frac{\sin \pi\beta\,(b+c)}{(b+c)}\right]\ ,$$

$$C = \frac{bc}{2\pi}\left[\frac{\sin \pi\beta\,(a-d)}{(a-d)} - \frac{\sin \pi\beta\,(a+d)}{(a+d)}\right]\ ,$$

$$D = \frac{bd}{2\pi}\left[\frac{\sin \pi\beta\,(a-c)}{(a-c)} - \frac{\sin \pi\beta\,(a+c)}{(a+c)}\right]\ . \qquad \text{..... (C.7)}$$

Similarly, three additional expressions would be needed to account for the singularities when $(b = c)$, $(a = d)$ and $(a = c)$, respectively.

Subjected to the same condition as that of equation (C.6), the variance of equation (C.4b) is given by

$$Var\left\{\hat{r}_{k,i}(\tau)\right\} = \frac{1}{\beta M^2}\sum_{a=1}^{M}\sum_{c=1}^{M} g_{k,a}\, g_{k,c}\, p_{k,a}\, p_{k,c}\, \{A - B + C - D + E - F + G - H + J\}$$

where

$$A = \frac{1}{2\pi}\left[\frac{\sin \pi\beta\,(a-c)}{(a-c)} + \frac{\sin \pi\beta\,(a+c)}{(a+c)}\right],$$

$$B = \frac{1}{2\pi^2}\left\{\left[\frac{\cos \pi\beta(a-c) - 1 + \pi\beta(a-c)\sin \pi\beta(a-c)}{(a-c)^2}\right] + \left[\frac{\cos \pi\beta(a+c) - 1 + \pi\beta(a+c)\sin \pi\beta(a+c)}{(a+c)^2}\right]\right\},$$

$$C = -\frac{1}{2\pi^2 c}\left\{\left[\frac{\cos \pi\beta(c-a) - 1}{(c-a)}\right] + \left[\frac{\cos \pi\beta(c+a) - 1}{(c+a)}\right]\right\},$$

$$D = \frac{1}{2\pi^2}\left\{\left[\frac{\cos \pi\beta(a-c) - 1 + \pi\beta(a-c)\sin\pi\beta(a-c)}{(a-c)^2}\right] + \left[\frac{\cos \pi\beta(a+c) - 1 + \pi\beta(a+c)\sin\pi\beta(a+c)}{(a+c)^2}\right]\right\},$$

$$E = \frac{1}{2\pi^3}\left\{\left[\frac{\pi^2\beta^2(a-c)^2\sin \pi\beta(a-c) - 2\sin\pi\beta(a-c) + 2\pi\beta(a-c)\cos\pi\beta(a-c)}{(a-c)^3}\right] + \left[\frac{\pi^2\beta^2(a+c)^2\sin \pi\beta(a+c) - 2\sin\pi\beta(a+c) + 2\pi\beta(a+c)\cos\pi\beta(a+c)}{(a+c)^3}\right]\right\},$$

$$F = \frac{1}{2\pi^3 c}\left\{\left[\frac{\sin \pi\beta(c-a) - \pi\beta(c-a)\cos\pi\beta(c-a)}{(c-a)^2}\right] + \left[\frac{\sin \pi\beta(c+a) - \pi\beta(c+a)\cos\pi\beta(c+a)}{(c+a)^2}\right]\right\},$$

$$G = -\frac{1}{2\pi^2 a}\left\{\left[\frac{\cos \pi\beta(a-c)-1}{(a-c)}\right] + \left[\frac{\cos \pi\beta(a+c)-1}{(a+c)}\right]\right\},$$

$$H = \frac{1}{2\pi^3 a}\left\{\left[\frac{\sin \pi\beta(a-c) - \pi\beta(a-c)\cos \pi\beta(a-c)}{(a-c)^2}\right] + \left[\frac{\sin \pi\beta(a+c) - \pi\beta(a+c)\cos \pi\beta(a+c)}{(a+c)^2}\right]\right\},$$

$$J = \frac{1}{2\pi^3 ac}\left\{\left[\frac{\sin \pi\beta(a-c)}{(a-c)} - \frac{\sin \pi\beta(a+c)}{(a+c)}\right]\right\}. \qquad \text{..... (C.8)}$$

An additional expression stemming from the singularity condition when $(a=c)$ is required and can be easily obtained by the reader. Now, when all the indices are not equal, the variance of (C.4b) is given by

$$Var\left\{\hat{r}_{k,i}(\tau)\right\} = \frac{1}{\beta M^2}\sum_{a=1}^{M}\sum_{b=1}^{M}\sum_{c=1}^{M}\sum_{d=1}^{M} g_{k,a}\, g_{k,c}\, p_{k,b}\, p_{k,d} \frac{1}{\pi^2(b^2-a^2)(d^2-c^2)}\{A - B + C - D\}$$

where

$$A = \frac{2ac}{\pi}\left[\frac{\sin \pi\beta(b-d)}{(b-d)} - \frac{\sin \pi\beta(b+d)}{(b+d)}\right],$$

$$B = \frac{2ad\cos(\pi c)\cos(\pi d)}{\pi}\left[\frac{\sin \pi\beta(b-c)}{(b-c)} - \frac{\sin \pi\beta(b+c)}{(b+c)}\right],$$

$$C = \frac{2bc\cos(\pi a)\cos(\pi b)}{\pi}\left[\frac{\sin \pi\beta(a-d)}{(a-d)} - \frac{\sin \pi\beta(a+d)}{(a+d)}\right],$$

$$D = \frac{2bd\cos(\pi a)\cos(\pi b)\cos(\pi c)\cos(\pi d)}{\pi}\left[\frac{\sin \pi\beta(a-c)}{(a-c)} - \frac{\sin \pi\beta(a+c)}{(a+c)}\right]. \qquad \text{..... (C.9)}$$

Concerns regarding the singularities conditions when $(b=c)$, $(a=d)$ and $(a=c)$, respectively, must be addressed and can be easily obtained by the reader.

As for the covariance in equation (C.5), it is given by

$$Cov\left\{ r_{k,i}(\tau)\hat{r}_{k,i}(\tau) \right\} = \frac{1}{\beta M^2} \sum_{a=1}^{M} \sum_{c=1}^{M} g_{k,a}\, g_{k,c}\, p_{k,a}\, p_{k,c} \{A - B + C - D + E - F\}$$

where

$$A = \frac{1}{2\pi^2}\left\{\left[\frac{\cos \pi\beta(a-c) - 1 + \pi\beta(a-c)\sin\pi\beta(a-c)}{(a-c)^2}\right] + \left[\frac{\cos \pi\beta(a+c) - 1 + \pi\beta(a+c)\sin\pi\beta(a+c)}{(a+c)^2}\right]\right\},$$

$$B = \frac{1}{2\pi^3}\left\{\left[\frac{\pi^2\beta^2(a-c)^2\sin \pi\beta(a-c) - 2\sin\pi\beta(a-c) + 2\pi\beta(a-c)\cos\pi\beta(a-c)}{(a-c)^3}\right] + \left[\frac{\pi^2\beta^2(a+c)^2\sin \pi\beta(a+c) - 2\sin\pi\beta(a+c) + 2\pi\beta(a+c)\cos\pi\beta(a+c)}{(a+c)^3}\right]\right\},$$

$$C = \frac{1}{2\pi^3 c}\left\{\left[\frac{\sin \pi\beta(c-a) - \pi\beta(c-a)\cos\pi\beta(c-a)}{(c-a)^2}\right] + \left[\frac{\sin \pi\beta(c+a) - \pi\beta(c+a)\cos\pi\beta(c+a)}{(c+a)^2}\right]\right\},$$

$$D = -\frac{1}{2\pi^2 a}\left\{\left[\frac{\cos \pi\beta(a-c) - 1}{(a-c)}\right] + \left[\frac{\cos \pi\beta(a+c) - 1}{(a+c)}\right]\right\},$$

$$E = \frac{1}{2\pi^3 a}\left\{\left[\frac{\sin \pi\beta(a-c) - \pi\beta(a-c)\cos \pi\beta(a-c)}{(a-c)^2}\right] + \left[\frac{\sin \pi\beta(a+c) - \pi\beta(a+c)\cos \pi\beta(a+c)}{(a+c)^2}\right]\right\},$$

$$F = \frac{1}{2\pi^3 ac}\left\{\left[\frac{\sin \pi\beta(a-c)}{(a-c)} - \frac{\sin \pi\beta(a+c)}{(a+c)}\right]\right\}$$

......(C.10)

when it is subjected to the conditions $(a = b)$ and $(c = d)$. Once again, the singularity when $(a = c)$ leads to an additional expression which the reader can easily evaluate. The covariance for the case when all the indices are not equal, similar to the result obtained in equation (C.7), is given by

$$Cov\left\{ r_{k,i}(\tau)\hat{r}_{k,i}(\tau) \right\} = \frac{1}{\beta M^2} \sum_{a=1}^{M} \sum_{b=1}^{M} \sum_{c=1}^{M} \sum_{d=1}^{M} g_{k,a}\, g_{k,c}\, p_{k,b}\, p_{k,d} \frac{4}{\pi^2 (b^2 - a^2)(d^2 - c^2)} \cdot \{ -A + B + C - D \}$$

where

$$A = \frac{ac}{2\pi}\left[\frac{\sin \pi\beta\,(b-d)}{(b-d)} - \frac{\sin \pi\beta\,(b+d)}{(b+d)}\right],$$

$$B = \frac{ad\,\cos(\pi c)\cos(\pi d)}{2\pi}\left[\frac{\sin \pi\beta\,(b-c)}{(b-c)} - \frac{\sin \pi\beta\,(b+c)}{(b+c)}\right],$$

$$C = \frac{bc}{2\pi}\left[\frac{\sin \pi\beta\,(a-d)}{(a-d)} - \frac{\sin \pi\beta\,(a+d)}{(a+d)}\right],$$

$$D = \frac{bd\,\cos(\pi c)\cos(\pi d)}{2\pi}\left[\frac{\sin \pi\beta\,(a-c)}{(a-c)} - \frac{\sin \pi\beta\,(a+c)}{(a+c)}\right].$$

..... (C.11)

Here, concerns for the singularities conditions when $(b = c)$, $(a = d)$ and $(a = c)$, respectively, must be addressed. Note that the expressions for the variances and covariance of the partial crosscorrelation functions are also valid for the objective function of the optimization process by setting $\beta = 1$.